FLOW AND HEAT TRANSFER CHARACTERISTICS OF MICROENCAPSULATED PHASE CHANGE MATERIAL SLURRY IN A COIL HEAT EXCHANGER

A Dissertation

by

MINSUK KONG

Submitted to the Office of Graduate and Professional Studies of
Texas A&M University
in partial fulfillment of the requirements for the degree of

DOCTOR OF PHILOSOPHY

Chair of Committee,	Jorge L. Alvarado
Committee Members,	Sai C. Lau
	Yassin A. Hassan
	Michael B. Pate
Head of Department,	Andreas A. Polycarpou

December 2015

Major Subject: Mechanical Engineering

ABSTRACT

The use of enhanced heat transfer fluid and heat exchanger can improve the performance of thermal energy systems. Microencapsulated phase change material (MPCM) slurry is considered as an enhanced heat transfer fluid and can be used in heat transfer applications because of the higher heat capacity of MPCM slurry, which can improve heat transfer performance. In addition, coil heat exchangers (CHX) have been used in various heat transfer applications due to their compact structure and superior heat transfer performance. However, little is known about how MPCM may exhibit enhanced heat transfer performance in CHX. Therefore, flow and heat transfer characteristics of MPCM slurry in CHX have been investigated.

Fully instrumented pressure drop and heat transfer test sections were built to investigate pressure drop and the local convective heat transfer characteristics of MPCM slurry in a coiled tube, which resembles a CHX. The thermophysical properties of MPCM slurry were measured and characterized experimentally. The viscosity results show that MPCM slurry with a mass fraction of 10.9 % or less can be considered as a Newtonian fluid. Pressure drop and heat transfer experiments were conducted at different mass fractions of MPCM slurries under turbulent flow conditions. The pressure drop results indicate that higher viscosity of MPCM slurry increases pressure drop, which is greater than water. Furthermore, the correlated friction factor curve of MPCM slurry compares well with previous correlations used for homogeneous Newtonian fluids. The heat transfer results indicate that phase change process of the PCM enhances the

heat transfer coefficient of MPCM slurry. However, the heat transfer coefficient of MPCM slurry still is lower than that of water due to decreased momentum transfer. The experimental results also show that secondary flows are imminent and lead to variations in heat transfer coefficient within the coiled tube. Useful correlations have been postulated to predict friction factor and Nusselt number of MPCM slurry in a coiled tube, respectively. Energy evaluation analyses were conducted to determine the benefits of using MPCM slurry in terms of heat transfer performance and heat capacity, respectively. The results show that MPCM slurry cannot enhance the heat transfer performance due to the high viscosity and low latent heat of fusion of the PCM, but it can considerably improve the heat capacity.

DEDICATION

This dissertation is dedicated to my family:

For their love, support and encouragement throughout my educational years

ACKNOWLEDGEMENTS

I would like to thank my advisor, Dr. Jorge L. Alvarado, for his constant guidance, mentorship, and encouragement during the course of this research work. He has always taught me a lot to complete the project and I would like to thank him for giving me the opportunity to do this research.

I wish to thank Dr. Wilson Terrell for his valuable comments and encouragement during the entire research years. I have learned lots of things about experimental study and analysis work. I would like to thank my committee members, Dr. Sai C. Lau, Dr. Yassin A. Hassan, and Dr. Michael B. Pate for their kind assistance and valuable comments on my research. I also wish to thank Dr. Curt Thies for his technical support on my research project.

In addition, I would like to thank my friends, Sungwon Kim, Eunseok Kim, Jeongmoon Park, Qibo Li, Chun-Wei Yao, Taolue Zhang, Kun Yu for their wholehearted support.

In closing, I would like to thank my parents for their unconditional love and support. I wish to thank my lovely wife, Youjin Oh, for her love and dedication, and thank my son, Nathan Yunsu Kong, for his birth and cute tricks.

TABLE OF CONTENTS

LIST OF FIGURES

LIST OF TABLES

1. INTRODUCTION

Energy consumption in cooling and heating systems in buildings has grown rapidly in recent decades. Advanced heat transfer systems using geothermal energy, solar heat, and waste heat have been applied in buildings to conserve energy. However, these systems still require large amounts of heat transfer fluids to be able to operate efficiently and cost effectively. Therefore, increasing the effective heat carrying capacity of heat transfer fluids should result in energy and cost savings.

In the past three decades, the use of microencapsulated phase change material (MPCM) slurry as an enhanced heat transfer fluid has been considered to be very promising for saving energy in thermal energy systems. MPCM slurry can improve the thermal performance of heat transfer systems through its high heat capacity enhanced by phase change materials (PCM) that undergo phase change under certain conditions. The PCM absorbs or releases heat equivalent to its latent heat of fusion with no significant change of temperature during the phase change process. However, MPCM slurries usually need heat exchangers with relatively high surface area for adequate heat transfer given the higher heat capacity and observed lower heat transfer rates. Therefore, appropriate heat exchangers should be used to harness the potential of MPCM slurries.

A coil heat exchanger (CHX) is widely used in many applications including heating, ventilating, and air conditioning (HVAC) systems, chemical processing, and nuclear reactors. The CHX can accommodate a large heat transfer area in a small space and ensure high heat transfer rate partly due to the secondary flows induced by its

configuration. However, little is known about how MPCM may exhibit enhanced heat transfer performance in a CHX. Thus, understanding the flow and heat transfer characteristics of MPCM slurry in CHX is very important and necessary.

1.1 Purpose and Objectives

The purpose of this study was to gain a better understanding about hydraulic and heat transfer characteristics of MPCM slurry in CHX, and to determine how MPCM slurry can enhance the thermal performance of the CHX. The experimental results obtained from this study will be used to provide guidelines and basic data that can be used to design the heat transfer systems with MPCM and to determine their performance.

In order to attain the purpose of this study, the following objectives were identified:

1. Measure and characterize thermophysical properties of MPCM slurries.
2. Measure pressure drop of MPCM slurries in a CHX under turbulent flow conditions and examine the effects of the MPCM's mass fraction and fluid velocity on pressure drop.
3. Postulate a correlation for the prediction of friction factor of MPCM slurries in a CHX.
4. Measure and characterize local convective heat transfer of MPCM slurries in the CHX under turbulent flow conditions and investigate the effects of the MPCM's mass fraction, fluid velocity and heat flux on the heat transfer coefficient.

5. Investigate how Nusselt number is affected by the presence of microcapsules that make up MPCM slurry in a CHX taking into account the phase change process.
6. Postulate a correlation for estimating Nusselt number of MPCM slurries in a CHX.
7. Determine and quantify the benefits of using MPCM slurries in a CHX by comparing with water using the performance efficiency coefficient (PEC) and the figure of merit for heat capacity (FOMHC) approaches.

1.2 Overview

This dissertation is comprised of six chapters. Chapter II provides a literature review of MPCM slurries and coil heat exchangers. Characterization of MPCM slurry is presented in Chapter III, and the experimental heat transfer and pressure drop systems used for the study are described in Chapter IV. Chapter V presents heat transfer and pressure drop results, and analysis of hydraulic and thermal performance of MPCM slurry. Chapter VI presents concluding remarks and recommendations for future studies.

2. LITERATURE REVIEW*

Microencapsulated phase change material (MPCM) slurries have had an increasingly important role as heat transfer fluids because of their high heat carrying capacity induced by the latent heat of fusion, which in turn can improve the performance of the heat transfer systems. In addition, studies of flow patterns and heat transfer performance in coil heat exchangers (CHX) have been performed due to the extensive use of CHXs in commercial and industrial applications. In this chapter, a review of past studies related to MPCM slurries and CHXs is presented.

2.1 Microencapsulated Phase Change Material Slurry

MPCM slurry has been studied and tested in heat transfer systems because of its high heat carrying capacity enhanced by the phase change material (PCM) that undergoes phase change. The studies on MPCM slurries as a heat transfer fluid have been performed for the last three decades to understand the flow and heat transfer characteristics of MPCM slurries in heat transfer systems.

*Part of the data reported in this chapter is reprinted with permission from "Effect of secondary fluid motion on laminar flow heat transfer in helically coiled tubes" by A.N. Dravid, K.A. Smith, E.W. Merrill, P.L.T. Brian, 1970. AIChE J., 17 (5), pp. 1114-1122, Copyright [2004] by John Wiley and Sons

2.1.1 Thermophysical Properties of MPCM Slurry

Alvarado et al. [1] used and characterized MPCM consisting of n-tetradecane with an average size of 2-10 μm as a PCM and tetradecanol, which was used as a nucleating agent to reduce the supercooling effect. The experimental viscosity results showed that MPCM slurry exhibited a Newtonian-like behavior when the mass fraction was kept below 18 %, and that the MPCM's relative viscosity was independent of temperature. Alvarado et al. [2] also studied how to reduce subcooling (or supercooling) of microencapsulated n-tetradecane by adding nucleating agents such as silica fume (0.2 wt %) and tetradecanol (2 and 4 wt %). The results showed that tetradecanol was a better nucleating agent to suppress subcooling.

Taherian et al. [3] used and characterized methyl stearate as a PCM and the MPCM particle diameters were less than 5 μm. The viscosity of MPCM slurry was measured using a rotating drum viscometer. The viscosities increased with the mass fraction of MPCM in the slurries and decreased slightly with increasing temperature. The results also showed that MPCM slurries behaved like a Newtonian fluid at mass fraction less than 15 %.

Kong et al. [4] used methyl stearate encapsulated by polyurea and the average diameter of MPCM particles was approximately 5 μm. The measured viscosity of MPCM slurry increased with MPCM concentration and was about 2.5 to 2.8 times higher than water. They also found that MPCM slurry behaved as a Newtonian fluid at the tested mass fractions of 4.6 % and 8.7 %, which was consistent with previous experiments [1].

Yamagishi et al. [5] observed that surfactant agents were effective in reducing the viscosity of MPCM slurries, which behaved as Newtonian fluids at low volume fraction. Zhang and Zhao [6] found that the dynamic viscosity of MPCM slurries decreased as temperature increased. Overall, MPCM slurry can be considered as a Newtonian fluid at a high shear rate and a mass fraction of less than 20 %. Yang et al. [7] investigated rheological properties of microencapsulated tetradecane slurries and used four different shell materials such as polyvinyl acetate, polystyrene, polymethyl methacrylate and polyethyl methacrylate. Experimental results showed that the viscosity increased with the concentration of MPCM in the slurry and the shell materials slightly affected the apparent viscosity. Roy and Sengupta [8] used n-eicosane and stearic acid as phase change materials with two different wall thicknesses, comprising of around 15 % and 30 % of the total microcapsule volume. The results showed that the microcapsules with thinner walls were unable to withstand repeated thermal cycles. However, the microcapsules with thicker walls were found to be structurally and thermally stable.

Wang et al. [9] found that the relationship between shear stress and shear rate was perfectly linear, when the mass fraction of MPCM was less than around 30 %. It was found that the MPCM slurry can be generally considered as a Newtonian fluid. Additionally, the viscosity of MPCM slurry, with a mass fraction of less than around 30 %, was 1.5 to 8.5 times higher than water [10]. They also found that the MPCM slurry should be considered as a non-Newtonian fluid when the concentration was above 30 %.

At low volume fraction, MPCM slurries can be treated as homogeneous fluid and the viscosity can be calculated by using the Vand equation [11].

$$\frac{\mu_b}{\mu_f} = \left(1 - c_v - Ac_v^2\right)^{-2.5} \quad (1)$$

where $\frac{\mu_b}{\mu_f}$ is defined as relative viscosity, c_v is the volume fraction, and A varies for different materials and sizes.

Many researchers have used the Vand equation to predict the viscosity of the MPCM slurry. Yamagishi et al. [12] estimated the value of A in the Vand equation to be 3.7 for microencapsulated octadecane slurry with an average diameter of 6.3 μm. Mulligan et al. [13] obtained an A value of 3.4 for 10-30 μm diameter microcapsules in MPCM slurry. Wang et al. [9] showed that the value of parameter A was 4.4 for MPCM slurry with around 5 to 30 % mass fraction. Dammel and Stephan [14] found that this equation underestimated the viscosity of MPCM slurries because the MPCM particles were treated as ideal rigid sphere.

In summary, adding MPCM particles to carrier fluid increases the value of viscosity and MPCM slurry can be considered as a Newtonian fluid at low mass fractions.

2.1.2 Pressure Drops of MPCM Slurry

Alvarado et al. [1] conducted a series of experiments where pressure drop of MPCM slurries were measured under turbulent conditions. The data collected by Alvarado et al. [1] indicated a potential drag-reducing effect of MPCM slurry, which

could play a major role in reducing pressure drop. The experimental results showed that the pressure drop for the MPCM slurry at 5.9 % mass fraction was less than that for water. They suggested that a small amount of ruptured and released microcapsules into the carrying fluid could create favorable conditions for the drag-reducing effect and contribute to the reduction of pressure drop.

Taherian et al. [3] measured pressure drop of MPCM slurry in a circular horizontal tube, and experimental results showed that the pressure drop of MPCM slurries was higher than water. However, they found that the pressure drop of one of MPCM slurries, which contained the proprietary PCM, was close to or less than water. This could be attributed to the drag-reducing effect as reported by Alvarado et al. [1].

Kong et al. [4] measured pressure drop of MPCM slurry flowing through a coil heat exchanger. Experimental results showed that the pressure drop of MPCM slurry increased with increasing MPCM concentration and fluid velocity. Also, the pressure drop of MPCM slurry was slightly greater than that of water, even though the viscosity was about 2.5 to 2.8 times higher than for water.

Yamagishi et al. [5] studied the relationship between pressure drop and the mean fluid velocity and showed that pressure drop of MPCM slurry at 19.1 % volume fraction in a pipe was found to be 20 % greater than that of the carrier fluid at the same fluid velocity. However, they found that pressure drop of a 29.4 vol. % MPCM slurry was lower than pure water when the fluid velocity was in the range of 2.0 to 2.5 m/s because the slurry became laminarized. Additionally, Yamagishi et al. [12] measured pressure drop of MPCM slurries in a circular tube with no heat and showed that the friction factor

of MPCM slurries was approximately equal to that for water. However, pressure drop for 30 % volume fraction of MPCM slurry was lower than that of water because high viscosity led to laminarization of the slurry flow. They also claimed that turbulence was suppressed because particle size was smaller than the turbulence length scale. Crowe et al. [15] found that the small size of microcapsules ranged from 2 to 10 μm suppressed turbulence, which could have a major role in reducing pressure drop.

Inaba et al. [16] reported that the Blasius equation overestimated friction factor of MPCM slurry under turbulent flow because of the flow drag reduction effect of the fine particles. Inaba et al. [16] also studied the heat transfer rate-to-pumping power ratio at different Reynolds numbers. Under turbulent flow condition, the ratio of MPCM slurry was less than that of water, while the ratios of MPCM slurry and water were approximately equal under laminar flow condition. It was found that the enhancement of MPCM slurry was not as large as expected due to the increased pumping power [17, 18]. Chen et al. [19] showed that pressure drop of a 15.8 wt% MPCM slurry was apparently higher than that of water at the same velocity. The pressure drop slightly increased with a decrease of fluid temperature.

Overall, MPCM concentration in the slurry increases pressure drop, which is typically greater than that of carrier fluid due to the increased viscosity. However, pressure drop of MPCM slurry is lower than that of carrier fluid at certain conditions due to a drag-reducing effect or laminarization.

2.1.3 Heat Transfer Characteristics of MPCM Slurry

Alvarado et al. [1] conducted several experiments to determine the heat transfer characteristics of MPCM slurry under constant heat flux and turbulent conditions using a circular horizontal tube. The results indicated that the heat transfer coefficient increased considerably during the phase change process, even at low mass fractions. However, the enhancement was reduced due to the turbulence damping effect, when the mass fraction of MPCM in the slurries increased. They also found that the heat transfer coefficient was affected by the slurry velocity more significantly than by heat flux.

Taherian et al. [3] investigated the effect of flow rate, MPCM concentration and heat flux on heat transfer coefficients under turbulent flow conditions using a circular horizontal tube. The increased flow rate increased the heat transfer coefficient and moved the maximum heat transfer coefficient towards the test section outlet, as observed by Alvarado et al. [1] and Yamagishi et al. [12]. The heat transfer coefficient decreased with increasing the mass fraction of MPCM in the slurry at the same fluid velocity conditions because of the reduced momentum transfer. The increased heat flux shifted the maximum heat transfer coefficient towards the test section inlet but it did not significantly affect the magnitude of the maximum heat transfer coefficient value. Also, Taherian et al. [3] found that the effective heat capacities of MPCM slurry were considerably greater than those of water due to the latent heat of fusion of PCM.

Kong et al. [4] conducted heat transfer experiments to investigate the effect of using MPCM slurry flowing through a CHX on heat transfer performance. Experimental results showed that MPCM slurry led to heat transfer enhancement in the range of 13 %

to 29 %, because of the latent heat of fusion of PCM. It was also found that MPCM enhanced the overall heat transfer coefficients and heat exchanger effectiveness. To assess the benefits of using MPCM slurry, Kong et al. [4] used performance efficiency coefficient (PEC), which was defined as the ratio of the overall heat transfer coefficient ratio to the friction factor ratio between MPCM slurry and water. PEC values for the 4.6 % MPCM slurry were higher than one. It was clear that using MPCM slurry at low mass fraction could improve the overall performance of a CHX by increasing the amount of heat transfer, even though MPCM slurries have higher viscosity, which leads to higher pressure drop when compared to water.

Wang et al. [9] performed an experimental study to investigate the heat transfer characteristics of MPCM slurries at both laminar and turbulent flow conditions in a circular horizontal tube under constant heat flux conditions. The results showed that the local heat transfer coefficient of MPCM slurry was higher than that for water due to the latent heat of PCM. In turbulent flow, the local heat transfer coefficient varied with heat flux and the maximum heat transfer coefficient at high heat flux appeared earlier than at low heat flux. Wang et al. [9] also found that the average heat transfer coefficient was considerably affected by turbulence. Wang et al. [10] showed that the average Nusselt number of MPCM slurry was up to about 2.5 times higher than that for pure water in turbulent flow. Wang et al. [10] also proposed correlations for the estimation of the Nusselt numbers for laminar and turbulent flow conditions.

Yamagishi et al. [12] noticed that the local heat transfer coefficients of MPCM slurries in turbulent flow increased when PCM underwent phase change. The

experimental results showed that local heat transfer coefficients of MPCM slurry were higher than those of pure water and increased with the slurry fraction at the same Reynolds number. However, since increasing the slurry fraction caused a reduction in turbulence, the local heat transfer coefficient of MPCM slurry decreased as the slurry fraction increased under the same fluid velocity. Yamagishi et al. [12] also observed that the maximum value of the local heat transfer coefficient was found to depend upon the MPCM fraction in the slurry, the degree of turbulence, and the heating rate in the test section.

Inaba et al. [16] investigated the heat transfer characteristics of MPCM slurries comprising of microcapsules of 1.5 μm diameter made of n-tetradecane and 17 μm diameter microcapsules made of n-docosane as phase change materials. Inaba et al. [16] claimed that Nusselt number for the plural slurries with two kinds of sized slurries increased, and that the average heat transfer coefficient for the plural slurries was about 2.8 times greater than water.

Rao et al. [20] conducted an experimental study to investigate the heat transfer characteristics of MPCM slurries flowing through rectangular mini-channels at low Reynolds number. Rao et al. [20] were able to observe that MPCM slurry at a low mass flow rate showed better cooling performance when compared with that of water. Heat transfer coefficient and Nusselt number increased with mass fraction of MPCM at low Reynolds number. The heat transfer performance of MPCM slurries at higher mass fractions was less effective at higher mass flow rates because of the shorter residence time of the suspended MPCM particles within the mini-channels.

In summary, the use of MPCM slurry can significantly enhance the heat capacity when compared to water (carrier fluid) due to the latent heat of fusion of PCM. Heat transfer coefficient increases considerably during phase change process, but the average heat transfer coefficient of MPCM slurry is typically lower than that of water at the same fluid velocity condition. However, since heat transfer coefficient of MPCM slurry is strongly affected by the magnitude of latent heat of fusion, slurry viscosity, and phase change rate, MPCM slurry used under moderate conditions can lead to enhanced heat transfer performance.

2.2 Coil Heat Exchanger

Coil heat exchangers (CHX) are widely used in many applications including HVAC systems, chemical processing, and nuclear reactors. The CHX can accommodate a large heat transfer area in a small space and transfer a large amount of heat. Due to the extensive use of CHXs, a considerable number of studies for understanding flow patterns, pressure drop, and the heat transfer characteristics in the helically coiled heat exchanger have been performed.

2.2.1 Flow Characteristics in CHX

The curvature of a coil heat exchanger induces secondary flow patterns perpendicular to the main axial flow direction, as shown in Fig. 1 [21]. The secondary flow patterns arise due to the centrifugally induced pressure gradient. Fluid in the core of the tube moves towards the outer wall and then return to the inner portion of tube by

flowing back along the wall. As the Reynolds number (Re) mainly affects the flow in straight tubes, the flow in coiled tube is governed by the Dean number (De), that is the ratio of the square root of the product of inertial and centrifugal forces to viscous forces. The magnitude of the Dean number is used to quantify the intensity of the secondary flow and it can be determined by the following equation.

$$\mathrm{De} = \mathrm{Re}\sqrt{\frac{r}{R}} = \frac{\rho \cdot u_m \cdot d_i}{\mu}\sqrt{\frac{r}{R}} \tag{2}$$

where ρ , μ , u_m , d_i , r , and R are density and viscosity of the fluid, fluid mean velocity, diameter of inner tube of the heat exchanger, radius of inner tube, radius of coil.

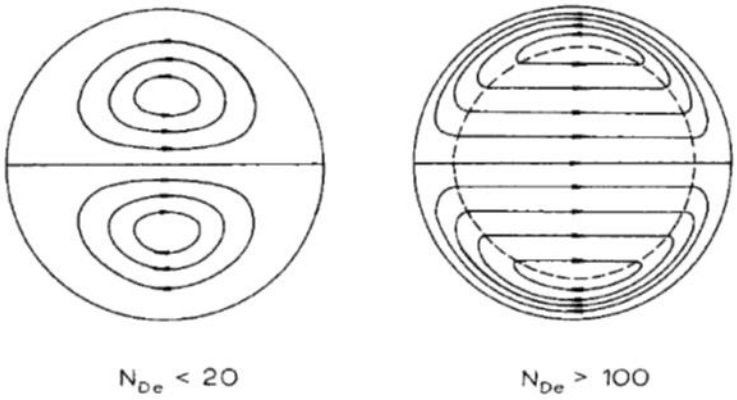

Fig. 1. Secondary flow field at low and high Dean numbers [21]

Dravid et al. [21] conducted a study of heat transfer characteristics for water flowing through coils under laminar flow. The numerical results showed that secondary flow induced the variation of wall temperature along the periphery of the tube and wall

temperature on the outer side was lower than on the inner side. Dravid et al. [21] found that cyclical oscillations in axial wall temperature occurred in the developing region due to secondary flow, which decayed and damped out in the fully developed region.

Huttl and Friedrich [22] conducted a direct numerical simulation for turbulent flow in helical coils. The numerical results showed that a secondary flow was induced due to the curvature and the maximum mean axial velocity moved from the pipe's center towards the outer wall. Huttl and Friedrich [22] also found that torsional forces induced by a coil pitch increased the secondary flow effect and changed its pattern, while having negligible effects on the axial velocity.

Yao and Berger [23] studied the ratio of entrance length for coiled tube to that for straight tube for fully developed flow and concluded that the entrance length for a coiled tube was approximately equal to half of a straight pipe. Shah and Joshi [24] noted that the entrance length for curved tubes was 20 to 50 % shorter than for a straight tube for most engineering applications for De greater than 200.

2.2.2 Transitional Flow Regime in CHX

The flow and heat transfer characteristics of fluids in coil heat exchangers depend on the flow regime such as laminar flow and turbulent flow. In general, the transition in the coil heat exchanger occurs at a higher Reynolds number than that in the straight tube due to the presence of secondary flow, that can stabilize the flow pattern. Since the critical Reynolds number at which the flow changes from laminar to turbulent

in a coil is a function of the curvature ratio, therefore, the critical Reynolds numbers for various coil heat exchangers have been defined.

Ito [25] proposed the empirical correlation to determine the critical Reynolds number for the curvature ratios (r/R) of coil heat exchangers in the range of 0.001 to 0.067.

$$\mathrm{Re}_{cri} = 2\left(\frac{r}{R}\right)^{0.32} \cdot 10^4 \tag{3}$$

Since the correlation proposed by Ito [25] did not give the critical Reynolds number for straight tubes, Srinivasan et al. [26] developed the following correlation based on their experiments for the curvature ratios ranged from 0.0097 to 0.135.

$$\mathrm{Re}_{cri} = 2100\left(1+12\left(\frac{r}{R}\right)^{0.5}\right) \tag{4}$$

The critical Reynolds number for the curvature ratios of CHXs in the range of 0.012 to 0.2 was determined by using the correlation by Schmidt [27], as shown in Equation (5).

$$\mathrm{Re}_{cri} = 2300\left(1+8.6\left(\frac{r}{R}\right)^{0.45}\right) \tag{5}$$

Kubair and Varrier [28] developed an equation to estimate the critical Reynolds number for the curvature ratios of coil heat exchangers in the range of 0.0005 to 0.103, as follows:

$$\mathrm{Re}_{cri} = 12730\left(\frac{r}{R}\right)^{0.2} \tag{6}$$

2.2.3 Flow Resistance in CHX

When a fluid flows through coils, a secondary flow is superimposed on the main flow and the maximum velocity tends to move towards the outer side of the tube. The flow resistance near the tube walls increases and pressure drop in the coil is greater than that in a straight tube. Thus, in order to determine the friction factors in various helically coiled tubes, correlations have been developed as shown below.

Ito [25] presented the results of the frictional resistance for turbulent flow through curved pipes with curvature ratios from 0.0015 to 0.061, and proposed empirical formulas to express friction factor for turbulent flow through curved pipes with satisfactory accuracy. For $\mathrm{Re}(r/R)^2$ ranged from 0.034 to 300, the empirical correlation is as follows [25]:

$$f_c = \frac{0.029 + 0.304\left[\mathrm{Re}\left(\frac{r}{R}\right)^2\right]^{-0.25}}{\left(\frac{R}{r}\right)^{0.5}} \tag{7}$$

For $\mathrm{Re}(r/R)^2$ less than 0.034, the friction factor of a curved pipe was practically equivalent to that of a straight pipe. The following empirical equation for large values of $\mathrm{Re}(r/R)^2$ was defined and used for $\mathrm{Re}(r/R)^2$ greater than 6 [25].

$$f_c = \frac{0.316}{\left[\mathrm{Re}\left(\frac{r}{R}\right)\right]^{0.2} \cdot \left(\frac{R}{r}\right)^{0.5}} \tag{8}$$

Mishra and Gupta [29] measured pressure drop of water flowing through sixty helical coils in the laminar and turbulent regions. For laminar flow, friction factor was calculated using the following correlation [29].

$$f_c = f_s\left(1 + 0.033\left(\log \mathrm{De_m}\right)^4\right) \tag{9}$$

$$\mathrm{De_m} = \mathrm{Re}\sqrt{\frac{D_t}{2R_c\left[1+\left(\frac{p}{2\pi R_c}\right)^2\right]}} \tag{10}$$

where $1 < \mathrm{De} < 3000$

$0.00289 < {}^{r}\!/_{R} < 0.155$

$0 < {}^{p}\!/_{D_c} < 25.4$

${}^{p}\!/_{D_c}$ is a ratio of pitch to coil diameter and the Fanning friction factor $\left(f_s\right)$ for the straight tube in laminar flow condition was determined by the following equation.

$$f_s = \frac{16}{\mathrm{Re}} \tag{11}$$

For turbulent flow, the following correlation was obtained by the least-square analysis of all the turbulent flow data.

$$f_c = f_s + 0.0075\left(\frac{D_t}{D_c}\right)^{0.5} \tag{12}$$

$$D_c = 2R_c\left[1+\left(\frac{p}{2\pi R_c}\right)^2\right] \tag{13}$$

where $4500 < \mathrm{Re} < 100000$

$0.00289 < r/R < 0.155$

$0 < p/D_c < 25.4$

Mishra and Gupta [29] used the Fanning friction factor (f_s) for the straight tube in turbulent flow condition, given by Blasius [30], as follows:

$$f_s = \frac{0.079}{\mathrm{Re}^{0.25}} \tag{14}$$

where $4000 < \mathrm{Re} < 100000$

Srinivasan et al. [26] conducted an experimental study on twelve coils with curvature ratios from 0.0097 to 0.135. The experiments were conducted with water and oil under laminar to turbulent conditions. The correlation for the estimation of the friction factors for laminar flow was defined as follows [26]:

$$f_c = \frac{6.7\sqrt{\frac{D_t}{D_c}}}{\mathrm{De}^{0.5}} \tag{15}$$

where $30 < \mathrm{De} < 300$

$0.0097 < D_t/D_c < 0.135$

The equation used to predict the friction factor in the transitional region is as follows [26]:

$$f_c = \frac{1.8}{\left(\mathrm{Re}\sqrt{\frac{D_c}{D_t}}\right)^{0.5}} \tag{16}$$

where $300 < \mathrm{De} < \mathrm{De}_{cri}$

$$0.0097 < D_t / D_c < 0.135$$

De_{cri} is critical Dean number and determined by multiplying a square root of curvature ratio by critical Reynolds number calculated by the Equation (4).

The friction factor for turbulent flow was predicted by the following equation [26].

$$f_c = \frac{0.084\left(\frac{D_t}{D_c}\right)^{0.2}}{\mathrm{De}^{0.2}} \tag{17}$$

where $\mathrm{De}_{cri} < \mathrm{De} < 14000$

$$0.0097 < D_t / D_c < 0.135$$

Additional experiments were performed to investigate the effects of helical coil pitch on flow resistance, varying from 0.0381m to 0.2032m. The influence of coil pitch was insignificant because the variation in friction factors was ± 4 %.

2.2.4 Heat Transfer Characteristics in CHX

Seban and McLaughlin [31] conducted an experimental study to determine the local heat transfer characteristics in two helical coils, having curvature ratios of 1/17 and 1/104, for laminar flow of oil and turbulent flow of water under constant wall flux boundary conditions. For laminar flow, the Reynolds number was in the range of 15 to 5600 and the Prandtl number was from 100 to 657. Seban and McLaughlin [31] showed that the heat transfer coefficient on the outer surface was higher than on the inner surface, and both values were greater than those in straight tubes. The results in laminar flow also

indicated that the thermal entry length affected Nusselt number. The empirical formula to predict the Nusselt number was postulated as follows [31]:

$$\mathrm{Nu_c} = 0.644\left[\left(\frac{f_c}{8}\right)\mathrm{Re}^2\left(\frac{d}{x}\right)\right]^{1/3}\mathrm{Pr}^{1/3} \tag{18}$$

In addition, Seban and McLaughlin [31] suggested an alternative form in terms of the Reynolds number, friction factor, and Prandtl number, as follows.

$$\mathrm{Nu_c} = \mathrm{A}\left[\left(\frac{f_c}{8}\right)\mathrm{Re}^2\left(\frac{d}{x}\right)\right]^{1/3}\mathrm{Pr}^{1/3} \tag{19}$$

The value A was 0.13 for a coil with a curvature ratio of 1/17. Since the above correlation was not good for coils with a curvature ratio of 1/104, the value A should be adjusted by using a correction factor of 0.74 based on the Adler's theory [32]. For turbulent flow, the same experimental setup with water was used to determine the Nusselt number in the same coils as mentioned above. Reynolds number range was between 6000 and 65600, and the Prandtl number ranged from 2.9 to 5.7. The experimental results showed the ratios of the outside to inside heat transfer coefficients were of the order of 2 and 4 for coils with curvature ratios of 1/104 and 1/17, respectively. An empirical correlation for the estimation of the Nusselt number was postulated, and the Nusselt number from the correlation deviated by less than 10 % and 15 % for coils with curvature ratios of 1/104 and 1/17, respectively, when compared with the experimental Nusselt numbers.

$$\mathrm{Nu_c} = \frac{f_c}{8}\mathrm{Re}\,\mathrm{Pr}^{0.4} \tag{20}$$

$$f_c = f_s\left[\mathrm{Re}\left(\frac{r}{R}\right)^2\right]^{1/20} \tag{21}$$

$$f_s = 0.184\,\mathrm{Re}^{-0.2} \tag{22}$$

Rogers and Mayhew [33] conducted forced convection experiments with water in steam heated helically coiled tubes with curvature ratios of 0.093, 0.075 and 0.05 under turbulent flow conditions. The experimental results were more than 10 % higher than Kirpikov results [34] calculated by the following Equation (23) because Kirpikov [34] defined fluid properties at the bulk fluid temperature instead of using film fluid temperature.

$$\mathrm{Nu_c} = 0.0456\,\mathrm{Re}^{0.8}\,\mathrm{Pr}^{0.4}\left(\frac{r}{R}\right)^{0.21} \tag{23}$$

where $0.056 < r/R < 0.1$

$10000 < \mathrm{Re} < 45000$

Rogers and Mayhew [33] suggested that curvature ratio exponent in Kirpikov correlation [34] should be smaller based on experimental data. The experimental Nusselt numbers were also compared with Seban and McLaughlin's results [31] for a coil with curvature ratio of 1/17 and were about 10 % lower than Seban and McLaughlin correlation [31]. Furthermore, Rogers and Mayhew [33] postulated the correlation for Nusselt number, as follows.

$$\mathrm{Nu_c} = 0.021\,\mathrm{Re}^{0.85}\,\mathrm{Pr}^{0.4}\left(\frac{r}{R}\right)^{0.1} \tag{24}$$

where $0.05 < r/R < 0.093$

$10000 < \mathrm{Re} < 100000$

Mori and Nakayama [35] performed theoretical and experimental studies of fully developed laminar flow in a curved pipe under uniform heat flux condition. In the theoretical study, Mori and Nakayama [35] assumed that the flow was divided into the core region and the boundary layer along the wall. In addition, it was found that the additional flow resistance in a curved pipe was caused by a secondary flow. Mori and Nakayama [35] also postulated a ratio between the thermal boundary layer thickness and the velocity boundary layer thickness expressed in terms of Prandtl number. Through the boundary layer approximation, the theoretical correlation for Nusselt number in curved pipes was also postulated and expressed in terms of Dean number and the ratio of thermal boundary layer thickness to hydrodynamic boundary layer thickness. Experiments were performed by using a coil with a curvature ratio of 0.025 and the results were in good agreement with the theoretical correlation. Mori and Nakayama [36] also studied a fully developed turbulent flow under constant heat flux both theoretically and experimentally. From the boundary layer approximation, a correlation to predict average Nusselt number was postulated in terms of Reynolds number, curvature ratio, and Prandtl number. Experiments were performed with air flowing through curved pipes with curvature ratios of 1/18.7 and 1/40. The experimental results showed that Nusselt numbers agreed well with the theoretical values. Mori and Nakayama [37] extended their earlier work to the theoretical analysis of uniform wall temperature. The results showed that the formula for Nusselt number for uniform wall temperature condition was the

same as that for uniform heat flux. They also summarized all the formulae for the estimation of Nusselt number in coiled pipes under laminar and turbulent flow conditions, respectively, as follows [35-37]:

$$\mathrm{Nu_c} = \frac{0.864}{\left(\frac{\delta_t}{\delta}\right)} \mathrm{De}^{0.5}\left(1 + 2.35\mathrm{De}^{-0.5}\right) \tag{25}$$

where $30 < \left[\mathrm{Re}\left(\frac{r}{R}\right)^{0.5}\right] < \left[\mathrm{Re}_{cri}\left(\frac{r}{R}\right)^{0.5}\right]$

$1 < \mathrm{Pr} < \infty$

δ_t / δ is a ratio of thickness of thermal boundary layer to that of hydrodynamic boundary layer, and critical Reynolds number is determined using the Ito's correlation[25].

$$\mathrm{Nu_c} = \frac{\mathrm{Pr}^{0.4}}{41} \mathrm{Re}^{5/6}\left(\frac{r}{R}\right)^{1/12}\left[1 + \frac{0.061}{\left\{\mathrm{Re}\left(\frac{r}{R}\right)^{2.5}\right\}^{1/6}}\right] \tag{26}$$

where $0.4 < \left[\mathrm{Re}\left(\frac{r}{R}\right)^{2.5}\right]$

$1 < \mathrm{Pr}$

Jayakumar et al. [38] numerically studied the heat transfer characteristics of water under turbulent conditions in vertically-oriented helical coils and simulations were conducted both at constant wall heat flux and constant wall temperature boundary conditions. Jayakumar et al. [38] stated that Nusselt number on the outer side of the coil was the highest among all the points at a specified cross-section, while the inner side had the lowest Nusselt number values. The oscillatory motion of fluid particles led by the

combination of the centrifugal force, inertial force, and buoyancy force influenced heat transfer around the periphery at a cross section along the axial distance. This could lead to the periodic behavior of Nusselt number along the length of the tube. With respect to the influence of coil pitch on heat transfer, the torsional forces induced by the pitch led to oscillations of Nusselt number in the developing region. However, the pitch effect was not significant on the average Nusselt number. The correlation for the estimation of the average Nusselt number under the constant wall heat flux boundary condition was postulated by using a multiple regression analysis as follows:

$$\mathrm{Nu_c} = 0.085\mathrm{De}^{0.74}\mathrm{Pr}^{0.4}\left(\frac{r}{R}\right)^{0.1} \tag{27}$$

where $14000 < \mathrm{Re} < 70000$

$3000 < \mathrm{De} < 22000$

$3 < \mathrm{Pr} < 5$

$0.05 < r/R < 0.2$

In addition, Jayakumar et al. [38] showed that the correlation for constant wall temperature boundary condition gave almost the same value as the Nusselt number with constant heat flux as boundary condition.

Overall, heat transfer coefficients in a coiled tube are higher than those in a straight tube because of the presence of secondary flows. The secondary flow also leads to the difference of heat transfer coefficient between inner and outer surfaces of tube and the heat transfer coefficient on the outer surface is higher than on the inner surface because of higher axial velocity near the outside. Oscillatory behavior of heat transfer coefficient is observed due to the interaction of secondary flow with the main flow.

As seen in the literature review, even though a significant number of studies for CHXs have been conducted to investigate flow and heat transfer characteristics, little is known about the effects of MPCM slurries on pressure drop and heat transfer characteristics in CHX. Therefore, a study should be undertaken to understand the effects of phase change and dilute particle-laden fluids on both pressure drop and convective heat transfer in CHXs.

3. CHARACTERIZATION OF MICROENCAPSULATED PHASE CHANGE MATERIAL SLURRY

3.1 Description of MPCM

MPCM slurries produced by Thies Technology Inc. were used as heat transfer fluids in experiments. The phase change material (PCM) used in the study was butyl stearate, which is an organic compound. Each microcapsule was made by encapsulating the PCM using polyurea as shell material, which made up about 35 % of the total volume of each microcapsule. The MPCM particle size range used in the experiments was between 5 to 10 μm in diameter. Differential scanning calorimetry (DSC) tests were carried out by Thies Technology Inc. using a METTLER DSC unit to determine the thermal properties of MPCM. The DSC method based on ASTM C1784 [39], was used and the amount of energy absorbed or released was measured as a function of temperature at a constant heating and cooling rate of 5 ˚C/min, as shown in Fig. 2. The latent heat of fusion of the PCM was about 88 J/g and the onset and peak melting temperatures were 17.4 ˚C and 22.2 ˚C, respectively.

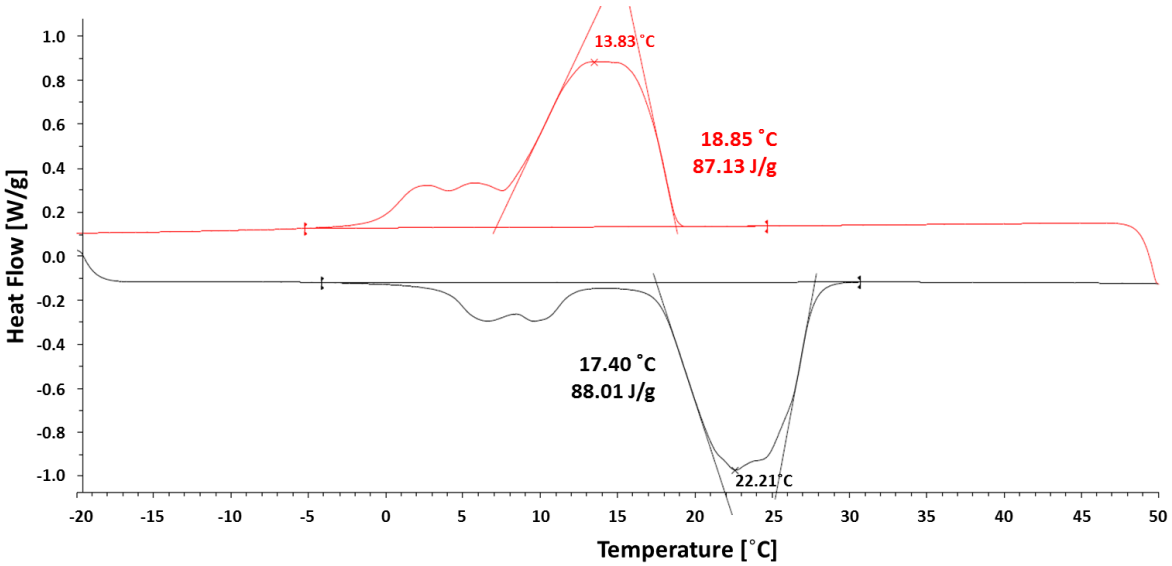

Fig. 2. DSC results

3.2 Thermophysical Properties of MPCM Slurry

To analyze the pressure drop and heat transfer results, thermophysical properties of MPCM slurries were measured and determined. Four different mass fractions of MPCM slurries were used as heat transfer fluids, as shown in Table 1.

Table 1. Concentration of MPCM in the slurry

Mass Fraction	Volume Fraction
2.1 %	2.4 %
5.9 %	6.8 %
8.3 %	9.6 %
10.9 %	12.5 %

3.2.1 Density

The density of MPCM slurry was determined by taking several samples from the heat transfer loop. The volume and mass of each sample were measured using a graduated beaker, a pipette, and a digital weight scale to determine the density of the MPCM slurry at different mass fractions. Density values of MPCM slurry at 10.9 %, 8.3 %, 5.9 %, and 2.1 % mass fractions are shown in Table 2. The measured densities were in good agreement with the values calculated by using the following equation [3], which are within 1 % of the experimental values.

$$\rho_{MPCMs} = \frac{1}{\frac{(1-MF)}{\rho_w} + \frac{MF}{\rho_{MPCM}}} \tag{28}$$

where ρ_w, ρ_{MPCM}, and MF are the density of water, the density of the MPCM, and the mass fraction of the MPCM in the slurry, respectively.

Table 2. Density of MPCM slurry

Fluid	Density, measured	Density, calculated	% Difference
Water [(1)]	998.2 kg/m^3	-	-
Butyl Stearate (PCM)[(2)]	860.0 kg/m^3	-	-
2.1 % MPCM slurry	990.4 kg/m^3	994.9 kg/m^3	-0.5 %
5.9 % MPCM slurry	986.6 kg/m^3	988.9 kg/m^3	-0.2 %
8.3 % MPCM slurry	982.0 kg/m^3	985.1 kg/m^3	-0.3 %
10.9 % MPCM slurry	978.3 kg/m^3	981.1 kg/m^3	-0.3 %

Note: Values are determined at 20 °C. [(1)] NIST Chemistry Webbook [40], [(2)] MatWeb [41]

3.2.2 Thermal Conductivity

Thermal conductivity is one of the important properties in heat transfer, since it is a measure of the material's ability to transfer heat within a medium. However, thermal conductivity measurement for the slurry is difficult because it is hard for microcapsules to be uniformly dispersed in a carrier fluid during a prolonged amount of time. Thus, in this study, thermal conductivity of the MPCM slurry was determined using the Maxwell correlation for homogeneous mixtures [42], which takes into account the mass fraction of MPCM in the slurry, thermal conductivity of water, and thermal conductivity of MPCM. The Maxwell correlation has been used to estimate well the thermal conductivity of particle-laden fluids [43, 44] and it has been used in previous studies [3, 10, 19] to determine thermal conductivity of MPCM slurry. The thermal conductivities of the MPCM slurries calculated using Equation (29) are shown in Table 3.

$$k_{MPCMs} = k_w \left(\frac{2k_w + k_{MPCM} + 2MF\left(k_{MPCM} - k_w\right)}{2k_w + k_{MPCM} - MF\left(k_{MPCM} - k_w\right)} \right) \tag{29}$$

where k_w and k_{MPCM} are thermal conductivities of water and MPCM, respectively. MF is the mass fraction of the MPCM in the slurry.

Table 3. Thermal conductivity of MPCM slurry

Fluid	Thermal Conductivity, calculated	% difference of thermal conductivity
Water [(1)]	0.601 W/m-˚C	-
Butyl Stearate (PCM)[(2)]	0.230 W/m-˚C	-
2.1 % MPCM slurry	0.591 W/m-˚C	-1.7 %
5.9 % MPCM slurry	0.573 W/m-˚C	-4.7 %
8.3 % MPCM slurry	0.563 W/m-˚C	-6.3 %
10.9 % MPCM slurry	0.551 W/m-˚C	-8.3 %

Note: Values are determined at 20 ˚C. [(1)] NIST Chemistry Webbook [40], [(2)] MatWeb [41]

3.2.3 Specific Heat

The specific heat of the MPCM slurry without phase change was calculated using the following equation.

$$c_{p,MPCMs} = c_{p,MPCM} \cdot MF + c_{p,w}(1 - MF) \tag{30}$$

where $c_{p,MPCM}$ and $c_{p,w}$ are the specific heat of MPCM and the specific heat of water, respectively. Specific heat of the MPCM slurry calculated using Equation (30) is shown in Table 4.

Table 4. Specific heat of MPCM slurry without phase change

Fluid	Specific Heat	% enhancement in specific heat
Water [(1)]	4.18 kJ/kg-˚C	-
Butyl Stearate (PCM) [(2)]	2.41 kJ/kg-˚C	-
2.1 % MPCM slurry	4.15 kJ/kg-˚C	-0.7 %
5.9 % MPCM slurry	4.08 kJ/kg-˚C	-2.4 %
8.3 % MPCM slurry	4.04 kJ/kg-˚C	-3.3 %
10.9 % MPCM slurry	3.99 kJ/kg-˚C	-4.5 %

Note: Values are determined at 20 ˚C. [(1)] NIST Chemistry Webbook [40], [(2)] MatWeb [41]

When MPCM particles undergo phase change, the specific heat of the MPCM slurry is strongly affected by the amount of the latent heat of fusion of the PCM, which is called the effective specific heat. Since the rate of heat transfer of the MPCM slurry is a combination of the sensible energy of the slurry and the latent heat of fusion of the PCM in the slurry, the difference between the inlet and outlet fluid temperatures is lower than that of a fluid without phase change, which can lead to increased specific heat. The effective specific heat was determined by the following equation.

$$c_{p,eff} = \frac{\dot{Q}}{\dot{m}_{MPCMs}\Delta T_{MPCMs}} \tag{31}$$

where $\dot{Q}$, $\dot{m}_{MPCMs}$ and ΔT_{MPCMs} are the heat transfer rate, the mass flow rate of the MPCM slurry, and the temperature difference between the inlet and outlet slurry temperatures.

In order to estimate the effect of using MPCM slurry on the enhancement of the specific heat, the effective specific heat of the MPCM slurry was calculated using the energy balance equation for a slurry temperature rise of 3 ˚C, as shown in Fig. 3. Specific heat of MPCM slurry increases with the mass fraction and the enhancement is up to 79 % when compared to water, when phase change takes place, which can lead to increased heat transfer performance.

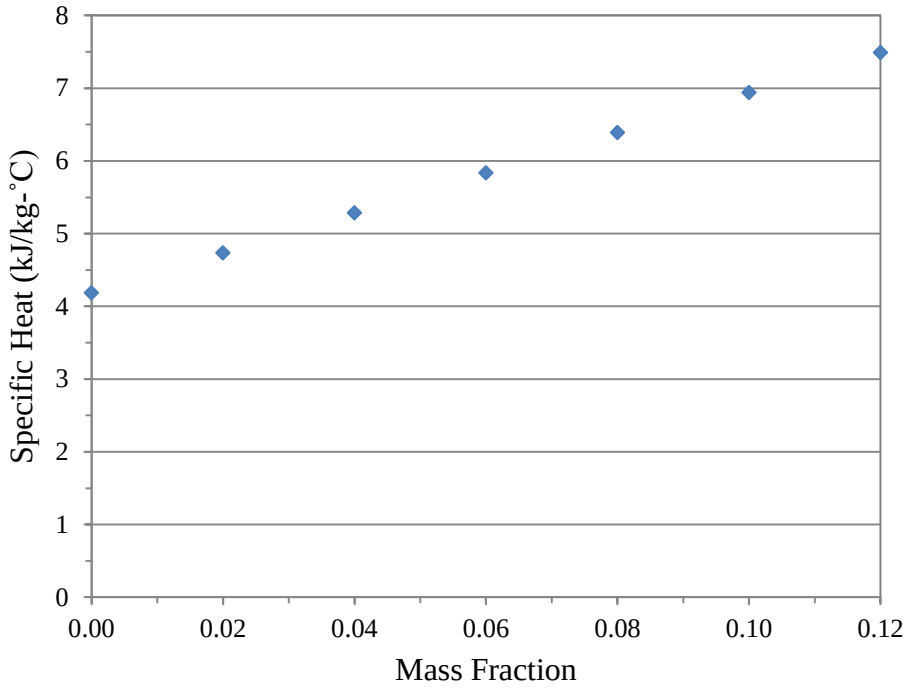

Fig. 3. Effective specific heat of MPCM slurry

3.2.4 Viscosity

Viscosity is an important property which is used to determine flow regime and predict hydrodynamic conditions. In addition, the viscosity plays a significant role in the performance efficiency of thermal energy systems by strongly affecting both pressure drop (pumping power) and momentum transfer. In this study, the apparent viscosity of MPCM slurries was measured using a coaxial cylinder viscometer from Brookfield Engineering Laboratories Inc. The viscometer used in this study consisted of a controller, a spindle, and a container. While the spindle inside the cylinder rotates at certain rotational speed, the viscometer can provide the viscosity of the fluid by measuring the torque generated by the fluid. In order to control fluid temperature, the container was

connected to a chiller, which circulated water at a constant temperature. A UL adapter, including a container and spindle, was used to obtain accurate measurements for low viscosity fluids [1] and the viscometer was calibrated using a reference fluid.

Figures 4 (a), (b), (c), and (d) show the apparent viscosity of MPCM slurries at different mass fractions as a function of shear rate. The viscosity was measured at three different rotational speeds, 50 RPM (= 61.7 rad/sec), 60 RPM (= 74.1 rad/sec), and 100 RPM (= 123.4 rad/sec). The shear rate was calculated using the following equation.

$$\gamma = \frac{2\omega R_c^2}{R_c^2 - R_s^2} \tag{32}$$

where ω is the angular velocity of the spindle (rad/sec) [$\omega = 2\pi N / 60$] where N is the spindle speed in RPM. R_c and R_s are the radius of the container (1.38 cm) and the radius of the spindle (1.2575 cm), respectively.

The experimental results clearly showed that the viscosity of MPCM slurry is independent of shear rate and the coefficient of variation $\left(\frac{\sigma}{\bar{X}}\right)$ of the viscosity is less than 1.2 %. It was found that the MPCM slurry behaves as a Newtonian fluid at the tested mass fractions ranging from 2.1 % to 10.9 %, which is consistent with previous experiments [1, 3, 4, 12].

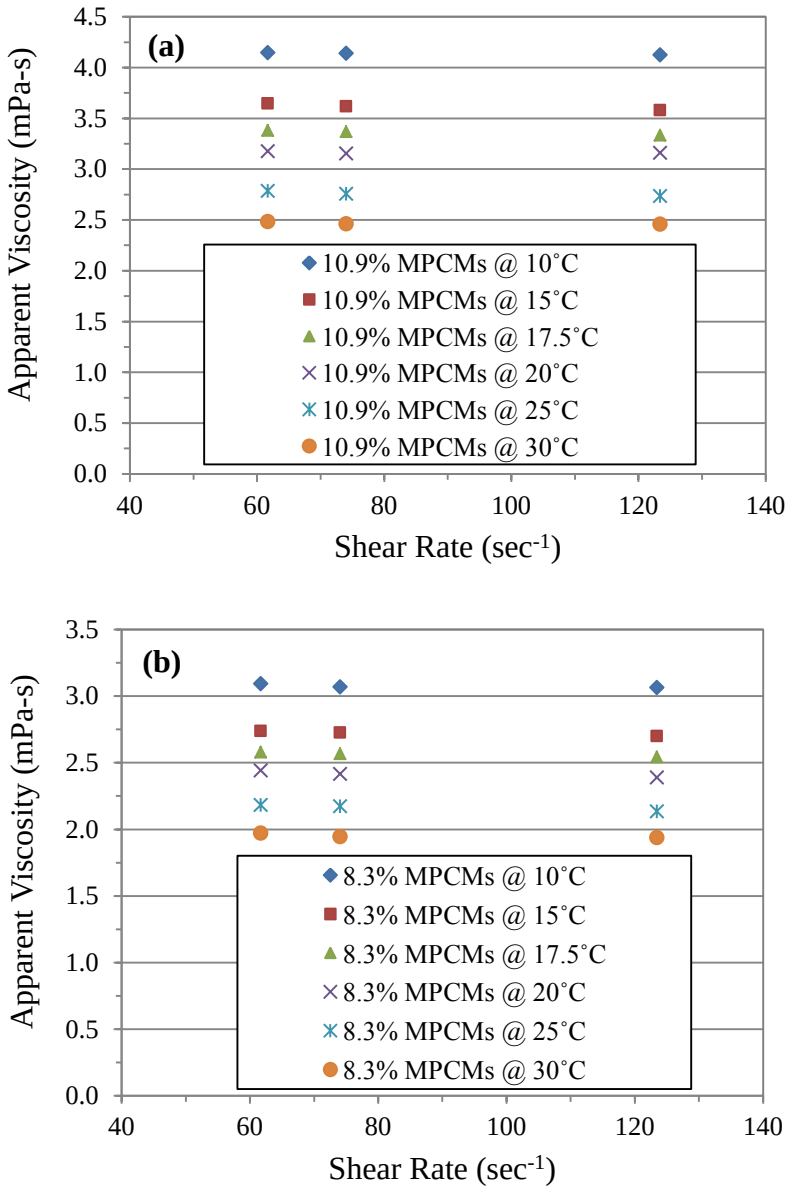

Fig. 4. Apparent viscosity of MPCM slurry as a function of shear rate at (a) 10.9 % MPCMs, (b) 8.3 % MPCMs, (c) 5.9 % MPCMs, (d) 2.1 % MPCMs

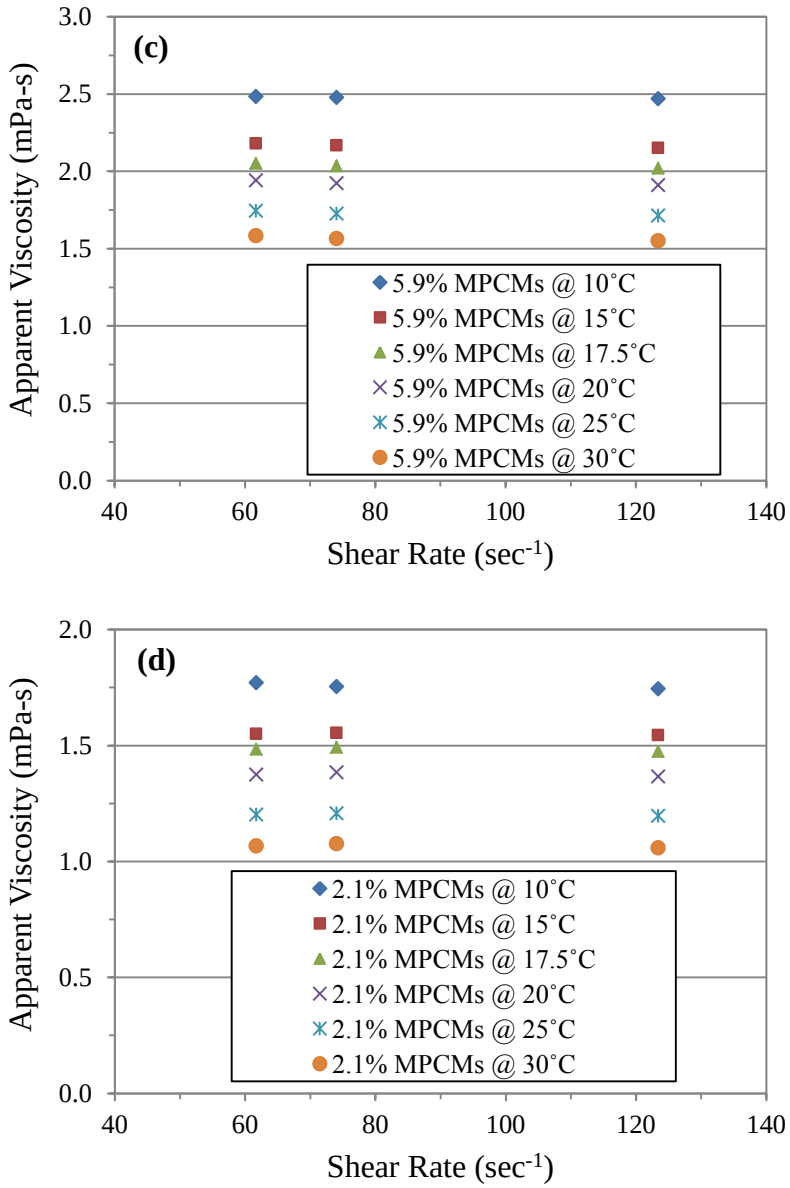

Fig. 4 Continued.

Figure 5 shows the apparent viscosity of MPCM slurries as a function of temperature. The viscosity of the MPCM slurry was measured at different temperatures, which were within the range of the working temperatures in the heat transfer

experiments. It was observed that the apparent viscosity of the MPCM slurries depends on the mass fraction of MPCM in the slurry and the temperature of the slurry. The viscosity at constant temperature increased with the concentration of MPCM dispersed in water, while increasing the slurry temperature reduced the apparent viscosity. The experimental results clearly show that the viscosity of the MPCM slurries is about 1.3 to 3.2 times higher than water, depending on the mass fraction of MPCM. The relative viscosity of the MPCM slurry is shown in Fig. 6. The relative viscosity is defined as the ratio of the apparent viscosity of the slurry to the viscosity of pure water. The experimental results show that the relative viscosity of the MPCM slurries is independent of temperature, which is consistent with previous studies [1, 4, 12].

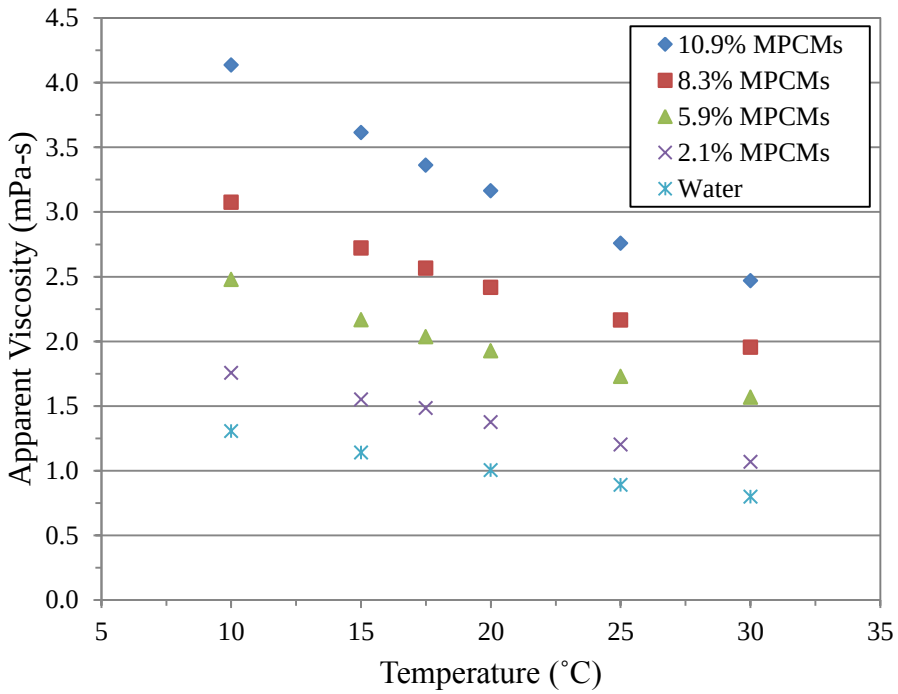

Fig. 5. Apparent viscosity of MPCM slurry as a function of temperature

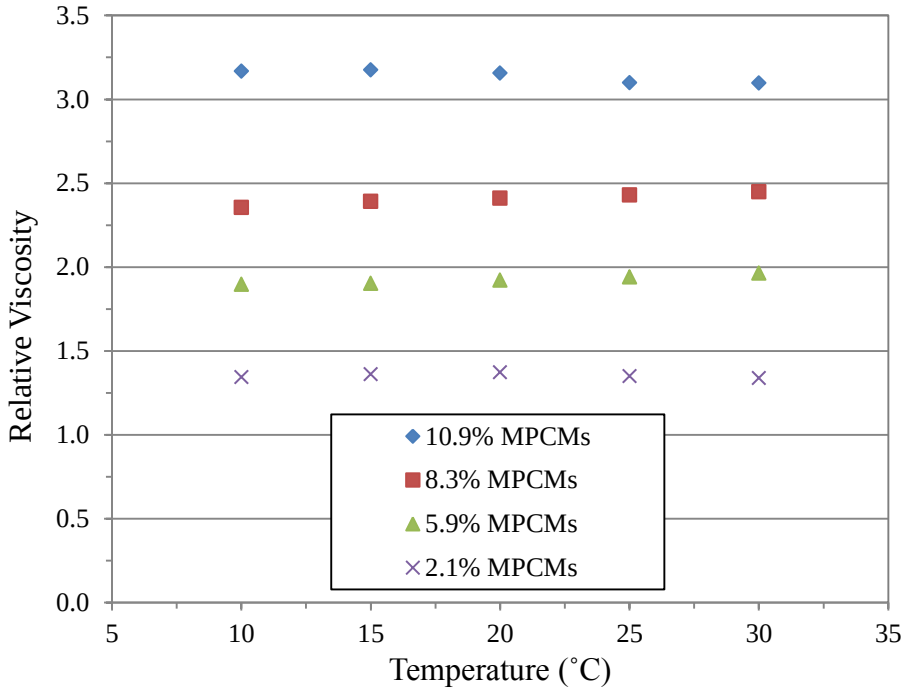

Fig. 6. Relative viscosity of MPCM slurry as a function of temperature

The Vand equation [11] was used to estimate the viscosity of the slurry, which is defined as: $\mu_r = \left(1 - c_v - \mathrm{A}c_v^2\right)^{-2.5}$, where μ_r is the relative viscosity, c_v is the volume fraction, and A is a constant that takes into account the shape and rigidity of the particles in the fluid. For comparison purposes, Figure 7 shows the relative viscosity as a function of volume fraction using the Vand equation and the experimental results. The results show that the Vand correlation (A=1.16) underestimates the viscosity of MPCM slurry, which was observed in previous studies [12, 14]. This could be attributed to that MPCM particles are not ideal rigid spherical particles [14]. In addition, the results show that the relative viscosity is about 1.4 times greater than that for Alvarado et al. [1]. This was also expected because the shape of microcapsules used in Alvarado et al. [1] was

spherical. The use of spherical particles can increase maximum packing fraction compared to oblate or elongated particles [45]. By increasing maximum packing fraction at constant volume fraction should lead to lower viscosity due to the increased free volume that particles can move without resistance or lower rate of collisions [45, 46].

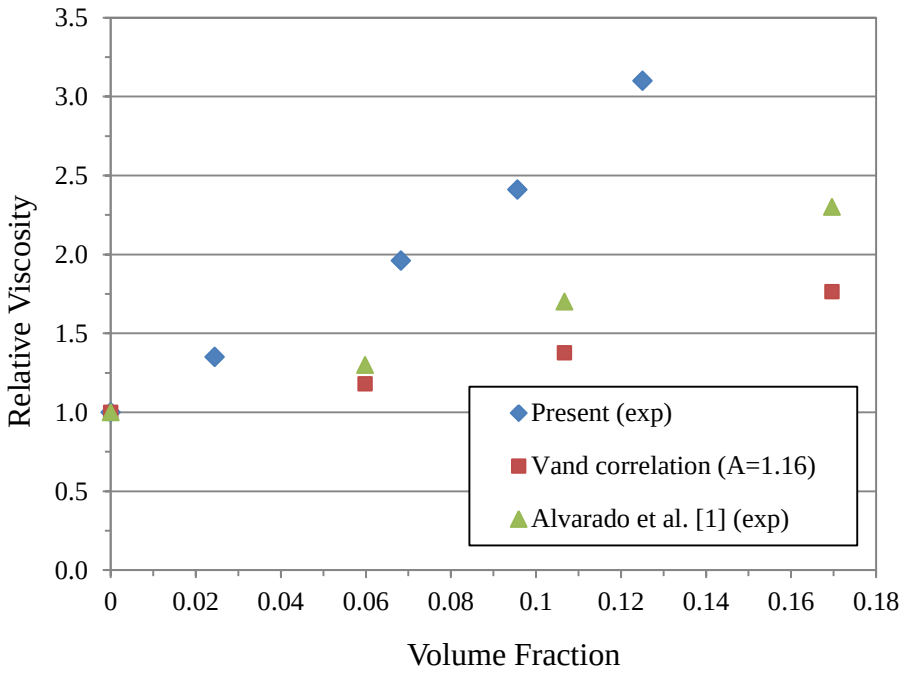

Fig. 7. Relative viscosity of MPCM slurry as a function of volume fraction

The Andrade equation was used for estimating fluid viscosity as a function of fluid temperature, which is defined as: $\mu = \mathrm{A} \cdot \exp\left(\frac{\mathrm{B}}{\mathrm{T}}\right)$ where A and B are constants, and T is absolute temperature (*K*) [47, 48]. Based on the relationship between fluid viscosity and temperature, a multiple regression analysis was performed to postulate a

correlation for predicting apparent viscosity of MPCM slurry as a function of the fluid temperature, T(*K*), and the mass fraction of the MPCM (*MF*) in the slurry, as follows:

$$\mu = 0.001(1 - MF)^{-9.55} \cdot \exp\left(\frac{2092.4}{\mathrm{T}}\right) \qquad \left(R^2 = 0.99\right) \tag{33}$$

where $0 \le MF \le 0.11$ and $283.15K \le \mathrm{T} \le 303.15K$

As shown in Fig. 8, the viscosity calculated by the correlation (33) is compared with the experimental values. The values of the correlation fit well with the experimental values which deviate by less than ± 6 %. From the correlation, it is clear that the apparent viscosity increases with mass fraction of MPCM in the slurry, and decreases with fluid temperature.

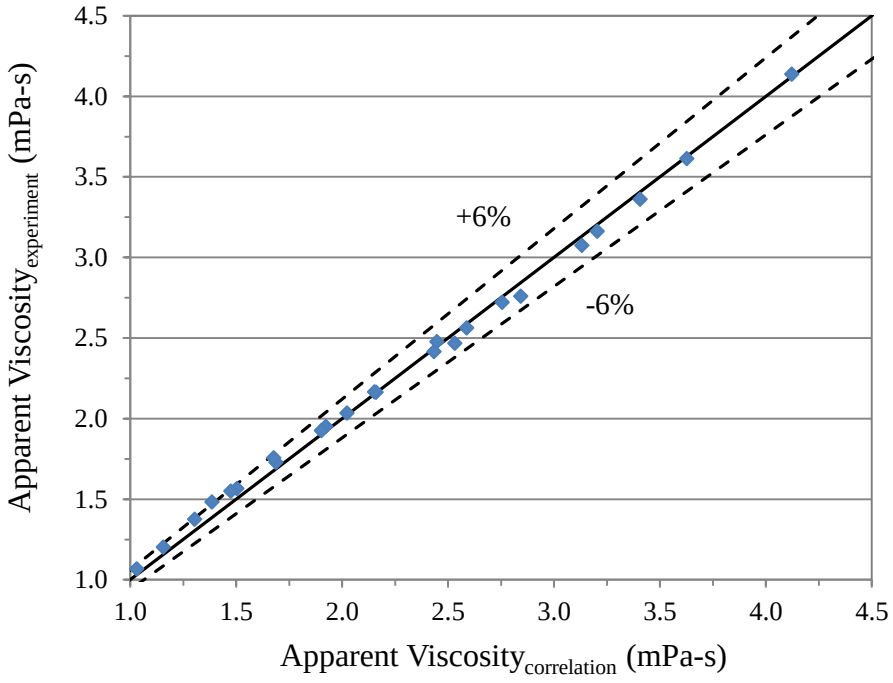

Fig. 8. Comparison of apparent viscosities between the experiment and correlation

Overall, the results show that MPCM slurry behaves as a Newtonian fluid at mass fraction less than 10.9 %, which were observed by previous studies [1, 3, 4, 12]. The experimental results also reveal that as the mass fraction of the MPCM in the slurry increases, the viscosity of the MPCM slurry increases, which is greater than that of water due to increased particle interactions [46, 49]. Thus, it can be inferred that the higher viscosity of MPCM slurry should lead to a reduction in thermal performance efficiency of energy system by increasing pumping power and decreasing momentum transfer under constant fluid velocity condition.

3.3 Durability of MPCM Slurry

Durability of MPCM is critically important for the implementation of MPCM slurry in industrial applications. To ensure that MPCM particles withstand continuous pumping conditions during long-term operations, the durability of the microcapsules should be determined. The durability of MPCM particles can also ensure that all the results obtained from the experiments are reliable and repeatable. Thus, many researchers have conducted durability experiments for long-term applications. Alvarado et al. [1] studied the durability of MPCM particles consisting of tetradecane as a PCM and a gelatin shell. The experimental results with small MPCM particles (2-10 μm) clearly showed no damage after 1200 circulation cycles, even though larger microcapsules were broken after 400 circulation cycles. These results were also observed by Yamagishi et al. [12]. In addition, Roy and Sengupta [8] reported that the

breakage of microcapsules decreased as the ratio of particle diameter to shell thickness decreased.

In this study, microcapsules in the range of 5 to 10 μm in terms of diameter were used and the effective specific heat of the slurries was used to evaluate the durability of MPCM particles [3, 4]. The change in the effective specific heat values during the experiments was investigated and the experimental values were also compared with the theoretical values to evaluate any degradation of effective specific heat of the MPCM slurry during the experiments. The experimental value of effective specific heat of the MPCM slurry was determined using Equation (31). Theoretical values were calculated based on Equation (34), assuming that all the MPCM particles underwent phase change.

$$c_{p,eff\,(theo)} = (1 - MF) \cdot c_{p,w} + MF \cdot c_{p,MPCM} + \frac{MF \cdot \lambda}{\Delta T_{MPCMs}} \tag{34}$$

where MF, $c_{p,w}$, $c_{p,MPCM}$, λ, and ΔT_{MPCMs} are the mass fraction of the MPCM in the slurry, the specific heat of water, the specific heat of MPCM, the latent heat of fusion of the PCM, and the temperature difference between the inlet and outlet slurry temperatures, respectively.

Figure 9 shows the effective specific heat of MPCM slurry as a function of the number of cycles, which was defined as $N_{cycles} = \frac{VF \cdot T}{V_{sys}}$ (where *VF*, *T*, and V_{sys} are volumetric flow rate (l/min), operating time (min) and system volume (l), respectively). The effective specific heat was determined at four different mass fractions of MPCM in the slurry (10.9 %, 8.3 %, 5.9 %, and 2.1 %), as shown in Figs. 9 (a), (b), (c), and (d),

respectively. The effective specific heats for the MPCM slurries were 7.7, 6.4, 5.5, and 4.6 kJ/kg-˚C for each corresponding mass fraction, respectively. The results revealed that effective specific heat remained constant and deviated by less than 1.5 % when compared to the theoretical values. It was found that the MPCM particles with 5 to 10 μm in diameter used in the study resisted continuous pumping condition (2200 circulation cycles) without any degradation of heat transfer performance. This also ensured that all the results obtained from the experiments are reliable and repeatable.

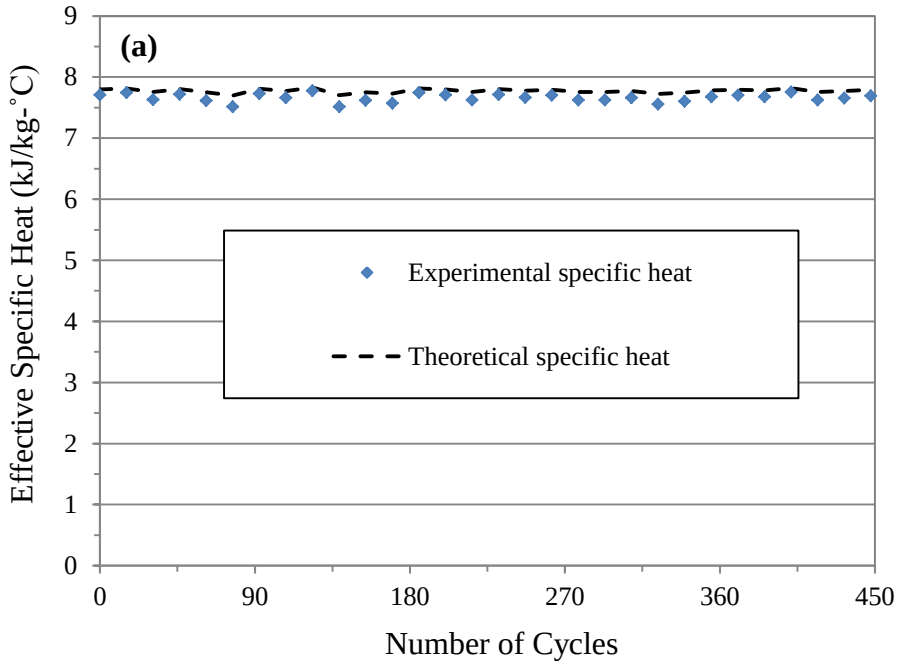

Fig. 9. Effective specific heat of MPCM slurry as a function of the number of cycles at (a) 10.9 % MPCMs, (b) 8.3 % MPCMs, (c) 5.9 % MPCMs, (d) 2.1 % MPCMs

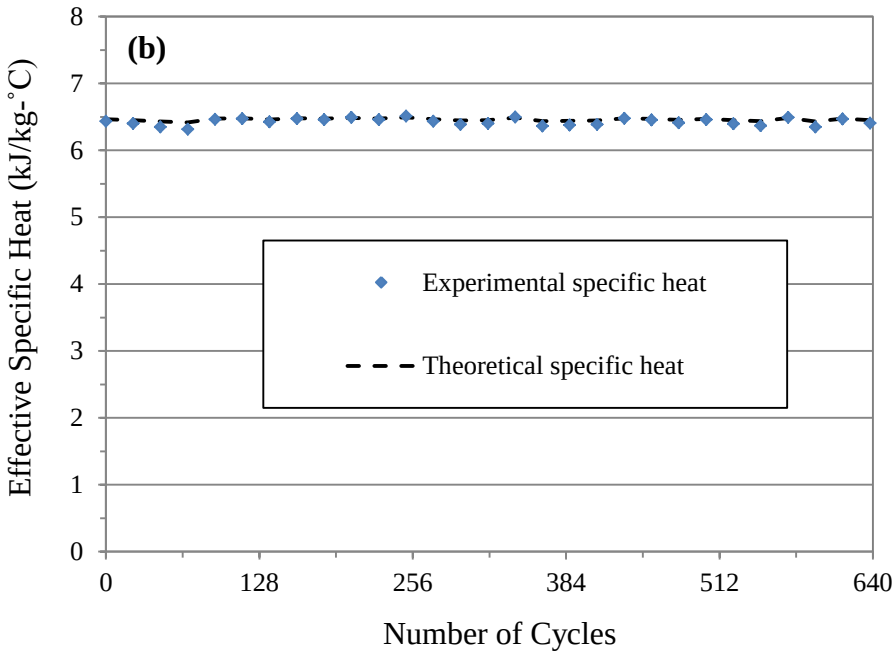

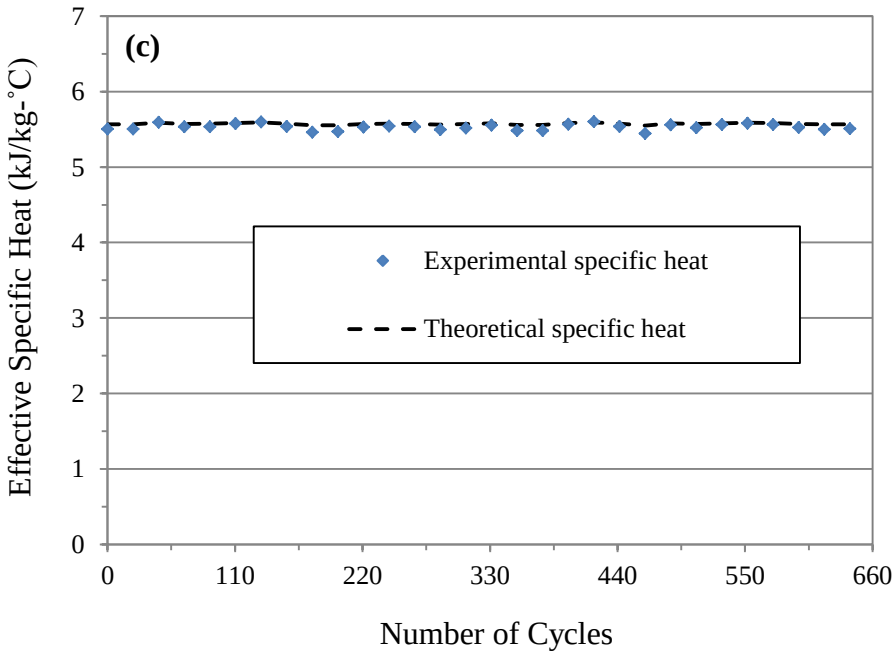

Fig. 9 Continued.

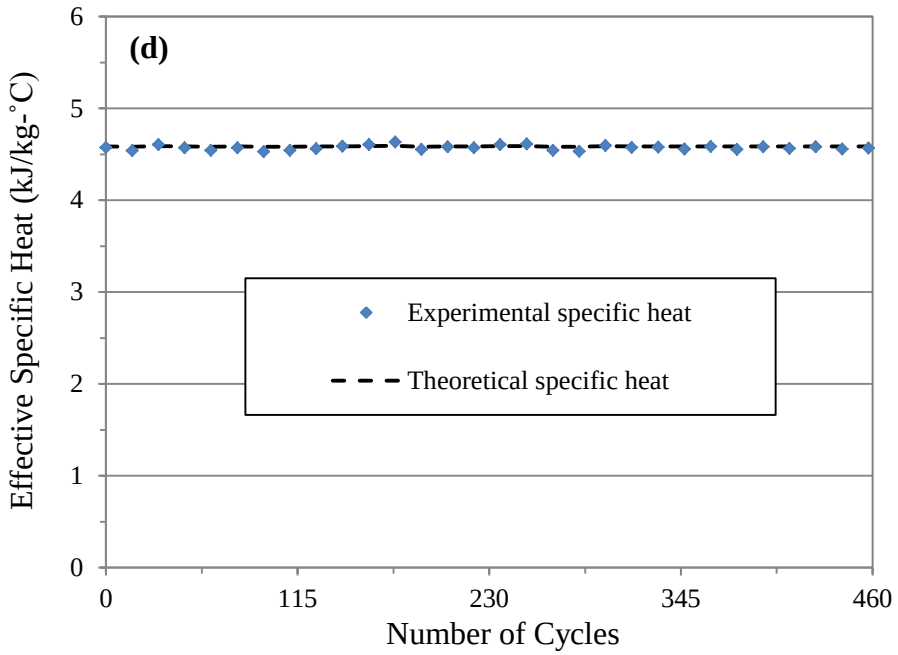

Fig. 9 Continued.

4. DESCRIPTION OF HEAT TRANSFER AND PRESSURE DROP EXPERIMENTAL SYSTEM

4.1 Purpose and Description of Experimental System

An experimental setup was designed and built in order to experimentally determine the pressure drop and heat transfer characteristics of MPCM slurry flowing through a coil heat exchanger. A schematic diagram of the experimental setup is shown in Fig. 10. The experimental setup mainly consisted of two loops for MPCM slurry and cold water. The MPCM slurry loop contained a heat transfer test section, a pressure drop test section, a preheater (PH1), a progressive cavity pump (P1), an electromagnetic flow meter (FM1), a differential pressure transducer (DPT1), and a sampling station (SS1). The cold-water loop consisted of an air-cooled water chiller (CH1), a Coriolis flow meter (FM2), and a coaxial heat exchanger (HX1). The cold water supplied by the air-cooled water chiller (CH1) was circulated through the annulus of the heat exchanger (HX1) to cool the MPCM slurry to ensure complete crystallization of the phase change material. The MPCM slurry delivered by the progressive cavity pump (P1) was circulated through the heat transfer test section where it was fully melted in the section. The heat transfer characteristics of MPCM slurries were investigated for melting conditions only. The MPCM slurry was heated using a preheater (PH1) to maintain constant inlet temperature of the slurry entering the heat transfer test section. A sampling station (SS1) was used to take samples to determine thermophysical properties of

MPCM slurries. The pressure drop test section was used to measure pressure drop of MPCM slurries. All data were read directly from a data logger (DAQ).

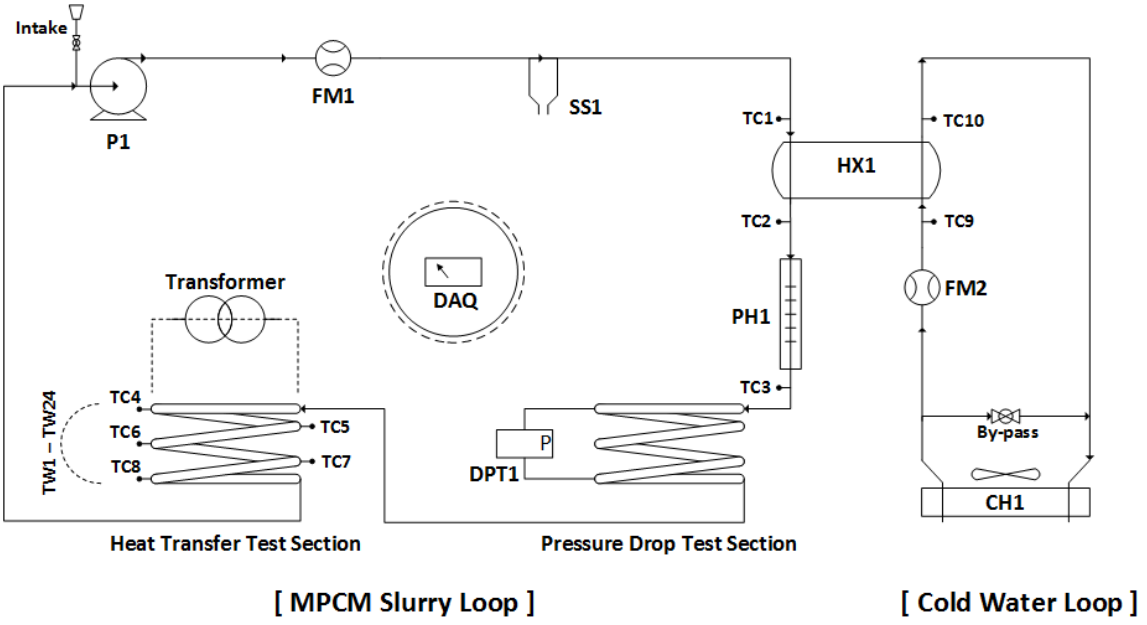

Fig. 10. Schematic diagram of experimental setup

4.2 Description of Heat Transfer Section

Figure 11 shows the instrumented heat transfer test section. A helically two-turn coiled tube was made of a 3/8-inch coiled copper tube (10.2 mm ID) with 2.6 m in length, which consisted of four 0.65 m long subsections. The coil diameter was 0.414 m with a specified curvature ratio (d/D) of 0.025, which is the ratio of a tube diameter (d) to a coil diameter (D). The copper tubing length guaranteed a full phase change transition and a 30 cm long straight tube (10.2 mm ID) was connected before the section to ensure fully developed flow conditions.

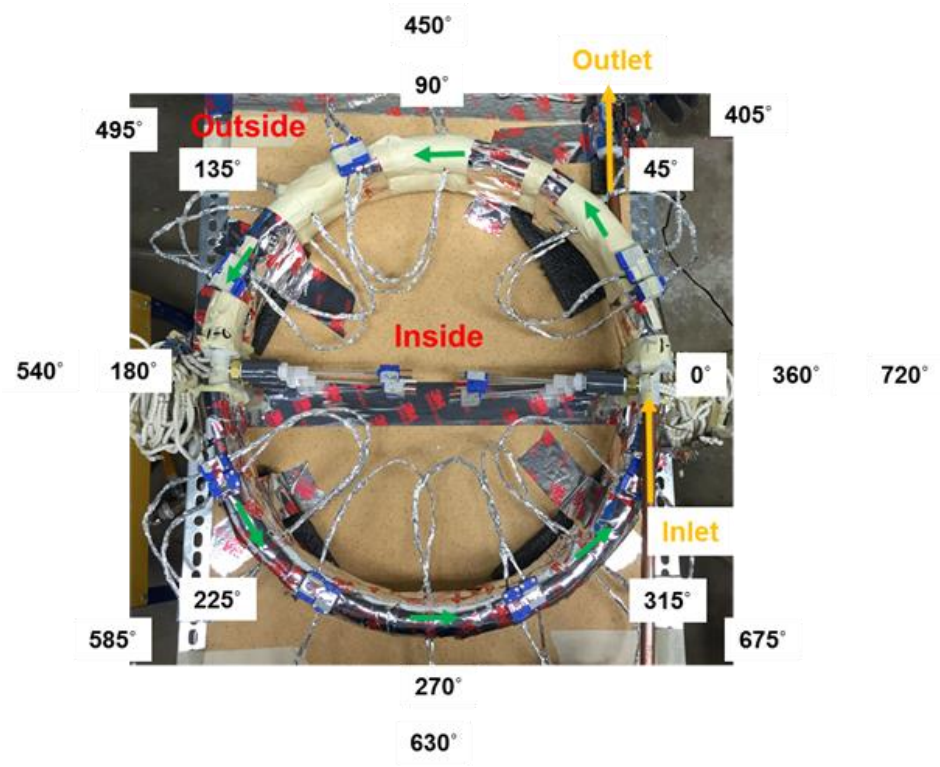

Fig. 11. Heat transfer test section

Each subsection had six T-type thermocouples, which were soldered in grooves cut longitudinally along the tube wall to measure surface temperature at different locations, as shown in Fig. 12. Thermocouple pairs were mounted on the outside and inside of the coiled tube at three different axial locations spaced evenly along the test section. The positions for the wall temperature thermocouples along the coiled tube periphery direction were determined based on the results of preliminary experiments, to determine suitable positions for wall temperature thermocouples by mounting the thermocouples on the inside, outside, top and bottom of the tube periphery at the same axial location. The experimental results showed that the wall temperatures on the top and

bottom of the coiled tube represented the average wall temperature in the periphery direction of the coiled tube. It was also found that the lowest and highest temperatures were observed on the outside and inside of the coiled tube, respectively, which is consistent with previous study [50].

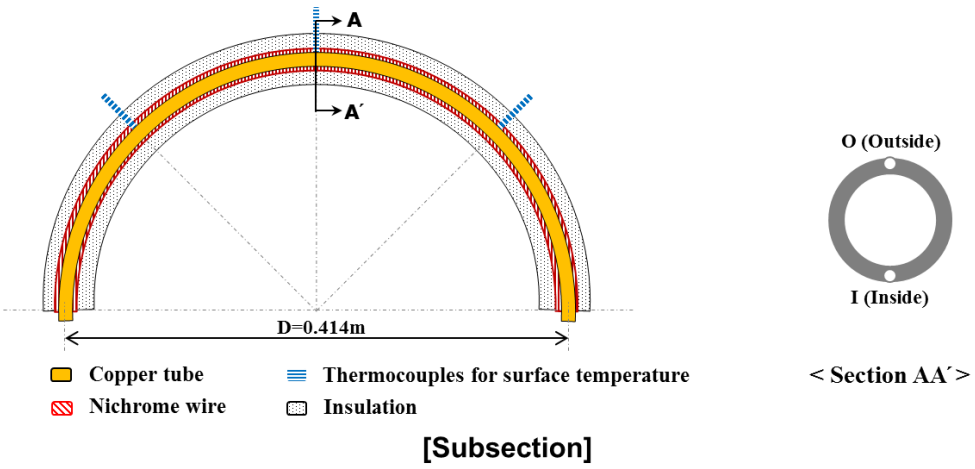

Fig. 12. Schematic of the subsection and thermocouple locations

The subsections were coated with paint to electrically isolate them from the nichrome wires, which were used as heating element. In order to provide constant heat flux, the insulated or coated nichrome wires were wound around the coated tube very evenly. Two independent nichrome wire sections were connected in parallel to a variable voltage transformer in each subsection. In order for each nichrome wire section to provide the same heat flux, the total length of each nichrome wire was adjusted externally. The heat transfer section was wrapped with a fiberglass insulation to minimize heat losses to the environment. Five T-type immersion thermocouples were

located before and after each subsection to measure bulk fluid temperatures. To ensure thermal isolation, PVC connectors were used to mount the thermocouples.

4.3 Description of Pressure Drop Section

A helically two-turn coiled tube was made of a 3/8-inch coiled copper tube (10.2 mm ID) with 2.6 m in length to measure pressure drops, as shown in Fig. 13. The coil diameter was 0.414 m with a curvature ratio (d/D) of 0.025. Pressure tap connectors were placed on the inlet and outlet of the coiled tube to measure pressure drop. To ensure hydraulically fully developed flow, a 30 cm long straight copper tube (10.2 mm ID) was connected before the section. The entire pressure drop section was wrapped with thermal insulation to minimize heat losses to the environment.

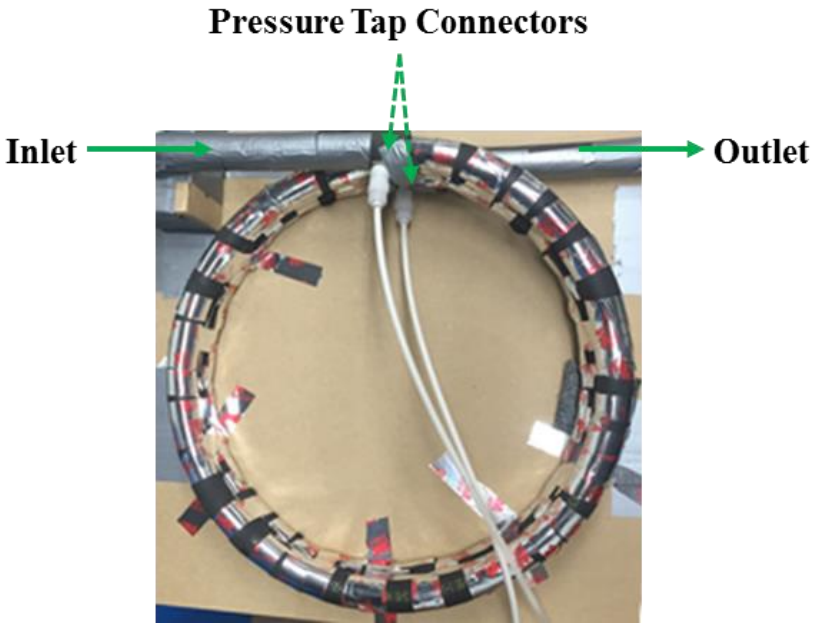

Fig. 13. Pressure drop test section

4.4 Description of Components (Devices and Sensors)

4.4.1 Pump and Air-cooled Water Chiller

A Moyno progressive cavity pump (P1) as shown in Fig. 14 was used to circulate MPCM slurries in the heat transfer loop. This pump has been found to be suitable for viscous slurries without causing damage to the solid particles in the slurry [1, 12]. The capacity of the pump is 18.9 l/min and the maximum operating pressure is 689.5 kPa. An air-cooled water chiller (CH1) was used to circulate the cold water to cool MPCM slurries to ensure complete solidification of the phase change material after melting in the heat transfer loop. The capacity of the chiller is 5 tons and the chiller uses the R22 refrigerant as a cooling medium. Figure 14 shows the air-cooled water chiller used in the experiment.

Fig. 14. Progressive cavity pump (left) and air-cooled water chiller (right)

4.4.2 Heat Exchanger

As shown in Fig. 15, a coil heat exchanger (HX1) manufactured by Turbotec with a capacity of 2.5 tons was used for exchanging heat between the cold water and MPCM slurry to ensure that the phase change material with the MPCM particles fully

crystalized. The outer tube of the heat exchanger was made of carbon steel, while the inner tube of the heat exchanger was made of copper with a corrugated surface to enhance heat transfer. Water and MPCM slurry flowed through the outer and inner tube sides of the heat exchanger, respectively.

Fig. 15. Coil heat exchanger

4.4.3 Flow Measuring Devices

An electromagnetic flow meter (FM1) with an accuracy of ± 0.5 %, manufactured by Omega, was used to measure flow rate of the MPCM slurries flowing through the heat transfer loop. The electromagnetic flow meter basically measures volumetric flow rates of electrically conductive materials on the basis of Faraday's Law of electromagnetic induction. The electromagnetic flow meter is suitable for measurement of flow of slurries without compromising the accuracy of the measurement [1, 4]. The full scale of the flow meter is 94.6 l/min with an output of 4 to 20 mA. A Coriolis flow meter (FM2) from Endress+Hauser Promass was also used to measure the

flow rate of cold water. The Coriolis flow meter measures the mass flow rate by using Coriolis force generated in oscillating systems. The Coriolis force can cause a slight distortion of the measuring tube and is directly proportional to mass flow rate. The Coriolis flow meter used can measure the flow rate ranging from 0 to 31.753 kg/min with an accuracy of ± 0.1 %. The two flow meters used in the experiments are shown in Fig. 16.

Fig. 16. Electromagnetic flow meter (left) and Coriolis flow meter (right)

4.4.4 Thermocouples

Immersion type thermocouples (T-type) were used to measure fluid temperatures and the T-type thermocouple wires installed on the surface of the coiled tube were used to measure tube wall temperatures. The thermocouples were manufactured by Omega and their accuracy is ± 0.4 %. All the thermocouples were calibrated by using water as a heat transfer fluid under isothermal conditions throughout the entire experimental system.

4.4.5 Differential Pressure Transducer

A Rosemount differential pressure transducer (DPT1) was used to measure pressure difference of MPCM slurry flowing through the pressure drop test section. The pressure transducer can measure the pressure difference ranged from 0 to 344.8 kPa with ± 0.04 % accuracy of the full range.

4.4.6 Variable Transformers and Power Meter

Two Staco variable voltage transformers were used to provide voltage to the nichrome heating wires to set constant heat flux conditions. The variable transformers were selected to provide variable output voltage that could be adjusted from 0 to 117 % of the input voltage. It could operate on 240 V input and the output voltage ranged from 0 to 280 V. The allowable power was 6.7 kVA and maximum current was 28 Amps. Two voltage transformers provided voltage to the heat transfer section and the preheater, respectively. A Fluke power meter was used to measure voltage and current, which were used to determine the electrical power delivered to each subsection.

4.4.7 Data Acquisition Unit

An Agilent data acquisition unit was used to record data from thermocouples, pressure transducer and flow meters. The data logger (34970A) with two 20-channel multiplexers was used. The Agilent Bench Link Data Logger software was used to control the data logger through a 34970A unit to record all the data.

5. CHARACTERIZATION OF PRESSURE DROP AND HEAT TRANSFER OF MICROENCAPSULATED PHASE CHANGE MATERIAL SLURRY

The flow and heat transfer characteristics of fluids strongly depend on the flow regime, laminar flow or turbulent flow. In general, the transition in the coil heat exchanger occurs at a higher Reynolds number than in the straight tube due to the presence of a secondary flows, which stabilize the flow pattern and attenuate velocity fluctuations. Correlations [26, 27] were used to estimate the critical Reynolds number to determine flow conditions for turbulent flow in this study. Figure 17 shows the critical Reynolds number as a function of curvature ratio. As a result, the critical Reynolds number for the coil with a curvature ratio of 0.025 used in this study is about 6000. The Reynolds number range of the experiments was from 6000 to 25000; therefore, the flow regime was mainly turbulent.

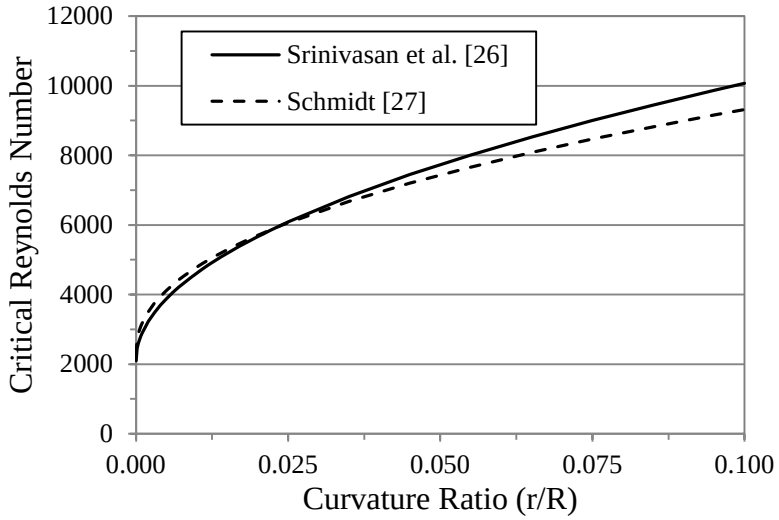

Fig. 17. Critical Reynolds number as a function of curvature ratio

5.1 Validation of Experiments

5.1.1 Pressure Drop Measurements

In order to validate the pressure drop measurement, the pressure drop of water flowing through a test section was measured using a differential pressure transducer. The fluid velocity varied from 0.7 to 2.9 m/s, with an equivalent Reynolds number range of 6500 to 27000, and the fluid temperature was maintained at 16.5 ˚C. All pressure drop data were recorded with an Agilent data logger when the water temperature and flow rate reached steady state conditions. Uncertainty propagation analysis was carried out using the multivariate error formula described in NIST Technical Note 1297 [51]. The experimental uncertainty in determining the associated friction factor was ± 6.4 %.

Figure 18(a) shows the pressure drop of water as a function of fluid velocity. The results clearly showed that pressure drop increases with fluid velocity. As shown in Fig. 18(b), the pressure drop results are expressed in terms of a Fanning friction factor, which is defined as:

$$f = \frac{d \cdot \Delta P}{2 \cdot \rho \cdot L \cdot u^2} \tag{35}$$

where ρ, d, L, and u are the fluid density, tube diameter, tube length , and fluid mean velocity, respectively.

The friction factor curves shown in Fig. 18(b) decreased with Dean number, which is the product of the Reynolds number and the square root of the curvature ratio (d/D). To validate the pressure drop measurements, the friction factor values from the present experiments were compared with the correlations from Srinivasan et al. [26] presented in

Equation (17) and Mishra and Gupta [29] shown in Equation (12). It was found that the present results are in good agreement with the previous results and deviate within 7 %.

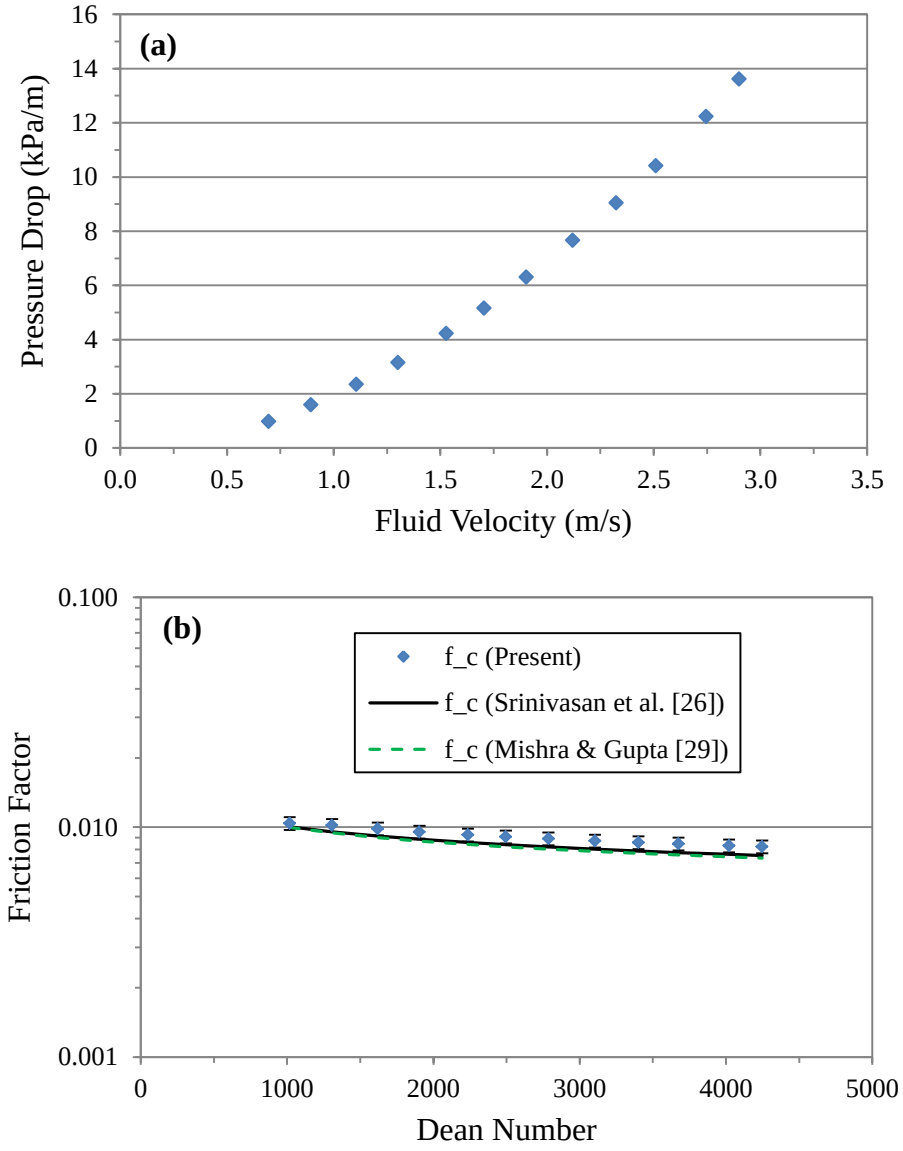

Fig. 18. (a) Pressure drop of water as a function of fluid velocity; (b) Friction factor as a function of Dean number

A multiple regression analysis was performed to postulate a correlation capable of predicting friction factor for water. The correlation is based on Dean number (De) and it is applicable for a coiled tube with a curvature ratio (r/R) of 0.025, as follows:

$$f_c = 0.035\mathrm{De}^{-0.17} \quad \left(R^2 = 0.99\right) \tag{36}$$

where $1000 \le \mathrm{De} \le 4000$

As shown in Fig. 19, the friction factor values calculated by the correlation (36) are compared with those of the experiments. The values of the correlation fit well with the experimental values and deviate by less than ± 1.5 %.

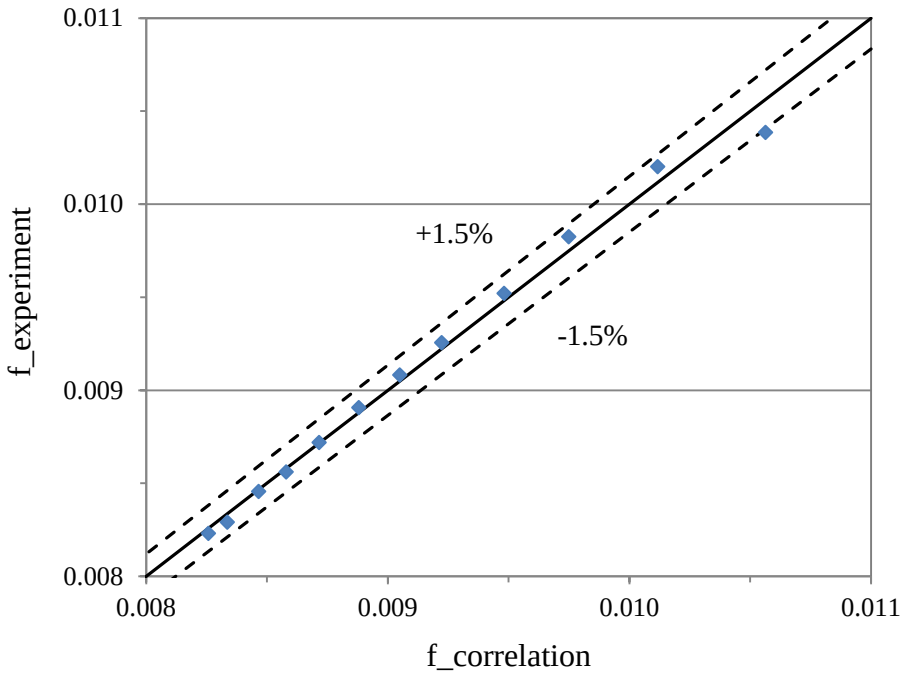

Fig. 19. Comparison of friction factors between the experiment and correlation

Overall, pressure drop results fitted well with the results calculated using previous correlations [26, 29], which indicate that pressure drop measurement using the present experimental setup is reliable and applicable for MPCM slurry.

5.1.2 Heat Transfer Measurements

For the validation of the heat transfer coefficient measurements, heat transfer experiments with water were conducted using an instrumented two-turn coiled tube and all the data were collected using a data acquisition system. The amount of power was measured to determine wall heat flux as boundary condition. The heat transfer coefficients were calculated using the following equation:

$$h = \frac{q''}{(T_w - T_b)} \tag{37}$$

where q'', T_w, and T_b are the wall heat flux, wall surface temperature, and bulk fluid temperature, respectively.

Nusselt numbers were determined using the following equation:

$$\mathrm{Nu} = \frac{h \cdot d}{k} \tag{38}$$

where d is the tube diameter and k is the fluid thermal conductivity determined at the fluid bulk temperature.

Heat transfer experiments were conducted using water as a heat transfer fluid at two different wall heat flux conditions (35.8 kW/m^2 and 25.4 kW/m^2). The fluid velocity varied from 0.7 to 2.5 m/s (equivalent Reynolds number range of 7500 to 24500). The

data were collected once all the physical variables reached steady state values. Uncertainty propagation analysis revealed that the experimental uncertainty for calculating Nusselt number was ± 3.1 %.

Figure 20 shows fluid bulk temperature as a function of angle from the start of the coil under constant heat flux (35.8 kW/m^2) condition. Experimental results clearly show that fluid bulk temperature linearly increases along the coil and the temperature gradient decreases with fluid velocity, as well as Reynolds number.

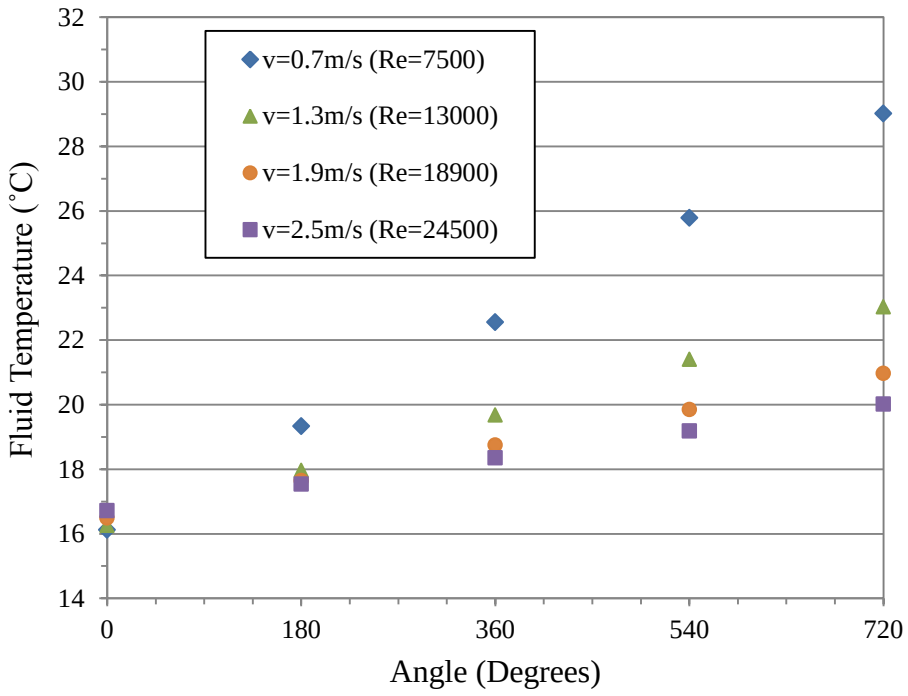

Fig. 20. Fluid temperature as a function of angle

Figure 21 shows variation of dimensionless wall temperature along the coil. The wall dimensionless temperature is defined as follows:

$$\theta_w = \frac{\left(T_w - T_{b,i}\right)}{\left(T_{b,o} - T_{b,i}\right)} \tag{39}$$

where T_w, $T_{b,i}$, and $T_{b,o}$ are the wall temperature, the inlet fluid temperature, and the outlet fluid temperature, respectively. The experimental uncertainty in determining the associated dimensionless wall temperature was ± 2.8 %.

Dimensionless wall temperatures on the inside ($\theta_{w,i}$) and the outside ($\theta_{w,o}$) of the tube were calculated using wall temperatures on the inside ($T_{w,i}$) and the outside ($T_{w,o}$) of the tube, respectively. Average dimensionless wall temperature (θ_w) was determined by averaging $\theta_{w,i}$ and $\theta_{w,o}$. The experimental results show that all the dimensionless wall temperatures linearly increase with angle from the start of the coil. As fluid velocity (Reynolds number) increases, the average dimensionless wall temperature (θ_w) increases because of greater momentum transfer within the coil [50]. The dimensionless wall temperature on the outside of the tube wall ($\theta_{w,o}$) is always lower than that on the inside of the tube wall ($\theta_{w,i}$) under constant fluid velocity condition, which can be attributed to the maximum fluid velocity being shifted towards the outside of the tube due to the centrifugal force effect of the coil. In addition, formation of the secondary flows could also play a role in the distribution of peripheral temperature.

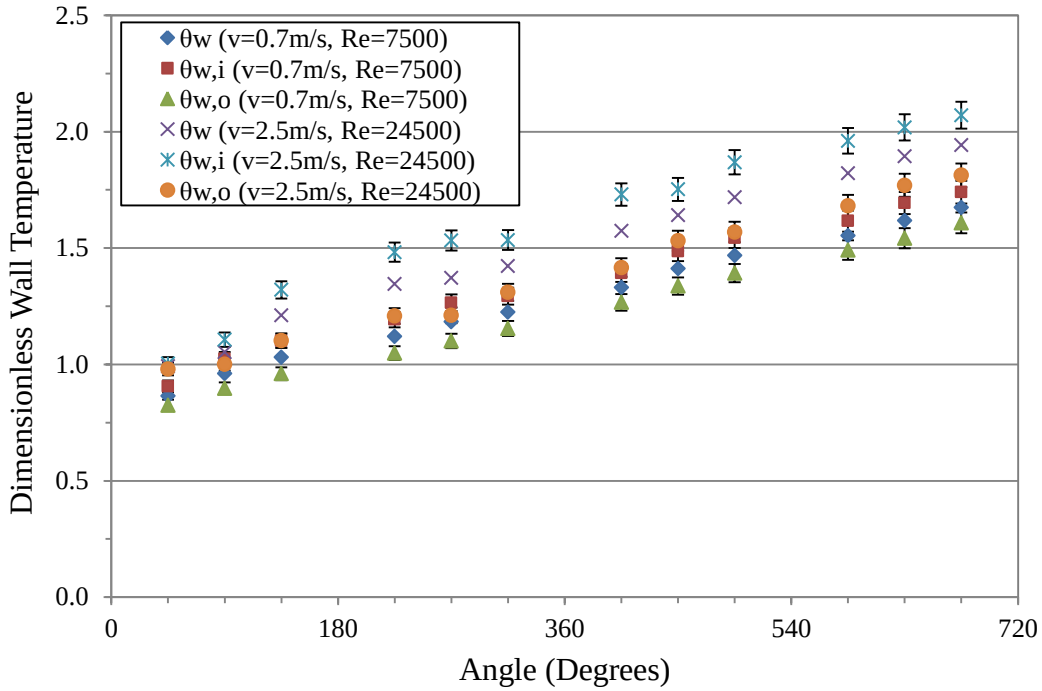

Fig. 21. Dimensionless wall temperature as a function of angle

Figure 22 shows Nusselt number as a function of Reynolds number. The values of Nusselt number are compared with the results calculated using the correlations of Seban and McLaughlin [31] and Mori and Nakayama [36]. The results show that Nusselt numbers increased with Reynolds number due to increased momentum transfer, while heat flux variations have no effect on Nusselt number. Also, the values of Nusselt numbers agree well with those from previous correlations and deviate within 3.5 %.

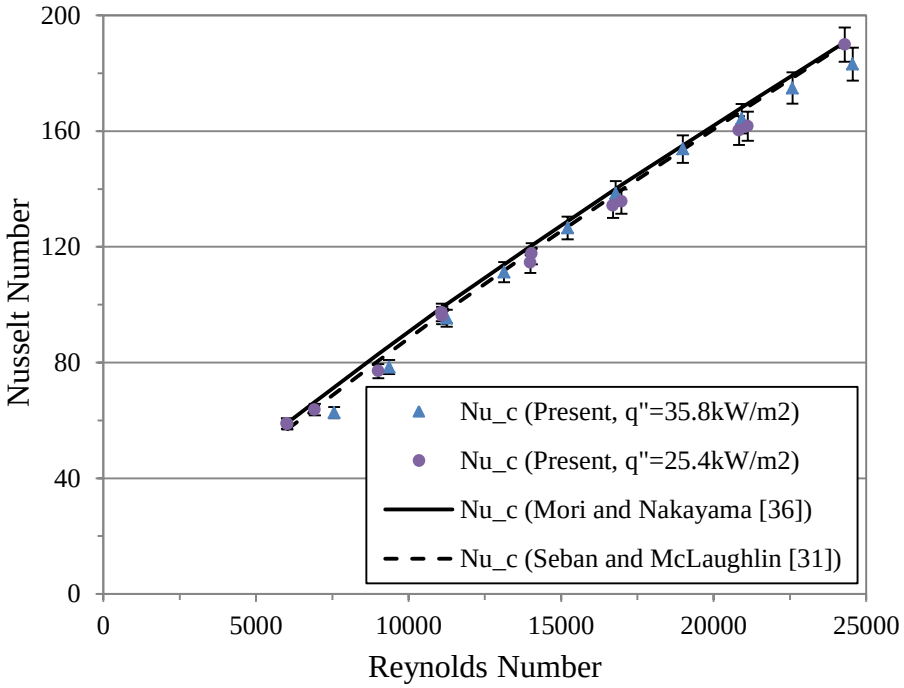

Fig. 22. Comparison of Nusselt numbers

A multiple regression analysis was performed to formulate a correlation capable of predicting Nusselt number for water flowing through the coiled tube with a curvature ratio (r/R) of 0.025. The correlation is based on the Reynolds (Re) and Prandtl (Pr) numbers, as follows:

$$\mathrm{Nu_c} = 0.02\,\mathrm{Re}^{0.84}\,\mathrm{Pr}^{0.4} \qquad \left(R^2 = 0.99\right) \tag{40}$$

where $7500 \le \mathrm{Re} \le 24500$

$6.7 \le \mathrm{Pr} \le 7.6$

As shown in Fig. 23, the Nusselt number values of the correlation (40) are compared with those of the experiments. The values of the correlation are in good agreement with the experimental values and deviate by less than ± 4 %. From the correlation, it is clear

that the Nusselt number increases with Reynolds number and Prandtl number. It is also clear that Reynolds number plays a more significant role in increasing the magnitude of Nusselt number rather than Prandtl number, which is indicative of the effect of fluid momentum, bulk motion, on heat transfer.

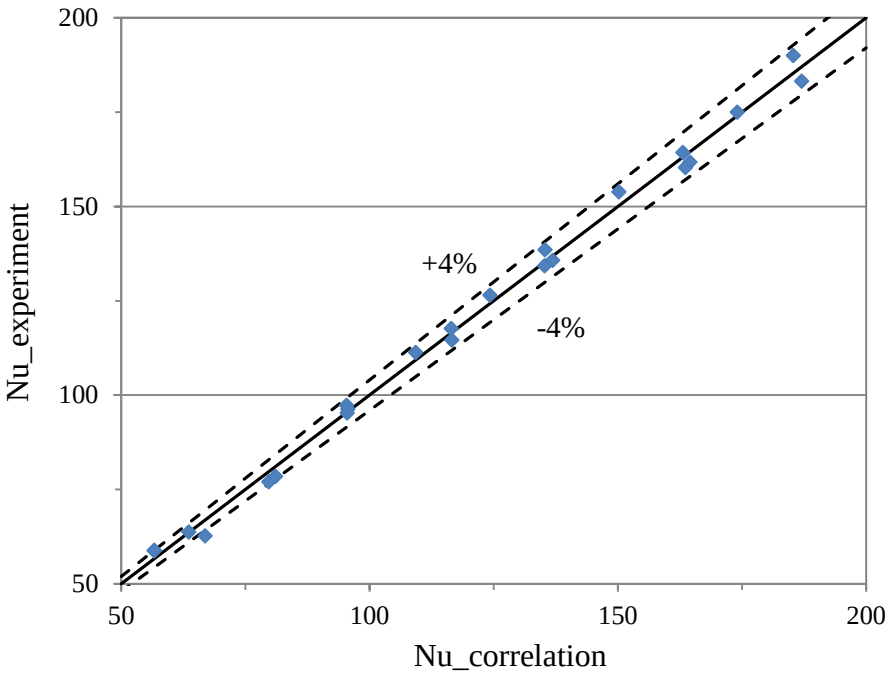

Fig. 23. Comparison of Nusselt numbers between the experiment and correlation

Overall, Nusselt number values obtained from the experiments were in good agreement with the results calculated using previous correlations, which indicate that heat transfer coefficient measurements using the present experimental setup is reliable and applicable for MPCM slurry.

5.2 Experiments with MPCM Slurry

5.2.1 Pressure Drop Measurements

The pressure drop experiments were conducted to determine the pressure drop of MPCM slurry at four different mass fractions. The pressure drop of MPCM slurry flowing through the pressure drop test section shown in Fig. 10 was measured, when the slurry reached steady-state conditions in terms of temperature and flow rate. The test conditions for the pressure drop experiments are shown in Table 5.

Table 5. Test conditions for the pressure drop experiments

Fluid	Fluid Velocity	Reynolds Number	Fluid Temperature
2.1 % MPCM slurry	1.9 – 2.9 m/s	13000 – 19600	16.5 ˚C
5.9 % MPCM slurry	1.9 – 2.9 m/s	9300 – 14000	16.5 ˚C
8.3 % MPCM slurry	1.9 – 2.9 m/s	7300 – 11000	16.5 ˚C
10.9 % MPCM slurry	1.9 – 2.9 m/s	6000 – 8500	16.5 ˚C 20.5 ˚C

Figure 24 shows the pressure drop of 10.9 % MPCM slurry at different slurry temperatures as a function of fluid velocity to determine the effect of PCM's states on the pressure drop. When the slurry temperatures are set at 16.5 ˚C and 20.5 ˚C, the PCM is expected to be at solid state and liquid state, respectively. The results showed that the difference of the pressure drop is small and negligible. This could be attributed to the

shell material, which was always in contact with the carrier fluid and other particles [9] regardless of the phase change process taking place within each microcapsule.

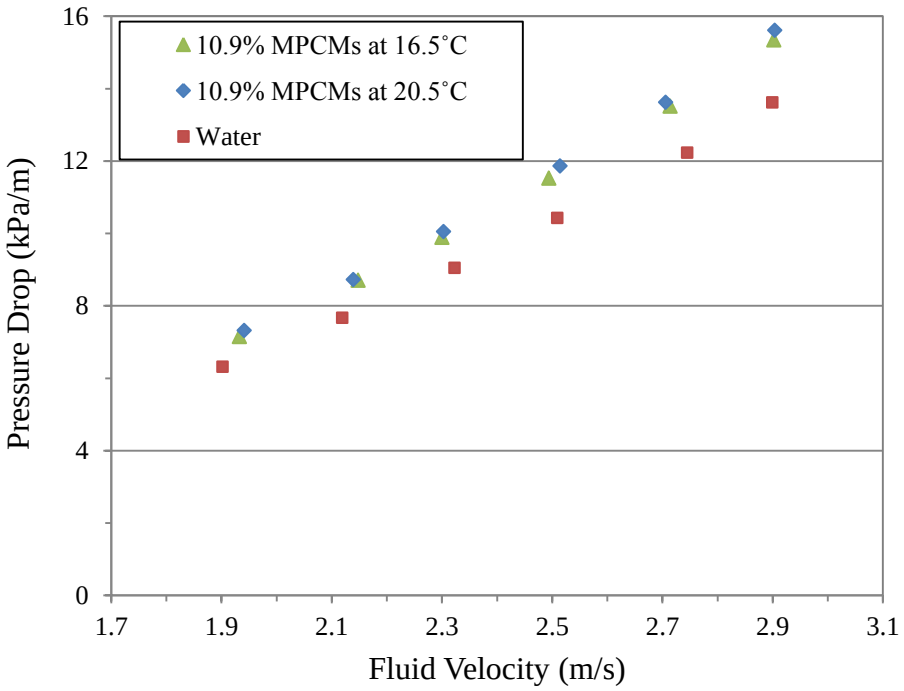

Fig. 24. Pressure drop of 10.9 % MPCM slurry as a function of fluid velocity

Figure 25 shows the pressure drop of MPCM slurry as a function of fluid velocity. The results showed that increasing the mass fraction of MPCM in the slurry and the fluid velocity results in increased pressure drop. The pressure drop of MPCM slurry was greater than that of water by up to 16 % due to increased viscosity. However, it was observed that pressure drop increased slightly with MPCM slurry, even though the viscosity was about 1.3 to 3.2 times higher than for water as shown in Fig. 5. These

phenomena might suggest the presence of a drag reduction effect between the MPCM slurry and the inner surfaces of the coiled tube as reported in earlier studies [1, 3, 12].

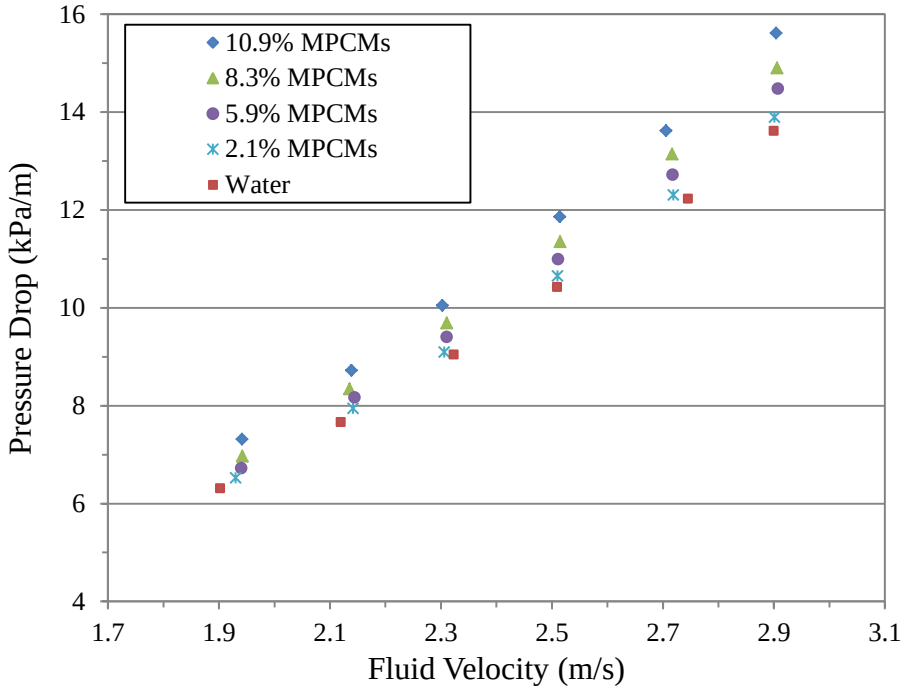

Fig. 25. Pressure drop of MPCM slurry as a function of fluid velocity

Figure 26 shows the friction factor of MPCM slurry as a function of Dean number. The experimental results show that the friction factor of the MPCM slurry decreases with Dean number. The friction factor of the MPCM slurry fits well with the friction factor calculated using previous correlation [26] for turbulent flow of homogeneous Newtonian fluid. This suggests that MPCM slurries can be considered as homogeneous Newtonian fluids. This characteristic of MPCM slurry was also observed in straight test section studies [9, 12].

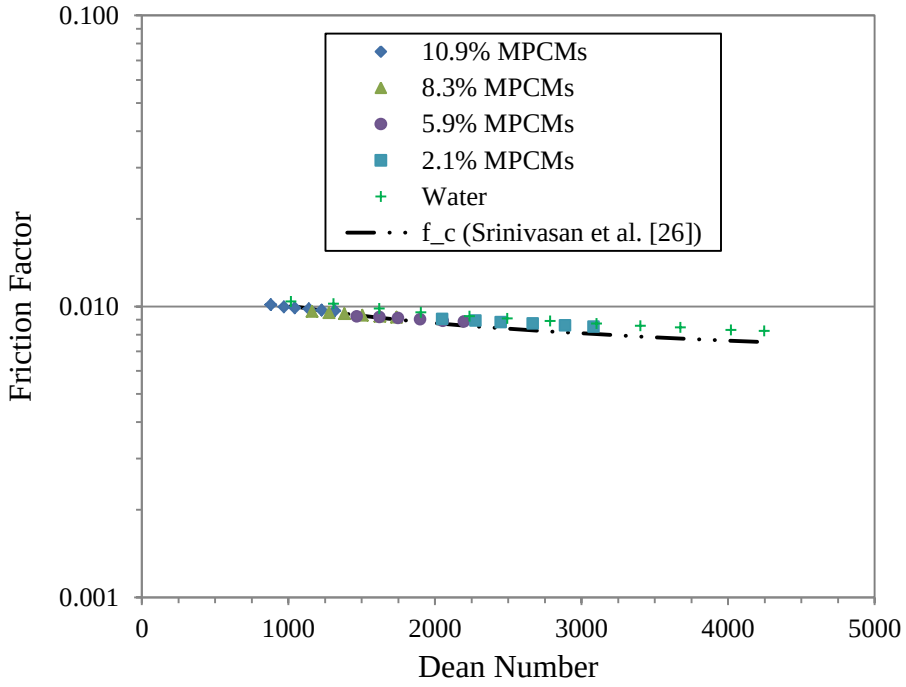

Fig. 26. Friction factor of MPCM slurry as a function of Dean number

A multiple regression analysis was performed to postulate a correlation for predicting friction factor of MPCM slurry as a function of Dean number. This correlation is applicable for a coiled tube with a curvature ratio (r/R) of 0.025.

$$f_c = 0.02\mathrm{De}^{-0.13} \quad \left(R^2 = 0.88\right) \tag{41}$$

where $1000 < \mathrm{De} < 4000$

As shown in Fig. 27, the friction factor values calculated by the correlation (41) are compared with those of the experiments. The values of the correlation fit well with the experimental values and deviate by less than ± 5 %. From the correlation, it is clear that the friction factor decreases with Dean number.

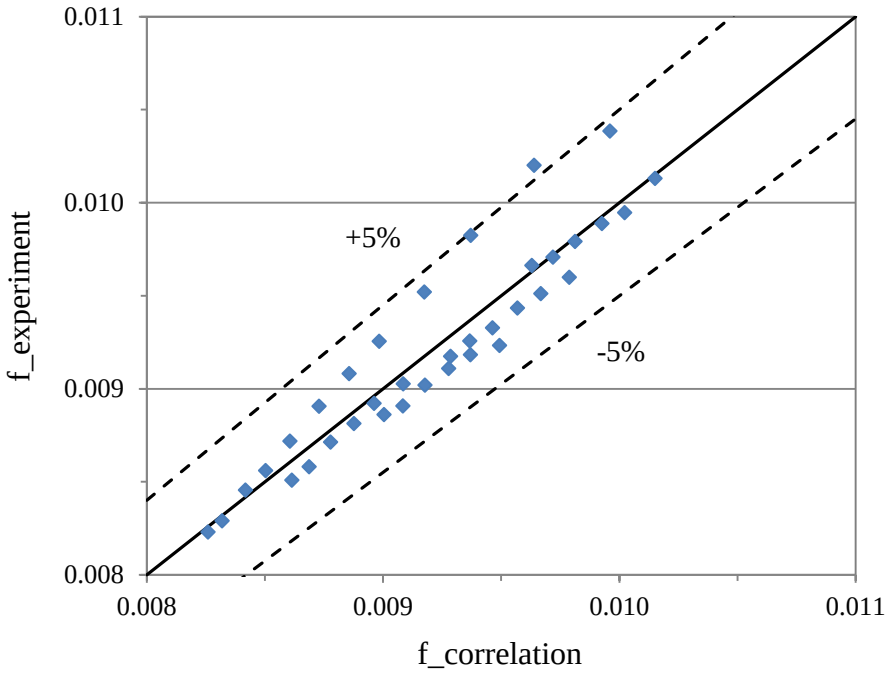

Fig. 27. Comparison of friction factor values between the experiment and correlation

Friction factor of MPCM slurry as a function of fluid velocity is shown in Fig. 28. Experimental results show that the friction factor decreases with fluid velocity. As the concentration of MPCM in the slurry increases at a constant fluid velocity, the friction factor values increases due to increased viscosity. It was found that more pumping power is needed to circulate the MPCM slurry when compared with water at a constant velocity (i.e. higher pressure drop when using MPCM).

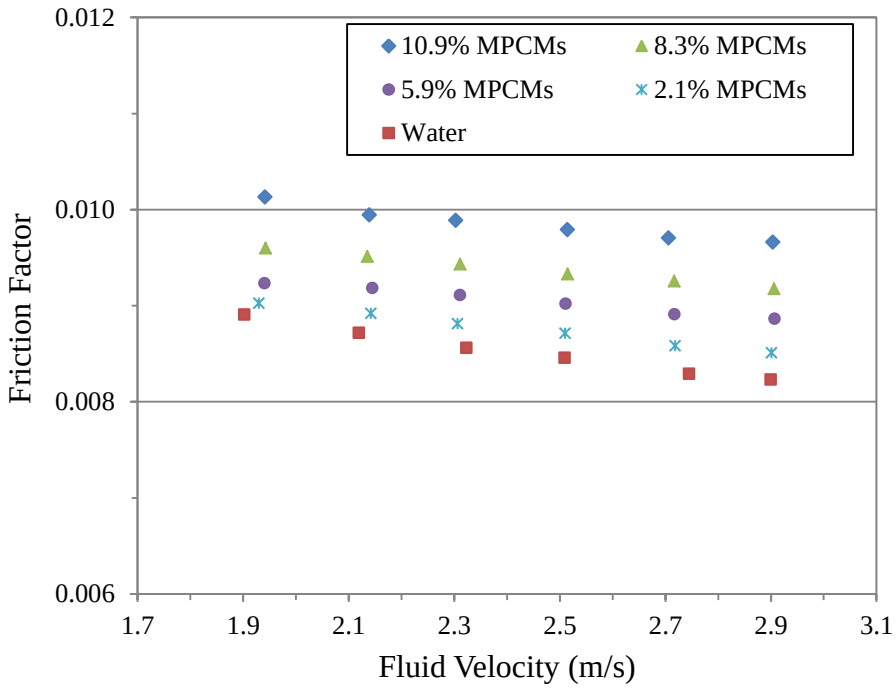

Fig. 28. Friction factor of MPCM slurry as a function of fluid velocity

In summary, pressure drop of MPCM slurry flowing through a CHX was higher than water at constant flow conditions and increased with mass fraction of MPCM in the slurry due to increased viscosity. The friction factor curve of MPCM slurry as a function of Dean number fitted well with previous correlation [26] used for homogeneous Newtonian fluids. The use of MPCM slurry always led to increased pressure drop (pumping power), which can negatively affect the energy efficiency of the thermal energy system.

5.2.2 Heat Transfer Coefficient Measurements

Heat transfer experiments were conducted to determine the convective heat transfer coefficient of MPCM slurry at four different mass fractions. Test conditions are shown in Table 6. The heat transfer characteristics of the MPCM slurry flowing through CHX were investigated for melting conditions only. To investigate the effects of MPCM particles, additional heat transfer experiments were conducted without a phase change of the PCM by setting the inlet temperature (20.5 ˚C) of MPCM slurry, which is greater than the melting temperature (17.4 ˚C) of the PCM. All the data were recorded when the slurry reached steady-state conditions in terms of temperature and flow rate.

Table 6. Test conditions for the heat transfer experiments

Fluid	Fluid Velocity (Reynolds Number)	Inlet Fluid Temperature	Heat Flux
Water	0.7 – 2.9 m/s (7500 – 24500)	16.5 ˚C	36 kW/m^2 25 kW/m^2
2.1 % MPCM slurry	1.9 – 2.9 m/s (14000 – 20500)	16.5 ˚C 20.5 ˚C	46 kW/m^2 28 kW/m^2
5.9 % MPCM slurry	1.9 – 2.9 m/s (9900 – 14500)	16.5 ˚C 20.5 ˚C	46 kW/m^2 37 kW/m^2
8.3 % MPCM slurry	1.9 – 2.9 m/s (7800 – 11400)	16.5 ˚C 20.5 ˚C	46 kW/m^2 42 kW/m^2
10.9 % MPCM slurry	1.9 – 2.9 m/s (5900 – 8700)	16.5 ˚C 20.5 ˚C	46 kW/m^2

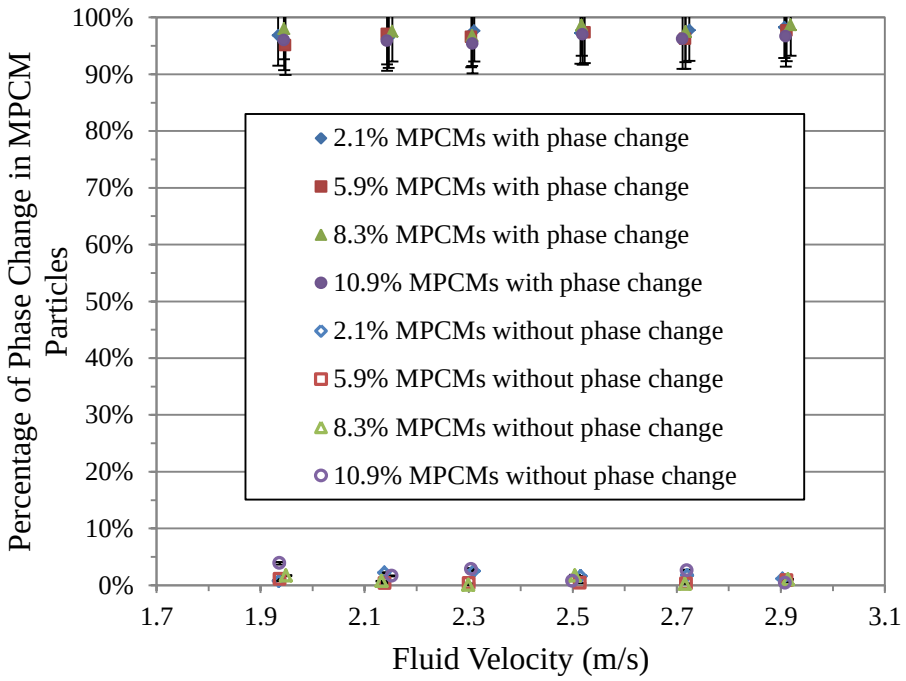

Fig. 29. Percentage of MPCM particles undergoing phase change

Determining the percentage of MPCM particles (ϕ) that underwent phase change is important in the heat transfer experiments with MPCM slurry to investigate the effects of the latent heat of fusion of the PCM on heat transfer characteristics. Energy balance calculations were performed using Equation (42).

$$\dot{Q} = \dot{m}_{MPCMs} \cdot \Delta T_{MPCMs} \left[(1 - MF) \cdot c_{p,w} + MF \cdot c_{p,PCM} \right] + \phi \cdot \dot{m}_{MPCMs} \cdot MF \cdot \lambda_{PCM} \qquad (42)$$

where $\dot{m}_{MPCMs}$, ΔT_{MPCMs}, MF, and λ_{PCM} are the mass flow rate of MPCM slurry, the fluid temperature difference of MPCM slurry, the mass fraction of MPCM in the slurry, and the latent heat of fusion of the PCM, respectively. $c_{p,w}$ is the specific heat of water

and $c_{p,PCM}$ is the specific heat of the PCM. The experimental uncertainty for calculating ϕ was ± 5.5 %.

Figure 29 shows the percentages of MPCM particles that underwent phase change, which were in the range of 95 to 98 % for the experiments with phase change of the PCM and 0 to 3.9 % for the experiments without phase change of the PCM.

Figure 30 shows fluid temperature profiles of MPCM slurries at mass fractions of 5.9 % and 10.9 % for several fluid velocities, which varied from 1.9 m/s to 2.9 m/s under constant heat flux (46 kW/m^2) condition. When fluid temperature reached the melting temperature (17.4 ˚C) of the phase change material (PCM), the temperature gradient decreased due to the phase change process of the PCM from solid to liquid. After complete phase change of the PCM, the temperature gradient increased. Theoretically, the slurry temperature should be constant during the phase change process but there was a slight temperature gradient in the experiments. This was because not all the MPCM particles underwent phase change at the same time [1, 12, 52]. The melting process of MPCM particles flowing through the coil was as follows: 1) MPCM particles near the wall underwent phase change by absorbing heat from the tube wall; 2) MPCM slurry near the wall transferred heat to the slurry in the core of the tube through fluid mixing due to turbulence and secondary flows; 3) as the slurry temperature increased, MPCM particles in the core of the tube underwent phase change. Since secondary flow in a CHX can redistribute fluid elements in a radial direction, it can improve the phase change process of the MPCM particles when compared to a straight tube case, where isotropic turbulence in the dominant transport mechanism.

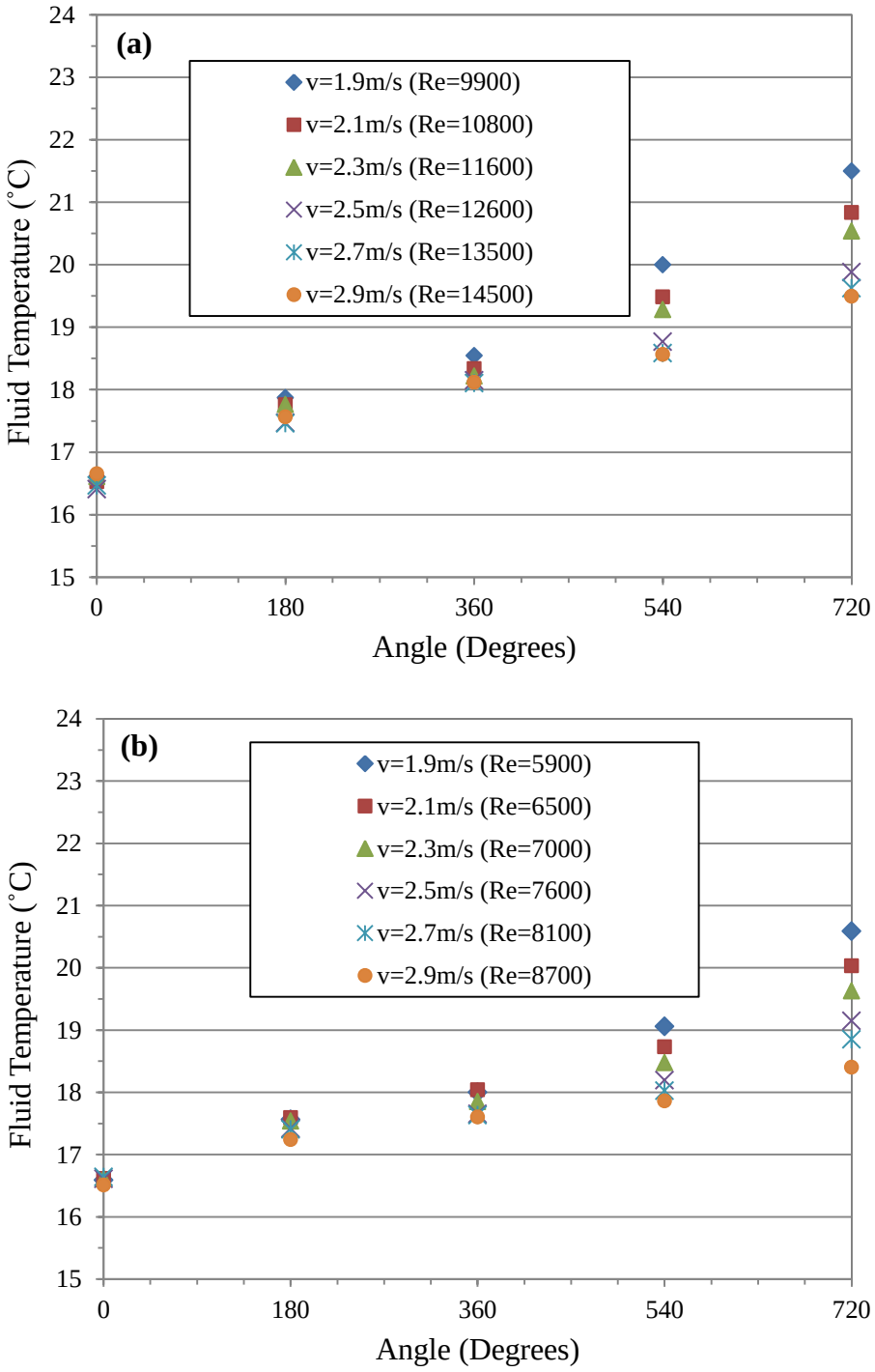

Fig. 30. Fluid temperature profile of MPCM slurry along the coiled tube at (a) 5.9 % MPCMs, (b) 10.9 % MPCMs

Figure 31 shows dimensionless wall temperatures for 5.9 % and 10.9 % MPCM slurries, which were determined using Equation (39). Average dimensionless wall temperatures (θ_w) for 5.9 % and 10.9 % MPCM slurries are shown in Figs. 31 (a) and (b), respectively. The figure shows that as fluid velocity increases, the dimensionless wall temperature increases due to greater momentum transfer [50]. The experimental results also show that the gradient of the dimensionless wall temperature changes during phase change process [9, 10], which mainly takes place in the test section between 180 and 360 degrees. Dimensionless wall temperatures on the inside ($\theta_{w,i}$) and the outside ($\theta_{w,o}$) of the tube for 5.9 % and 10.9 % MPCM slurries at two different fluid velocity conditions are shown in Figs. 32 (a) and (b), respectively. The experiment results show that the dimensionless wall temperature on the outside of the tube wall is always lower than that on the inside of the tube wall. This can be attributed to the centrifugal force induced by the tube curvature, which tends to shift the maximum axial fluid velocity toward the outside of the tube.

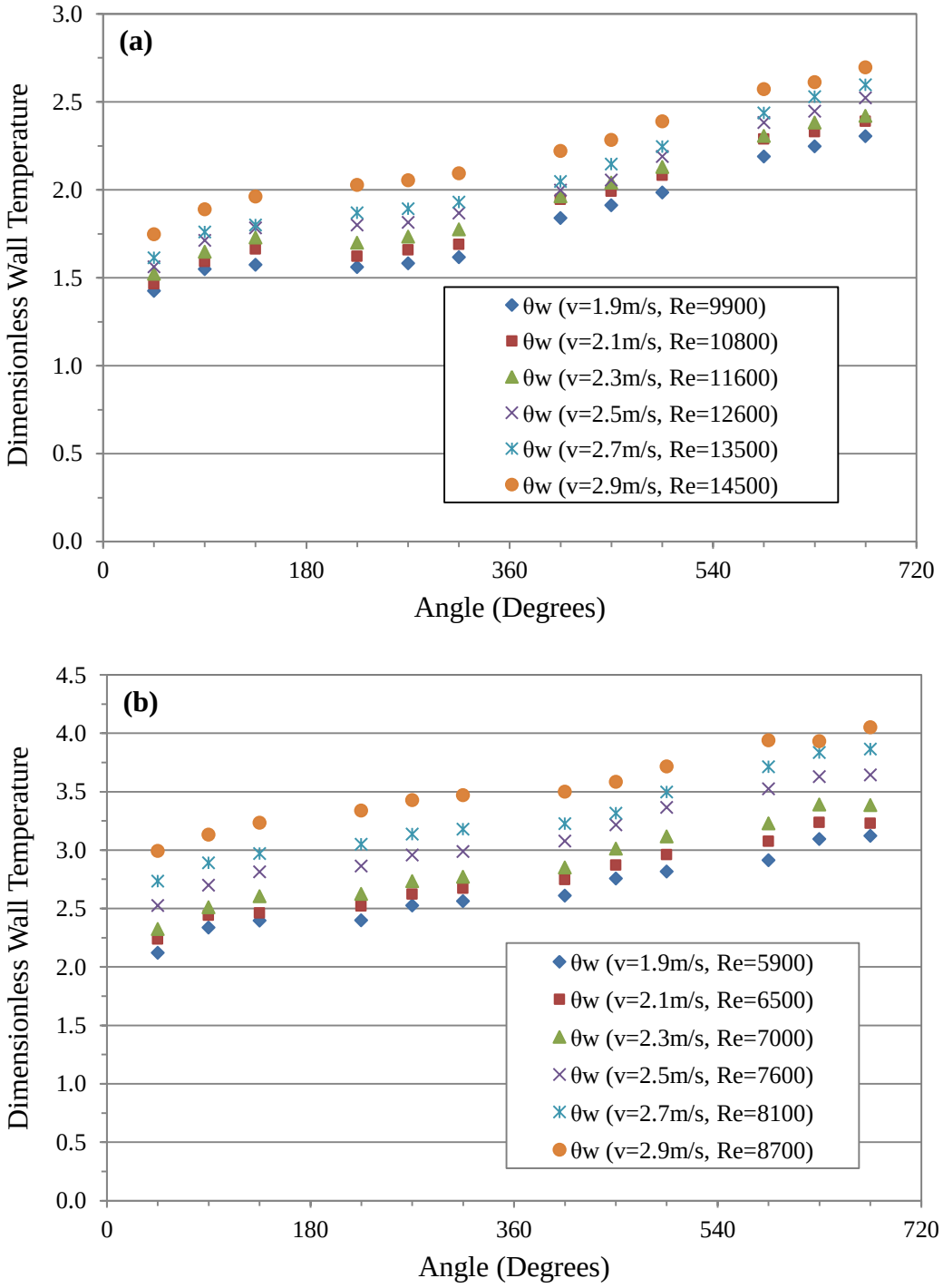

Fig. 31. Average dimensionless wall temperature of MPCM slurry at (a) 5.9 % MPCMs, (b) 10.9 % MPCMs

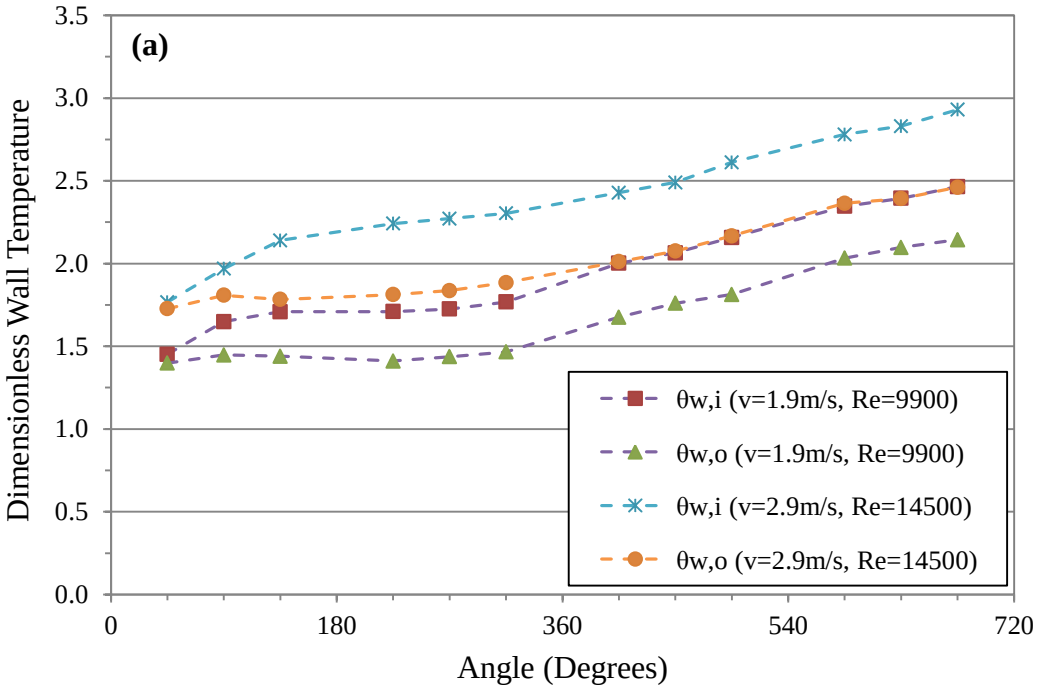

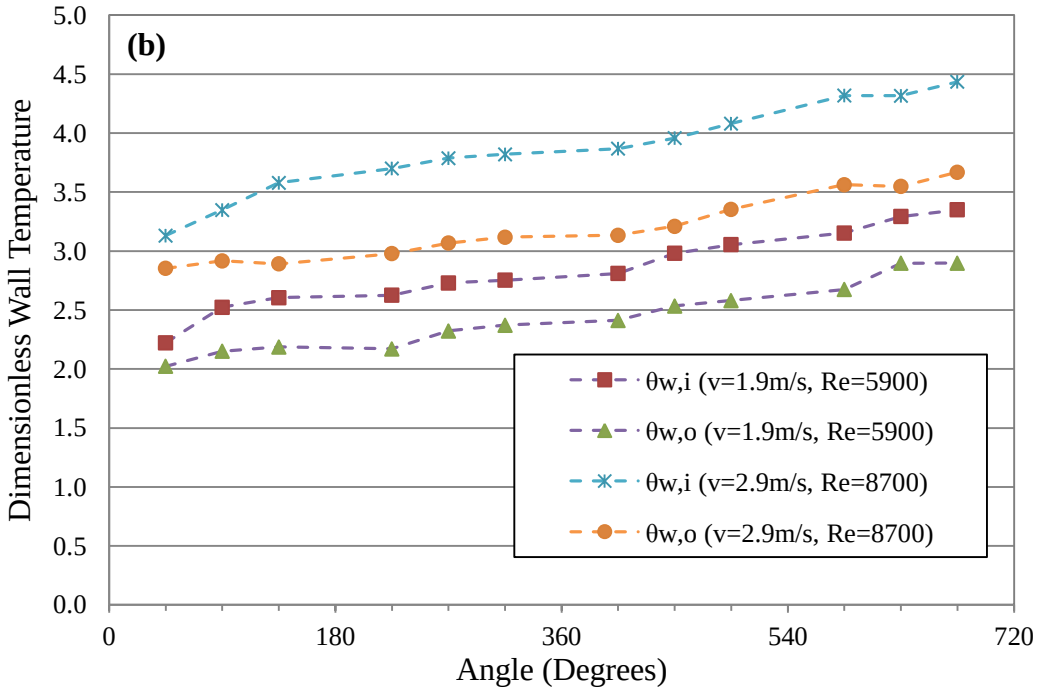

Fig. 32. Dimensionless wall temperatures on the inside and the outside of the tube at (a) 5.9 % MPCMs, (b) 10.9 % MPCMs

Figure 33 shows the difference of heat transfer coefficients between the outside (h_o) and the inside (h_i) of the wall as a function of angle. The experimental results show that the heat transfer coefficient difference increases with fluid velocity, which is about 18 to 27 % of the average heat transfer coefficient. This can be attributed to the intensified centrifugal force within the flow structure. Moreover, the centrifugal force induced by the coil curvature moves the location of maximum axial velocity toward the tube's outer region [53, 54]. Specifically, the shift in location is caused by the centrifugal force which is balanced by the radial pressure gradient as follows [54]:

$$\frac{\partial P}{\partial r} = \frac{\rho \cdot v^2}{R} \tag{43}$$

where ρ, v, and R are the density of fluid, axial fluid velocity, and the coil radius, respectively.

Furthermore, at higher Dean number, the location of maximum axial velocity shifts more to the outer region of the tube, which leads to greater fluid shear in the outer region than in the inner region inside the helical coil [54-56]. As a result, higher Dean number leads to a greater heat transfer coefficient difference as well as a higher heat transfer coefficient overall. The experimental results, Fig. 33, also show that the heat transfer coefficient difference ($h_o - h_i$) shows an oscillatory behavior, and the magnitude of the oscillation tends to increase with fluid velocity (Dean number), even though it has no effect on the average heat transfer coefficients. This is expected because the secondary flows in the helical coil affect the heat transfer coefficients around the periphery of the tube, which researchers [21, 50, 57, 58] have observed, specifically within the

developing region. Previous studies [21, 50, 57, 58] also reported that the oscillatory behavior of the heat transfer coefficient decays and damps out in the fully developed region. However, Jayakumar et al. [38] observed through numerical simulations that the fluid elements move within various trajectories and oscillate along the helically coiled tube. Jayakumar et al. [38] also found that Nusselt number fluctuates because of an overall spiral movement of the fluid generated by a combination of centrifugal, inertial, and buoyancy forces, even though the oscillations are marginal in the fully developed region.

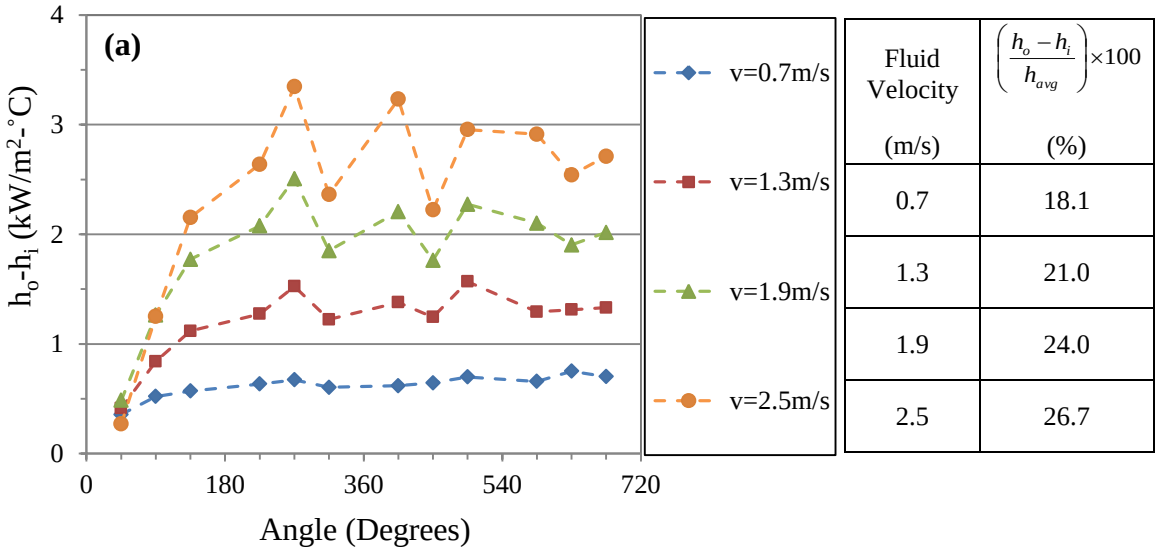

Fluid Velocity (m/s)	$\left(\frac{h_o - h_i}{h_{avg}}\right)\times 100$ (%)
0.7	18.1
1.3	21.0
1.9	24.0
2.5	26.7

Fig. 33. Difference of heat transfer coefficients between the outside and the inside of the tube for (a) water, (b) 5.9 % MPCM slurry without phase change, (c) 10.9 % MPCM slurry without phase change at different fluid velocities

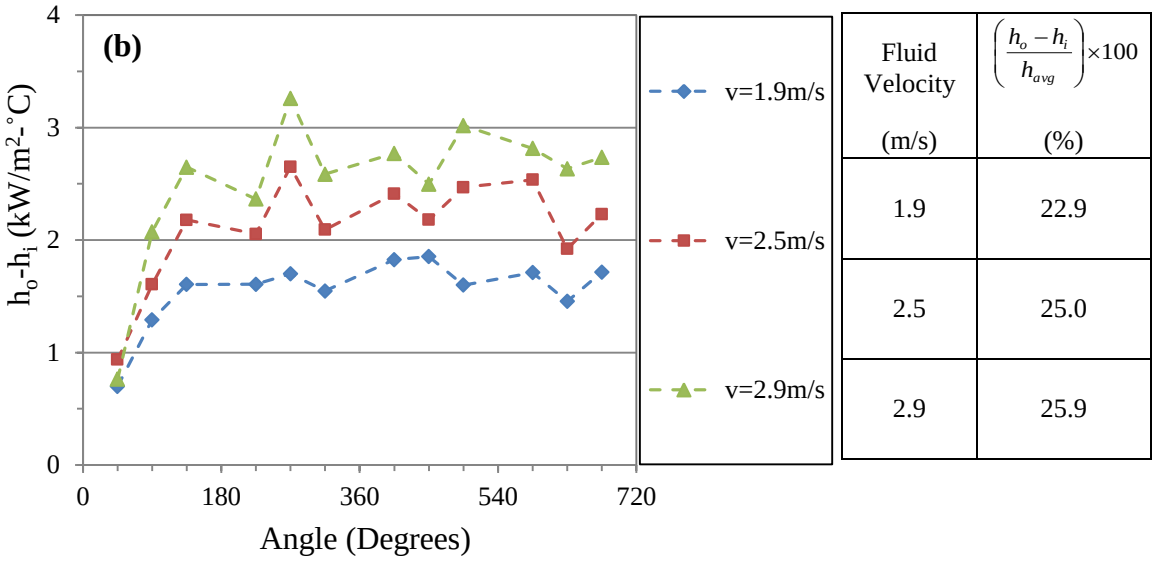

Fluid Velocity (m/s)	$\left(\frac{h_o - h_i}{h_{avg}}\right)\times 100$ (%)
1.9	22.9
2.5	25.0
2.9	25.9

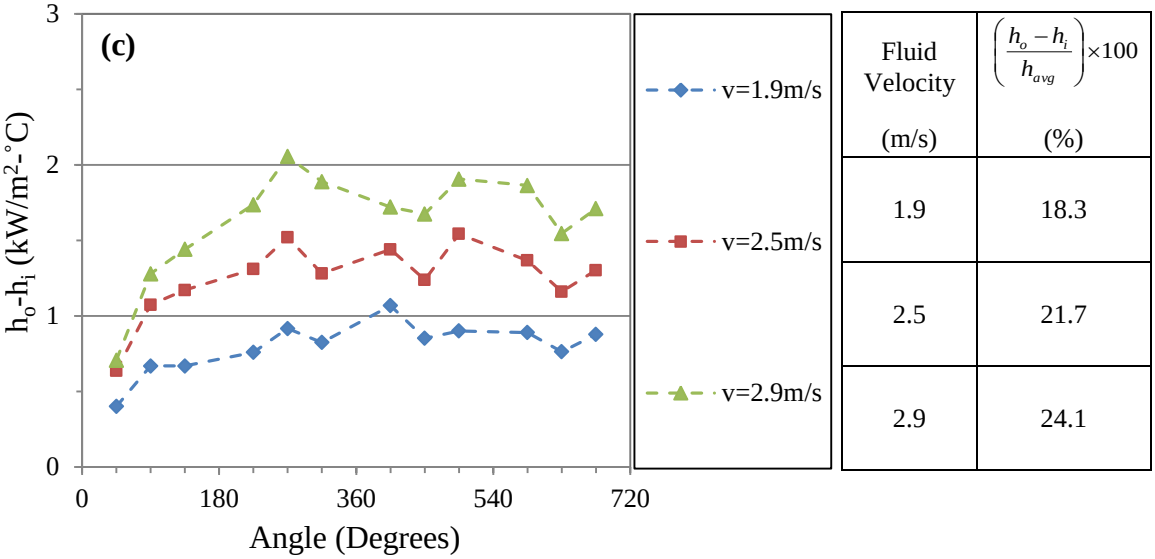

Fluid Velocity (m/s)	$\left(\frac{h_o - h_i}{h_{avg}}\right)\times 100$ (%)
1.9	18.3
2.5	21.7
2.9	24.1

Fig. 33 Continued.

Figure 34 shows the difference of the heat transfer coefficients for different mass fractions of MPCM slurries under constant fluid velocity condition. The experimental results show that the magnitude of heat transfer coefficient difference decreases with

mass fraction of MPCM in the slurry because of the increased viscosity at higher mass fractions. The experimental results suggest that higher viscosity attenuates and damps the oscillatory behavior of ($h_o - h_i$) and the secondary flows even at high velocities. Since the pressure losses are higher for MPCM at high mass fractions, it is expected that viscous effects would limit the intensity of secondary flows. The phase change process did not significantly affect the difference of heat transfer coefficients and the oscillations, as shown in Fig. 35.

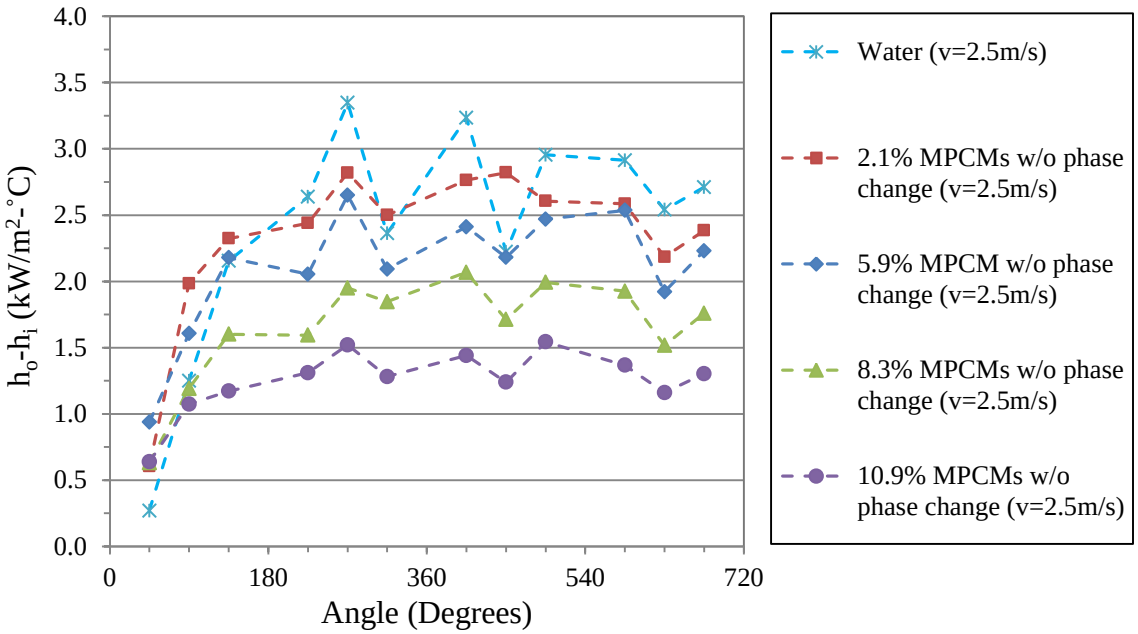

Fig. 34. Difference of heat transfer coefficients between the outside and the inside of the tube for different mass fractions of MPCM slurries

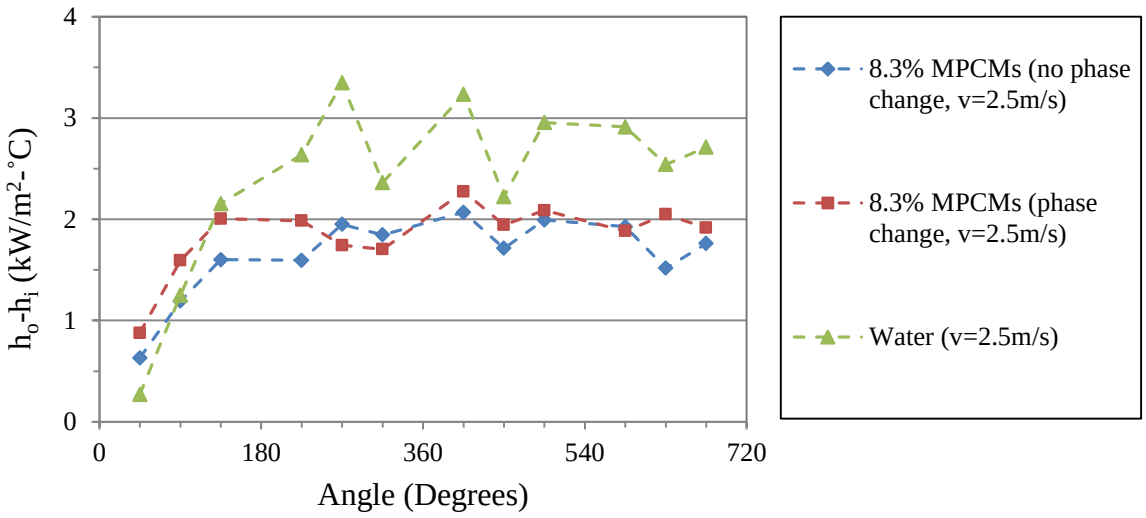

Fig. 35. Difference of heat transfer coefficients between the outside and the inside of the tube for 8.3 % MPCM slurry

Figure 36 shows Nusselt number as a function of fluid temperature for different mass fractions of MPCM slurries. Heat transfer experiments were conducted at different fluid velocities, which varied from 1.9 m/s to 2.9 m/s and at a constant heat flux (46 kW/m^2). The experimental results show that the Nusselt number increases during the phase change process due to the increased heat capacity generated by the latent heat of fusion of the PCM. The Nusselt number during the phase change process is higher than that the corresponding Nusselt number before and after the melting process. The latent heat of fusion of the PCM can enhance Nusselt number by increasing the specific heat of the MPCM slurry [59], but most importantly, the PCM keeps the temperature gradient within the fluid lower than in a single phase fluid case, which leads to greater heat transfer coefficient values. The experimental results clearly show that the Nusselt number increases with the fluid velocity (Reynolds number) due to the greater momentum transfer.

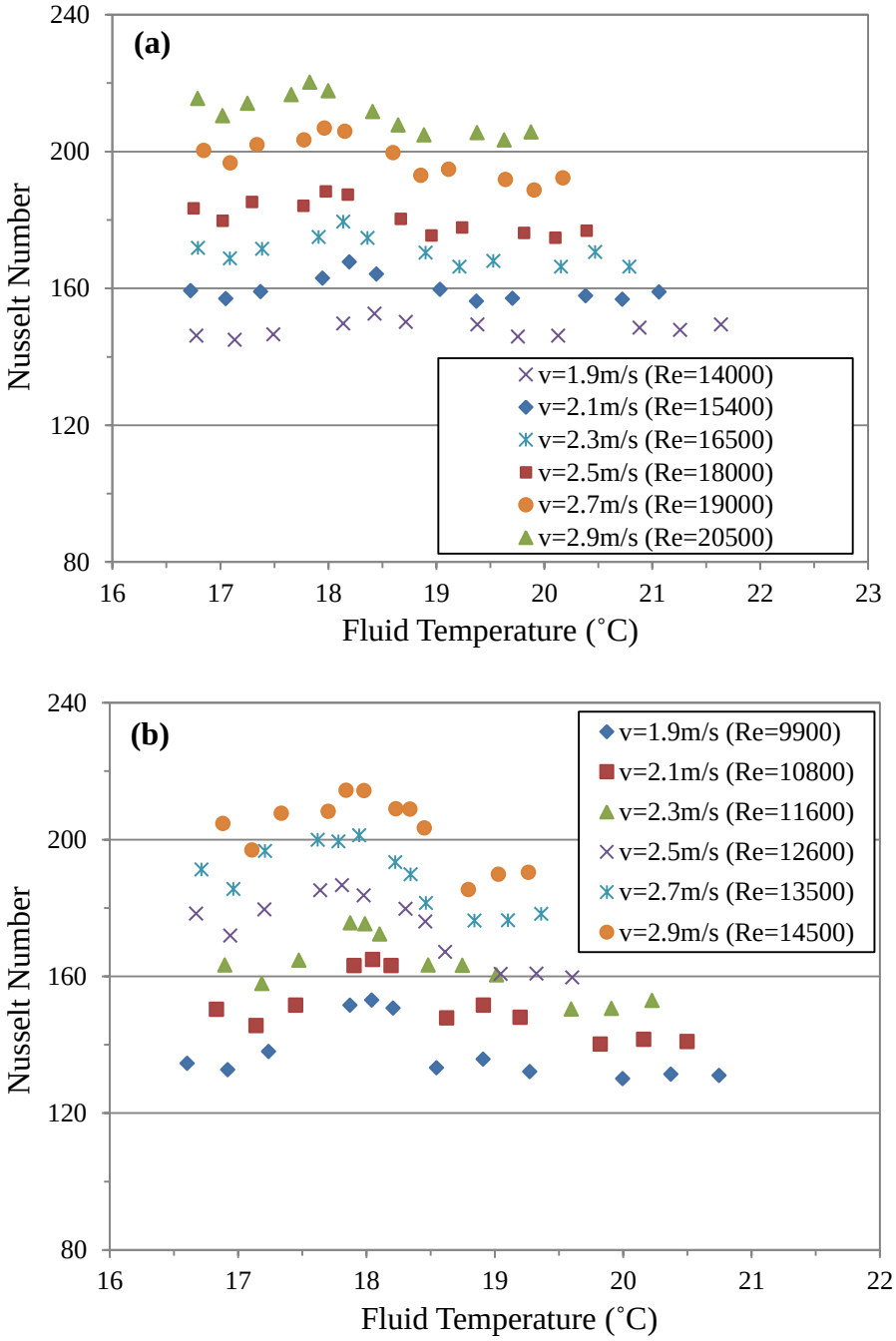

Fig. 36. Nusselt number of MPCM slurry as a function of fluid temperature at different fluid velocities at (a) 2.1 % MPCMs, (b) 5.9 % MPCMs, (c) 8.3 % MPCMs, (d) 10.9 % MPCMs

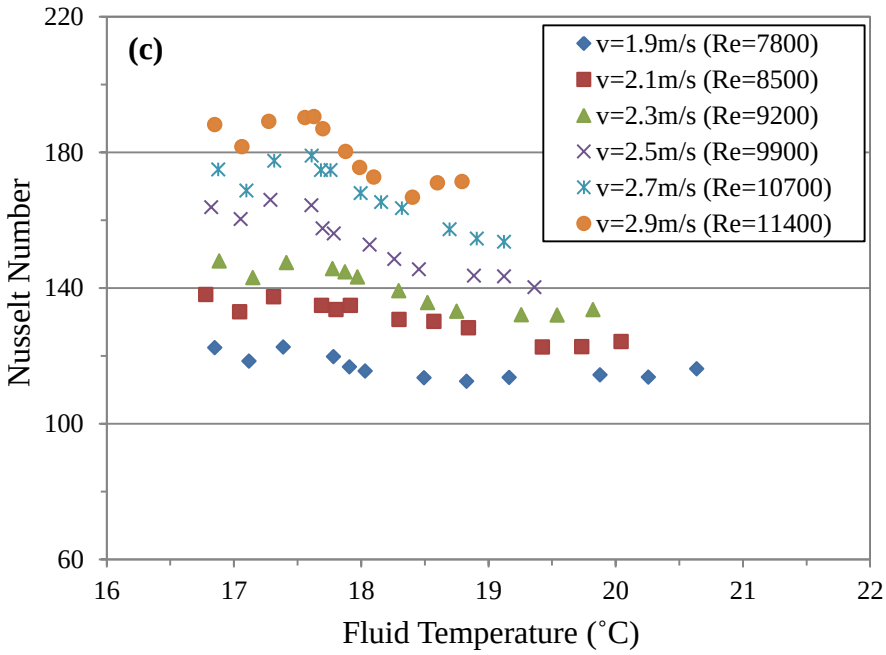

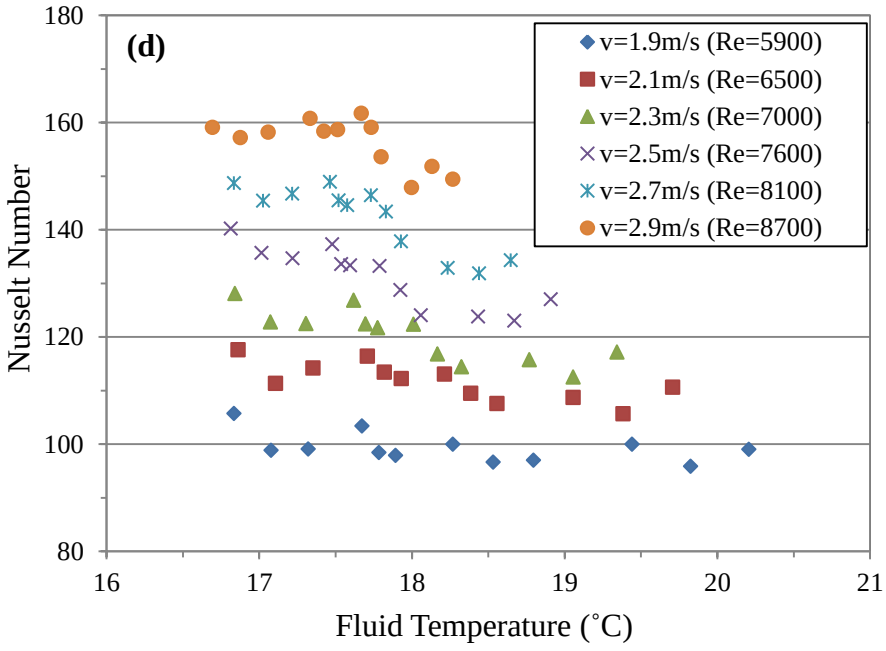

Fig. 36 Continued.

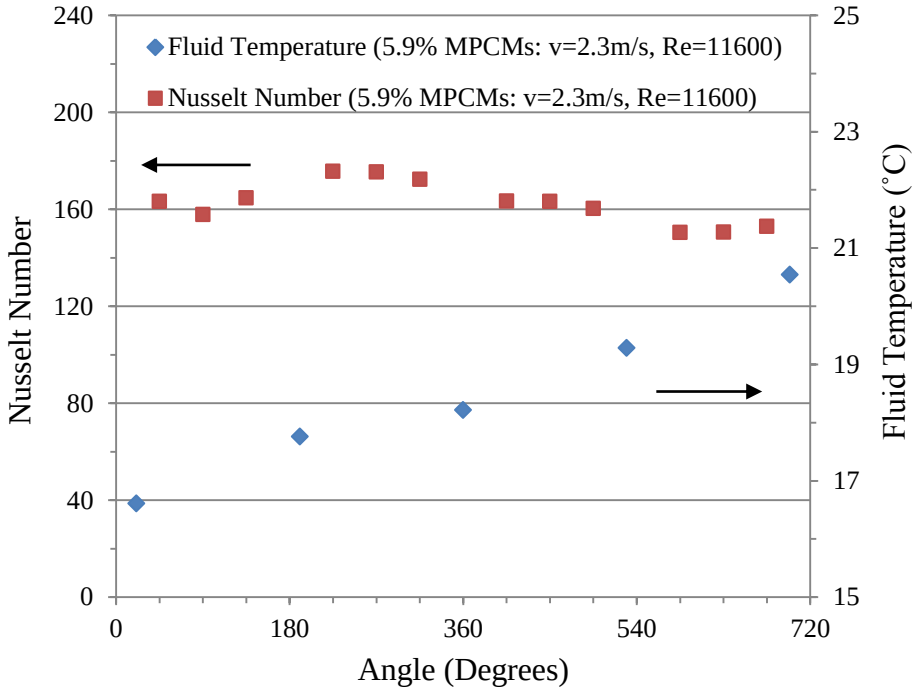

Fig. 37. Fluid temperature and Nusselt number as a function of angle for 5.9 % MPCM slurry at fluid velocity of 2.3 m/s

To clearly show the variations in Nusselt numbers along the coiled tube, the fluid temperature and Nusselt number as a function of angle for 5.9 % MPCM slurry at a fluid velocity of 2.3 m/s are shown in Fig. 37. Before the slurry temperature reached the melting temperature of the PCM, the Nusselt number increased slightly. This could be attributed to the small number of MPCM particles that underwent phase change because of the higher wall temperature than the melting temperature of the PCM. When the slurry temperature reached the melting temperature of the PCM, the Nusselt number considerably increased due to the phase change of the remaining MPCM particles. Then, since the number of MPCM particles that did not undergo phase change decreased, the

Nusselt number decreased again. After finishing the melting process, the Nusselt number remained almost constant, as is the case of the single phase fluid.

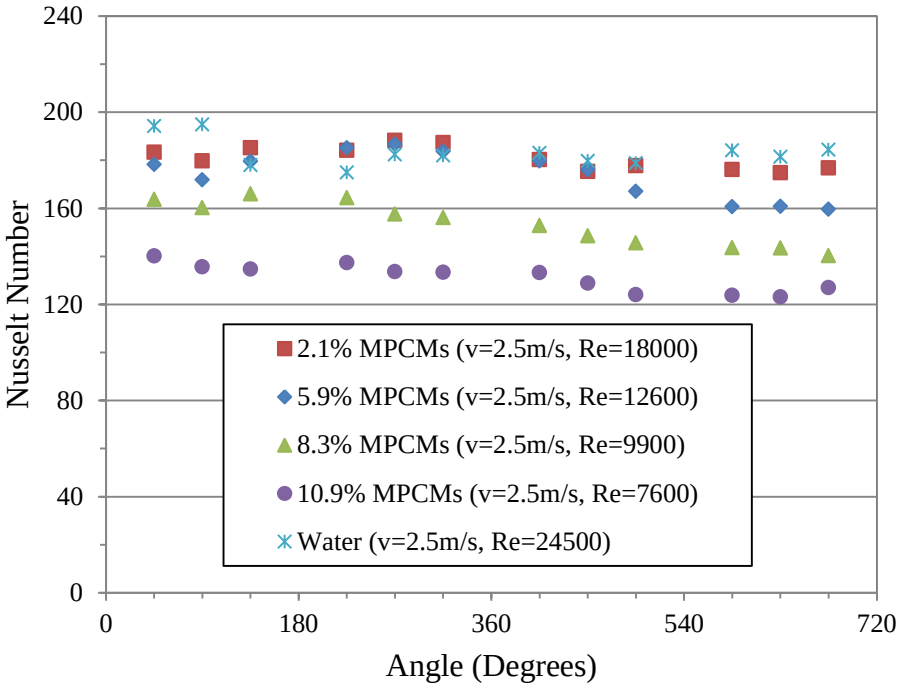

Fig. 38. Nusselt number as a function of angle at different mass fractions of MPCM slurries

Figure 38 shows the effects of mass fraction of MPCM in the slurry on Nusselt number at a constant fluid velocity (2.5 m/s) and constant heat flux (46 kW/m^2). The experimental results show that the average Nusselt number decreases with mass fraction of MPCM in the slurry, which is lower than that of water. Adding particles to a carrier fluid usually increases the fluid viscosity, which reduces the Reynolds number at the same fluid velocity due to the increased viscosity associated with particle loading. In turn, the lower turbulence decreases the momentum transfer and the Nusselt number as

well. In addition, the relatively low latent heat of fusion of the PCM (88 J/g) used in the study led to a lower Nusselt number than water. Organic phase change materials with a latent heat of fusion ranging from 150 to 200 J/g were typically used in previous studies [1, 3, 4, 9, 10, 12], which was approximately 1.7 to 2.3 times greater than that used in the study. For similar rheological properties of MPCM slurry, a higher latent heat of fusion can considerably enhance heat transfer performance. Kong et al. [4] reported that the overall heat transfer coefficient of MPCM slurry, having a latent heat of fusion of 152 J/g, was higher than that of water in a commercial coil heat exchanger.

The Nusselt number of MPCM slurry can also be affected by MPCM particle interactions within the fluid. In order to investigate the effects of MPCM particle interactions on Nusselt number, the Nusselt number of MPCM slurry without phase change of PCM was compared with that of a hypothetical fluid, assuming the following conditions:

- The fluid has no particles but matches the viscosity of the MPCM slurry
- The thermo-physical properties of the fluid are the same as those of MPCM slurries including density, viscosity, specific heat, and thermal conductivity
- The Nusselt number of the fluid is determined by using the correlation (Equation (26)) postulated by Mori and Nakayama [36], which is applicable for a coil with a curvature ratio of 0.025 and turbulent flow of homogeneous Newtonian fluid.

Figure 39 shows the Nusselt numbers of water, MPCM slurry with phase change, MPCM slurry without phase change, and a hypothetical fluid at a constant fluid velocity (2.5 m/s) and heat flux (46 kW/m^2). Figures 39 (a), (b), (c), and (d) show the results for

2.1 %, 5.9 %, 8.3 %, and 10.9 % MPCM slurries, respectively. As the results show, the ratio of Nusselt number of MPCM slurry without phase change to that of the hypothetical fluid increases from 1.02 to 1.08, when mass fraction increases from 2.1 % to 5.9 %. However, the ratio decreases at higher mass fractions. This suggests that microcapsules can enhance the heat transfer performance through the interactions of particles induced by a combination of the secondary flow and turbulence at a particular low mass fraction. At higher mass fraction of MPCM in the slurry, particle interactions negatively affect turbulence intensity leading to reduced momentum transfer. This phenomenon was observed in previous studies [60, 61].

Nusselt number of MPCM slurry with phase change was compared to the slurry without phase change to investigate the effect of the latent heat of fusion. The experimental results show that the latent heat of fusion of the PCM increases Nusselt number. It was also found that the ratio of Nusselt number of MPCM slurry with phase change to the slurry without phase change increases with mass fraction of MPCM in the slurry. This was expected because of the greater latent heat of fusion available for heat transfer, as the mass fraction of the MPCM increases.

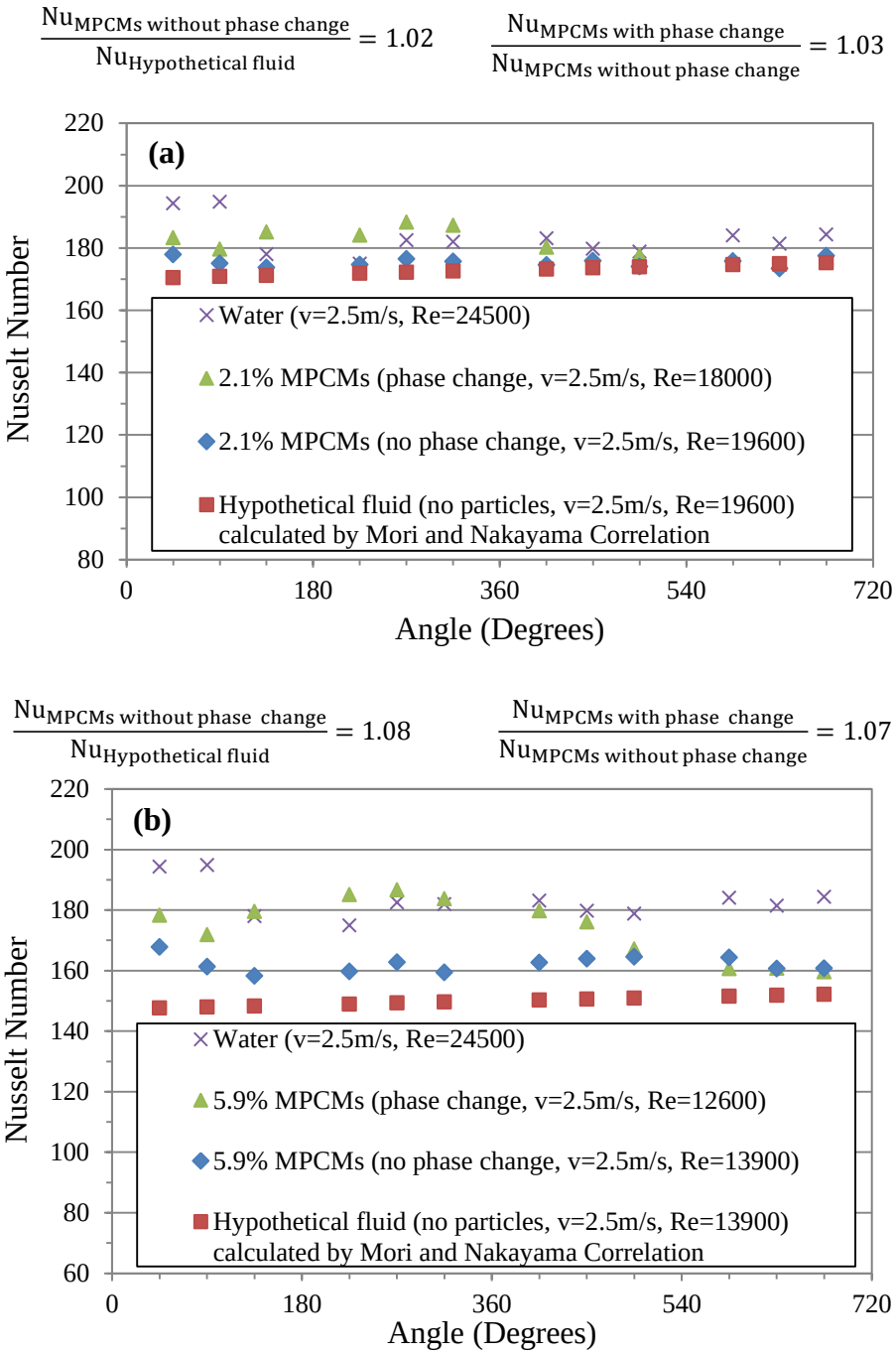

Fig. 39. Nusselt numbers of MPCM slurry with and without phase change and a hypothetical fluid at (a) 2.1 % MPCMs, (b) 5.9 % MPCMs, (c) 8.3 % MPCMs, (d) 10.9 % MPCMs

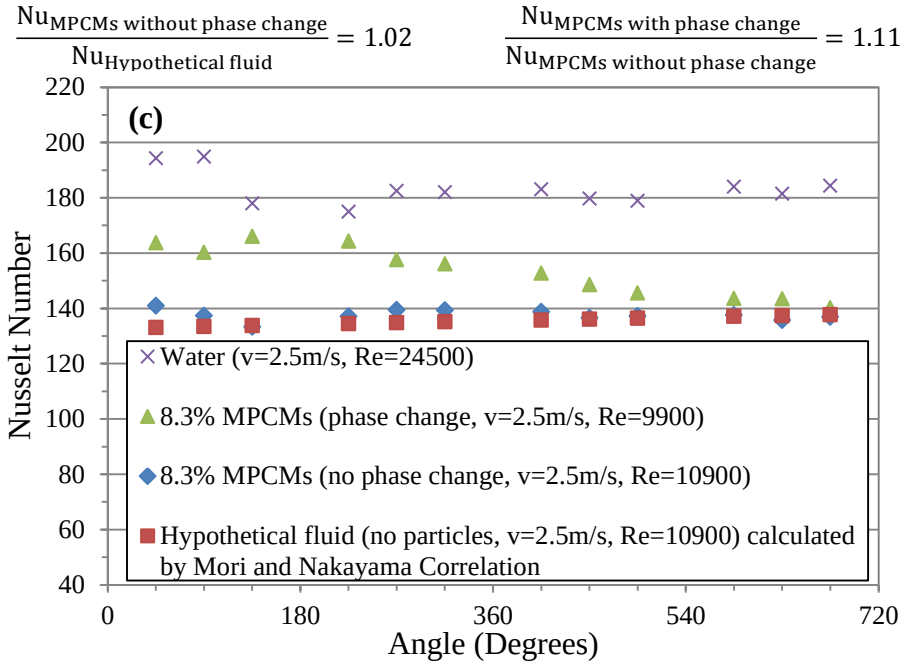

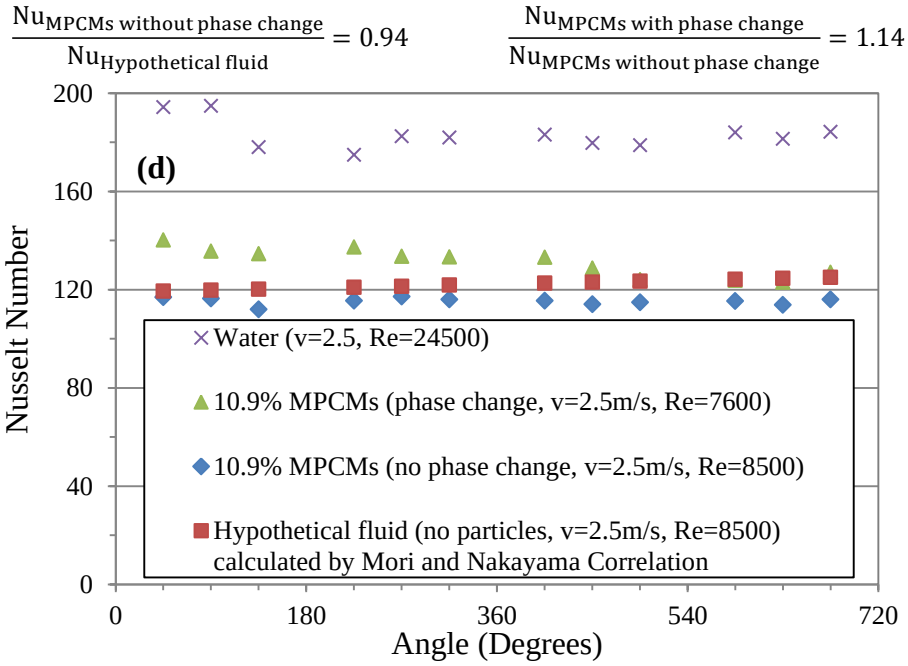

Fig. 39 Continued.

To investigate the effects of using a coiled tube on heat transfer performance of MPCM slurry, the heat transfer enhancement factor $\left(\frac{h_{MPCMs}}{h_w}\right)$ of MPCM slurry in the coiled tube was compared to that in a straight tube studied by Alvarado et al. [1]. As shown in Table 7, the heat transfer enhancement factor (0.73) in the coiled tube is higher than the one (0.6) for a straight tube. This is attributed to enhanced fluid mixing of the MPCM particles. To evaluate the effects of using a coiled tube on enhanced fluid mixing, the minimum required length of heat transfer section needed to ensure complete melting should be determined. It is hypothesized that better fluid mixing leads to a faster phase change process by allowing MPCM particles to interact with the heated surface energetically. Under ideal conditions, when the fluid reaches the melting point of the PCM, all the energy would then be used to melt the PCM while the carrier's fluid temperature remains constant or with a temperature rise of zero, as shown in Fig. 40. However, due to less than ideal mixing conditions, MPCM particles require a longer distance to melt inside the heat transfer section, which results in a temperature rise greater than zero.

Table 7. Comparison of heat transfer enhancement factors

Test section	Latent heat of fusion of PCM (J/g)	Mass fraction of MPCM (%)	Fluid velocity (m/s)	$\frac{h_{MPCMs}}{h_w}$	$\frac{L_{Ideal}}{L_{Actual}}$
Coiled Tube	88	8.3	1.9	0.73	0.78
Straight Tube	163	7.0	1.9	0.60	0.67

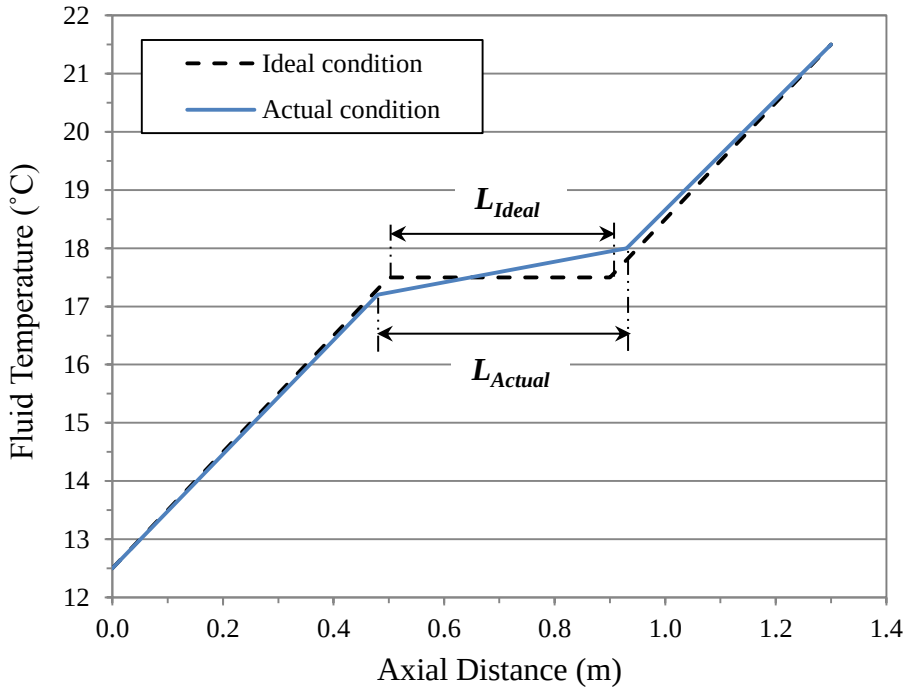

Fig. 40. Fluid temperature profile at ideal and actual conditions

One way to quantify the effects of enhanced mixing on melting, is by obtaining the ratio between the minimum required length for melting (i.e. temperature rise or slope of zero, or ideal case) and the actual length required for melting (i.e. actual temperature rise or slope of actual case), as follows:

$$MLR = \frac{L_{Ideal}}{L_{Actual}} \tag{44}$$

where MLR, L_{Ideal}, and L_{Actual} are the melting length ratio, ideal length for complete melting and actual length for complete melting, respectively. L_{Ideal} is as follows:

$$L_{Ideal} = \frac{MF \cdot \lambda \cdot \dot{m}}{q''(\pi d)} \tag{45}$$

where MF, λ, $\dot{m}$, q'', and d are the MPCM mass fraction, the latent heat of fusion of the PCM, the mass flow rate of the MPCM slurry, the heat flux, and the inner diameter of the tube, respectively.

Ideal length applies only when there is no temperature rise in the carrier fluid since all the energy is being absorbed by the phase change material in the form of latent heat. L_{Actual} was determined experimentally by noting the changes of the slope of the temperature curve along the axial direction. Specifically, the changes in slope associated with the onset of melting and complete melting were used as the limits of L_{Actual}, as shown in Fig. 40. As Table 7 shows, the melting length ratio (MLR) is greater for the coiled tube than for the straight tube even when taking into account the latent heat of fusion and mass fraction of the MPCM slurries. It is then inferred that better fluid mixing exists in the coiled loop than in the straight loop because of the presence of secondary flows, which leads to an enhanced phase change process of the PCM.

Figure 41 shows the Nusselt number of MPCM slurry as a function of fluid velocity at a constant fluid inlet temperature (16.5 ˚C) and heat flux (46 kW/m^2). The experimental results clearly show that Nusselt number increases with fluid velocity. This can be attributed to the combination of increased fluid velocity effect and intensified secondary flow effect [62]. As the MPCM mass fraction increases, the Nusselt number of the MPCM slurry decreases and is lower than water at the same fluid velocity. This is expected because the higher viscosity of MPCM slurry decreases the turbulence intensity and thus momentum transfer.

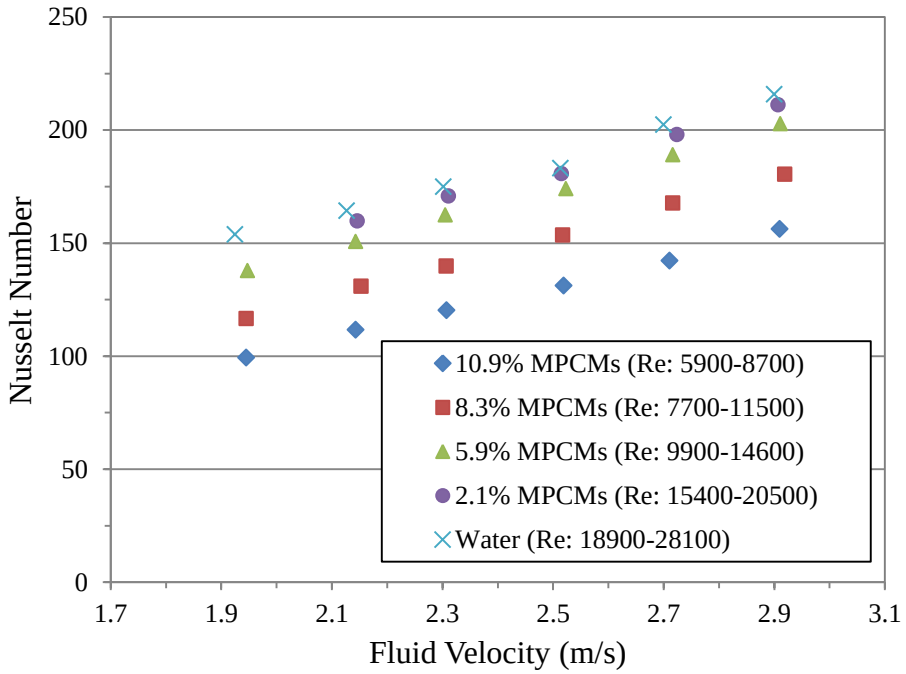

Fig. 41. Nusselt number of MPCM slurry as a function of fluid velocity

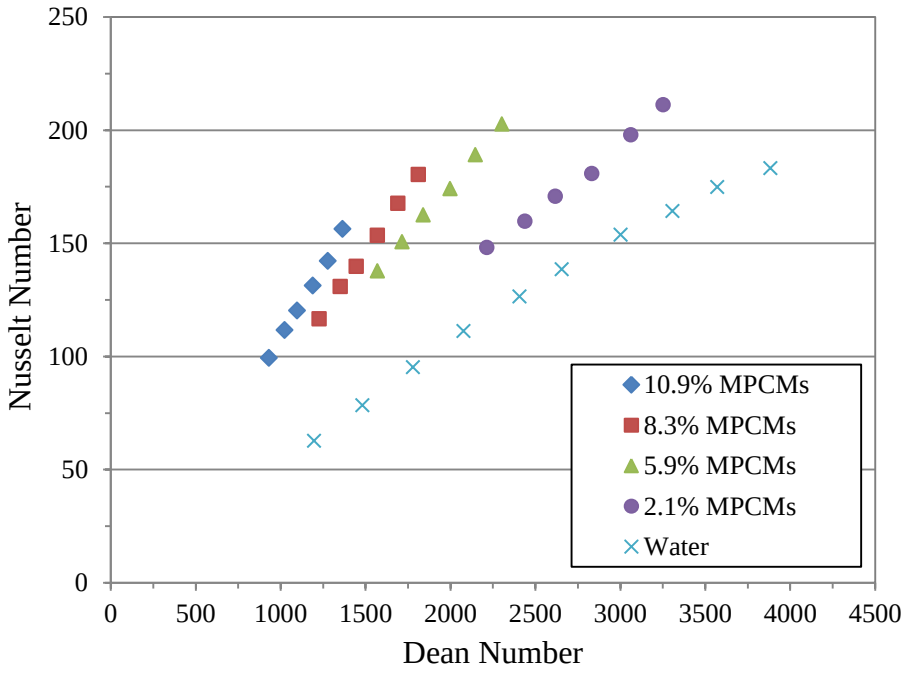

Fig. 42. Nusselt number of MPCM slurry as a function of Dean number

Figure 42 shows Nusselt number of MPCM slurry as a function of Dean number. The experimental results show that Nusselt number increases with Dean number and MPCM concentration due to the increased momentum and greater latent heat of fusion from the PCM. Based on the results, a multiple regression analysis was performed to formulate a correlation capable of predicting Nusselt number for MPCM slurry flowing through the coiled tube with a curvature ratio (r/R) of 0.025. The correlation is based on Dean number (De), mass fraction of MPCM in the slurry (MF), and Prandtl number (Pr), as follows:

$$\mathrm{Nu}_c = 0.03\mathrm{De}^{0.95}\left(1-MF\right)^{-0.19}\mathrm{Pr}^{0.4} \qquad \left(R^2 = 0.97\right) \tag{46}$$

where $1000 \le \mathrm{De} \le 4000$ and $0 \le MF \le 0.11$

As shown in Fig. 43, the Nusselt number values of the correlation (46) are compared with those of the experiments. The values of the correlation are in good agreement with the experimental values and deviate by less than ± 10 %. From the correlation, it is clear that the Nusselt number increases with Dean number, mass fraction of the MPCM, and Prandtl number. It is also clear that Dean number plays a more significant role in increasing the Nusselt number than the MPCM concentration and Prandtl number since its exponent in the correlation is greater than the other ones.

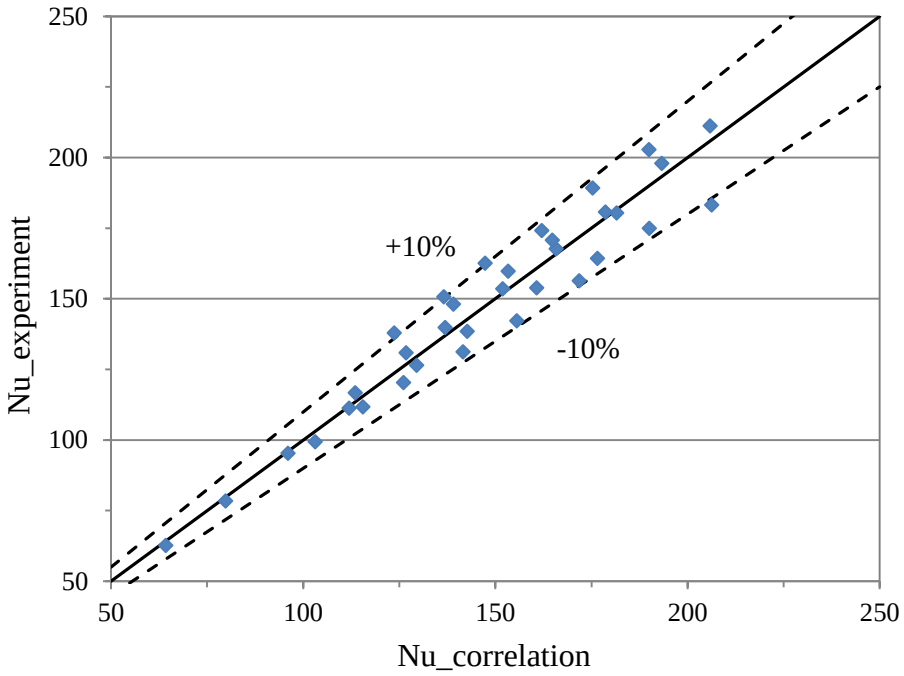

Fig. 43. Comparison of Nusselt numbers between the experiment and correlation

Additionally, the correlation for predicting Nusselt number was postulated in terms of Dean number and Prandtl number only, as follows:

$$\mathrm{Nu_c} = 0.04\mathrm{De}^{0.94}\mathrm{Pr}^{0.4} \qquad \left(R^2 = 0.97\right) \tag{47}$$

where $1000 \le \mathrm{De} \le 4000$

The correlation coefficient (R^2 =0.97) for the correlation is still high, even though the effect of MPCM's mass fraction is not considered directly. This is because the effect of the viscosity is taken into account by Dean number and the effect of the latent heat of fusion on Nusselt number is relatively insignificant given the PCM used in the study.

5.2.3 Energy Evaluation of MPCM Slurry

In order to determine the benefits of using MPCM slurry as a heat transfer fluid in terms of energy, the effects of both heat transfer and pressure drop on energy efficiency should be considered. Many researchers [63-67] have used a performance coefficient including both heat transfer and flow resistance characteristics to compare the overall performance of heat exchangers between new fluids and base fluids. In this study, the effect of using MPCM slurry was assessed using the performance efficiency coefficient (PEC) or Bergles number, which is defined as the ratio of Nusselt number ratio to friction factor ratio between MPCM slurry and water, and it is calculated as follows:

$$\mathrm{PEC} = \frac{\mathrm{Nu}_{\mathrm{ratio}}}{f_{ratio}} = \frac{\left(\frac{\mathrm{Nu}_{MPCMs}}{\mathrm{Nu}_{w}}\right)}{\left(\frac{f_{MPCMs}}{f_{w}}\right)} \tag{48}$$

where $\mathrm{Nu}_{\mathrm{MPCMs}}$, Nu_{w}, f_{MPCMs}, and f_{w} are the Nusselt numbers of MPCM slurry and water, the friction factors of MPCM slurry and water, respectively.

In addition, PEC values were determined using the results at a constant fluid velocity as suggested by Yu et al. [63] to definitely determine the benefits of using MPCM slurry as a heat transfer fluid.

Figure 44 shows the PEC values of MPCM slurry as a function of mass fraction of MPCM in the slurry. As the mass fraction of the MPCM in the slurry increases, the PEC values decrease and all are lower than one. The low PEC values can be attributed to that the viscosity of MPCM slurry should increase pressure drop and decrease turbulence

and momentum transfer. In addition, the relatively lower latent heat of fusion of the PCM (88 J/g) used in the study was low to promote enhancement of Nusselt number compared to that of water. Recently, Kong et al. [4] used methyl stearate microcapsules with a latent heat of fusion of 152 J/g and observed that PEC value for 4.6 % MPCM slurry was higher than one. It is evident that using MPCM slurry can enhance the overall performance of CHX by considerably increasing the heat transfer, even though the higher viscosity of MPCM slurry leads to a higher pressure drop (pumping power).

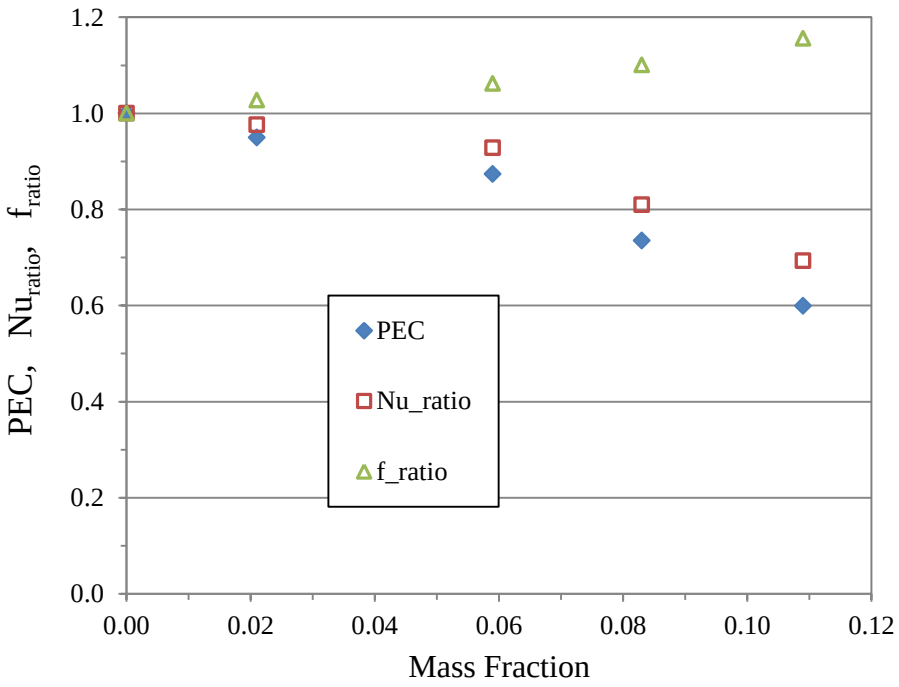

Fig. 44. Performance efficiency coefficient (PEC) as a function of mass fraction

The heat capacity of heat transfer fluid is one of the important properties in the thermal energy systems because heat capacity accounts for the amount of energy that the

fluid can carry with a raise in temperature. Thus, increased energy transferred can reduce the required flow rate of heat transfer fluid and consequently save energy through decreased pumping power. To evaluate the use of MPCM slurry as a heat transfer fluid from the heat capacity point of view, a figure of merit for heat capacity ($\mathrm{FOM_{HC}}$) is defined, as follows:

$$\mathrm{FOM_{HC}} = \frac{c_{p,ratio}}{f_{ratio}} = \frac{\left(\frac{c_{p,MPCMs}}{c_{p,w}}\right)}{\left(\frac{f_{MPCMs}}{f_w}\right)} \tag{49}$$

where $c_{p,MPCMs}$, $c_{p,w}$, f_{MPCMs}, and f_w are the effective specific heat of MPCM slurry, the specific heat of water, the friction factors of MPCM slurry and water, respectively.

Figure 45 shows the $\mathrm{FOM_{HC}}$ values of MPCM slurry as a function of mass fraction of MPCM in the slurry. The experimental results show that the $\mathrm{FOM_{HC}}$ values increase with MPCM's mass fraction, from 1.11 to 1.49. This can be attributed to the specific heat of the MPCM slurry, which significantly increases due to the latent heat of fusion of the PCM even at low mass fraction. It is found that the use of MPCM slurry can enhance the performance of the thermal energy systems by significantly increasing the heat capacity, even though the higher viscosity of MPCM slurry leads to the increased pumping power.

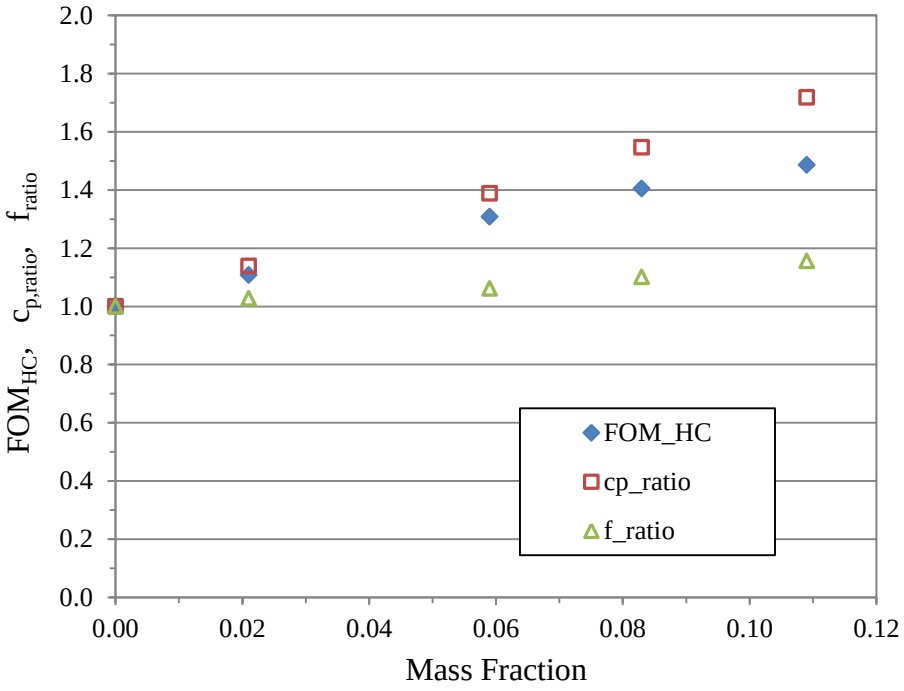

Fig. 45. Figure of merit for heat capacity (FOM_{HC}) as a function of mass fraction for ΔT of 3 ˚C

6. CONCLUSIONS

In the present experimental study, thermophysical properties of MPCM slurry were characterized and a variety of experiments for pressure drop and heat transfer coefficient measurements were conducted to investigate the flow and heat transfer characteristics of MPCM slurry in a helically coiled tube. Main observations and findings and recommendations for future work are as follows:

6.1 Concluding Remarks

Adding MPCM particles to water increased the viscosity due to particle interactions. MPCM slurry behaved as a Newtonian fluid at mass fractions less than 10.9 %. For the durability, MPCM particles used in the study resisted continuous pumping condition (2200 circulation cycles) without any degradation of heat transfer performance. From the pressure drop measurements, pressure drop of MPCM slurry increased with MPCM's mass fraction, which was higher than water because of the increased viscosity. Friction factor curve of MPCM slurry fitted well with previous correlation used for homogeneous Newtonian fluids and friction factor correlation was postulated as a function of Dean number only.

From the heat transfer experiments, Nusselt number of MPCM slurry significantly increased during the phase change process due to the increased heat capacity provided by the latent heat of fusion of the PCM. Nusselt number of MPCM slurry was lower than that of water at the same flow rate condition due to the decreased

momentum transfer. Difference of heat transfer coefficient between outside and inside regions of the coiled tube occurred because of a skewed axial fluid velocity generated by centrifugal force, which showed an oscillatory behavior due to the formation of secondary flows. In addition, the heat transfer coefficient difference decreased with mass fraction of MPCM due to higher viscosity and the viscous effect of MPCM slurry would limit the intensity of secondary flows. Fluid mixing in the radial direction induced by secondary flows led to an enhanced phase change process and increased heat transfer performance, when compared to MPCM heat transfer cases involving straight heat transfer sections. Moreover, the correlation for predicting Nusselt number of MPCM slurry in a coiled tube was postulated and Dean number played a more significant role in increasing Nusselt number than other parameters.

Energy evaluation was performed to determine the benefits of using MPCM slurry as a heat transfer fluid. Energy evaluation results revealed that using MPCM slurry do not have any enhancement in terms of performance efficiency coefficient due to the increased pressure drop, decreased momentum transfer, and low latent heat of fusion of the PCM used in the study. However, MPCM slurry increased the figure of merit in terms of heat capacity even at low mass fraction of MPCM in the slurry.

In summary, MPCM slurry can become a viable heat transfer fluid in thermal energy applications. MPCM slurry can significantly enhance heat capacity due to the latent heat of fusion of the PCM. MPCM slurry used under moderate conditions including high latent heat of fusion, low slurry viscosity, and high phase change rate can lead to enhanced heat transfer performance. In addition, a coil heat exchanger can be

appropriate for phase change process of PCM by enhancing fluid mixing induced by secondary flows. However, from the heat transfer performance point of view, optimum conditions still have to be identified to maximize the benefits of using MPCM slurry in the coil heat exchanger in future studies.

6.2 Future Studies

The following recommendations should be considered in future studies: 1) evaluation of heat transfer performance of MPCM slurry with a PCM with high latent heat of fusion in a coiled tube, 2) investigation of the effects of coil configurations including curvature and pitch on flow and heat transfer characteristics of MPCM slurry, 3) numerical simulation for MPCM slurry in the coiled tube to completely understand how MPCM particles behave inside the coiled tube and to determine the effect of flow behavior on heat transfer performance of MPCM slurry, 4) evaluation of the effects of MPCM particle material, particle shape, particle size, and particle size distribution on the pressure drop of MPCM slurry.

REFERENCES

[1] J.L. Alvarado, C. Marsh, C. Sohn, G. Phetteplace, T. Newell, Thermal performance of microencapsulated phase change material slurry in turbulent flow under constant heat flux, Int. J. of Heat and Mass Transfer 50 (2007) 1938-1952.

[2] J.L. Alvarado, C. March, C. Sohn, M. Vilceus, V. Hock, G. Phetteplace, T. Newell, Characterization of supercooling suppression of microencapsulated phase change material by using DSC, J. Therm. Anal. Calorim. 86 (2006) 505-509.

[3] H. Taherian, J.L. Alvarado, K. Tumuluri, C. Thies, C. Park, Fluid flow and heat transfer characteristics of microencapsulated phase change material slurry in turbulent flow, J. Heat Transfer 136 (2014) 061704-1-7.

[4] M. Kong, K. Yu, J.L. Alvarado, W. Terrell, Thermal performance of microencapsulated phase change material slurry in a coil heat exchanger, J. Heat Transfer 137 (2015) 071801-1-8.

[5] Y. Yamagishi, T. Sugeno, T. Ishige, An evaluation of microencapsulated PCM for use in cold energy transportation medium, Proc. Intersoc. Energy Convers. Eng. Conf. (1996) 2077-2083.

[6] G.H. Zhang, C.Y. Zhao, Thermal and rheological properties of microencapsulated phase change materials, Renewable Energy 36 (2011) 2959-2966.

[7] R. Yang, H. Xu, Y. Zhang, Preparation, physical property and thermal physical property of phase change microcapsule slurry and phase change emulsion, Sol. Energy Mater. Sol. Cells 80 (2003) 405-416.

[8] S.K. Roy, S. Sengupta, An evaluation of phase change microencapsules for use in enhanced heat transfer fluids, Int. Commun. Heat Mass Transfer 18 (1991) 495-507.

[9] X. Wang, J. Niu, Y. Li, X. Wang, B. Chen, R. Zeng, Q. Song, Y. Zhang, Flow and heat transfer behaviors of phase change material slurries in a horizontal circular tube, Int. J. Heat and Mass Transfer 50 (2007) 2480-2491.

[10] X. Wang, J. Niu, Y. Li, Y. Zhang, X. Wang, B. Chen, R. Zeng, Q. Song, Heat transfer of microencapsulated PCM slurry flow in circular tube, AIChE J. 54 (2008) 1110-1120.

[11] V. Vand, Theory of viscosity of concentrated suspensions, Nature 155, No. 3934 (1945) 364-365.

[12] Y. Yamagishi, H. Takeuchi, A.T. Pyatenko, N. Kayukawa, Characteristics of microencapsulated PCM slurry as a heat-transfer fluid, AIChE J. 45 (1999) 696-707.

[13] J.C. Mulligan, D.P. Colvin, Y.G. Bryan, Microencapsulated phase change material suspensions for heat transfer in spacecraft thermal systems, J. Spacecraft Rockets 33 (1996) 278-284.

[14] F. Dammel, P. Stephan, Heat transfer to suspensions of microencapsulated phase change material flowing through minichannels, J. Heat Transfer 134 (2012) 020907-1-8.

[15] C. Crowe, M. Sommerfeld, Y. Tsuji, Multiphase Flows with Droplets and Particles, CRC Press, Boca Raton, FL, 1998.

[16] H. Inaba, M.J. Kim, A. Horibe, Melting heat transfer characteristics of microencapsulated phase change material slurries with plural microcapsules having different diameters, J. Heat Transfer 126 (2004) 558-565.

[17] M. Delgado, A. Lazaro, J. Mazo, B. Zalba, Review on phase change material emulsions and microencapsulated phase change material slurries: materials, heat transfer studies and applications, Int. J. Heat Mass Transfer 16 (2012) 253-273.

[18] P. Zhang, Z.W. Ma, R.Z. Wang, An overview of phase change material slurries: MPCS and CHS, Renewable Sustainable Energy Rev. 14 (2010) 598-614.

[19] B. Chen, X. Wang, R. Zeng, Y. Zhang, X. Wang, J. Niu, An experimental study of convective heat transfer with microencapsulated phase change material suspension: laminar flow in a circular tube under constant heat flux, Exp. Therm. Fluid Sci. 32 (2008) 1638–1646.

[20] Y. Rao, F. Dammel, P. Stephan, G. Lin, Convective heat transfer characteristics of microencapsulated phase change material suspensions in minichannels, Heat Mass Transfer 44 (2007) 175-186.

[21] A.N. Dravid, K.A. Smith, E.W. Merrill, P.L.T. Brian, Effect of secondary fluid motion on laminar flow heat transfer in helically coiled tubes, AIChE J. 17 (1970) 1114-1122.

[22] T.J. Huttl, R. Friedrich, Influence of curvature and torsion on turbulent flow in helically coiled pipes, Int. J. Heat and Fluid Flow 21 (2000) 345-353.

[23] L.S. Yao, S.A. Berger, Entry flow in a curved pipe, J. Fluid Mech. 67 (1975) 177-196.

[24] R.K. Shah, S.D. Joshi, Convective Heat Transfer in Curved Ducts in Handbook of Single-Phase Convective Heat Transfer, John Wiley & Sons, New York, NY, 1987.

[25] H. Ito, Friction factors for turbulent flow in curved pipes, J. Basic Eng. (1959) 123-134.

[26] P.S. Srinivasan, S.S. Nandapurkar, F.A. Holland, Friction factors for coils, T. I. Chem. Eng. 48 (1970) T156-T161.

[27] E.F. Schmidt, Warmenbergang and drukverlust in rohrschlangen, Chem. Eng. Tech 13 (1967) 781-789.

[28] V. Kubair, C.B.S. Varrier, Pressure drop for liquid flow in helical coils, Trans. Indian Inst. Chem. Eng. 14 (1962) 93-97.

[29] P. Mishra, S.N. Gupta, Momentum transfer in curved pipes. I. Newtonian fluids, Ind. Eng. Chem. Proc. DD 18 (1978) 130-142.

[30] P.R.H. Blasius, Das aehnlichkeitsgesetz bei reibungsvorgangen in flüssigkeiten, Forschungsheft 131 (1913) 1-41.

[31] R.A. Seban, E.F. McLaughlin, Heat transfer in tube coils with laminar and turbulent flow, Int. J. Heat Mass Transfer 6 (1963) 387-395.

[32] M. Adler, Stromung in gekrummten rohren, Z. Angew. Math. Mech. 14 (1934) 257-275.

[33] G.F.C. Rogers, Y.R. Mayhew, Heat transfer and pressure loss in helically coiled tubes with turbulent flow, Int. J. Heat Mass Transfer 7 (1964) 1207-1216.

[34] A.V. Kirpikov, Heat transfer in helically coiled pipes, Trudi Moskov. Inst. Khim. Mashinojtrojenija 12 (1957) 43-56.

[35] Y. Mori, W. Nakayama, Study on forced convective heat transfer in curved pipes (1^{st} report, laminar region), Int. J. Heat Mass Transfer 8 (1965) 67-82.

[36] Y. Mori, W. Nakayama, Study on forced convective heat transfer in curved pipes (2^{nd} report, turbulent region), Int. J. Heat Mass Transfer 10 (1967) 37-59.

[37] Y. Mori, W. Nakayama, Study on forced convective heat transfer in curved pipes (3^{rd} report, theoretical analysis under the condition of uniform wall temperature and practical formulae), Int. J. Heat Mass Transfer 10 (1967) 681-695.

[38] J.S. Jayakumar, S.M. Mahajani, J.C. Mandal, K.N. Iyer, P.K. Vijayan, CFD analysis of single-phase flows inside helically coiled tubes, Comput. Chem. Eng. 34 (2010) 430-446.

[39] American International Society for Testing and Materials (ASTM) Standard C1784, 14, "Standard Test Method for Using a Heat Flow Meter Apparatus for Measuring Thermal Storage Properties of Phase Change Materials and Products," ASTM International, West Conshohocken, PA, 2014, DOI:10.1520/C1784-14, www.astm.org.

[40] National Institute of Standards and Technology (NIST), NIST Chemistry Webbook - Thermophysical Properties of Water, 2013, http://webbook.nist.gov/cgi/fluid.cgi?T=293.15&PLow=&PHigh=&PInc=&Applet=on&Digits=5&ID=C7732185&Action=Load&Type=IsoTherm&TUnit=K&PUnit=MPa&DUnit=mol%2Fl&HUnit=kJ%2Fmol&WUnit=m%2Fs&VisUnit=uPa*s&STUnit=N%2Fm&RefState=DEF.

[41] MatWeb, Material Property Data - Physical Properties of Butyl Stearate, 2013, http://www.matweb.com/search/DataSheet.aspx?MatGUID=9ce8f159202f428385dc5638c3210939&ckck=1.

[42] J.C. Maxwell, A treatise on electricity and magnetism, Dover Publications, Mineola, NY, 1954.

[43] U. Rea, T. McKrell, L. Hu, J. Buongiorno, Laminar convective heat transfer and viscous pressure loss of alumina-water and zirconia-water nanofluids, Int. J. Heat Mass Transfer 52 (2009) 2042-2048.

[44] E. Yakhshi-Tafti, S. Tamanna, H. Pearlman, Experimental investigation on the thermal and hydraulic performance of alumina-water nanofluids in single-phase liquid-cooled cold plates, J. Heat Transfer 137 (2015) 071703.

[45] S. Mueller, E.W. Llewellin, H.M. Mader, The effect of particle shape on suspension viscosity and implications for magmatic flows, Geophys. Res. Lett. 38 (2011) L13316.

[46] R. Greenwood, P.F. Luckham, T. Gregory, The effect of diameter ratio and volume ratio on the viscosity of bimodal suspensions of polymer lattices, J. Colloid Interface Sci. 191 (1997) 11-21.

[47] E. N. daC. Andrade, Theory of viscosity of liquid, Phil. Mag. 17 (1934) 497-511.

[48] R. Lakshmi, S.K. Athithan, An empirical model for the viscosity buildup of hydroxyl terminated polybutadiene based solid propellant slurry, Polym. Compos. 20 (1999) 346-356.

[49] S.K. Kawatra, T.C. Eisele, Rheological effects in grinding circuits, Int. J. Miner. Process. 22 (1988) 251-259.

[50] H. Inaba, W.I.A. Aly, N. Haruki, Flow and heat transfer characteristics of drag reducing surfactant solution in a helically coiled pipe, Heat Mass Transfer 41 (2005) 940-952.

[51] B.N. Taylor, C.E. Kuyatt, Guidelines for evaluating and expressing the uncertainty of NIST measurement results, NIST Technical Note 1297, NIST, Gaithersburg, MD, 1994.

[52] H. Taherian, J.L. Alvarado, System analysis of MPCM slurry enhanced with carbon nanotubes as heat transfer fluid, ASHRAE Trans. 116 (2010) AB-10-021.

[53] W.R. Dean, The stream-line motion of fluid in a curved pipe, Phil. Mag. J. Sci. 5 (1928) 673-695.

[54] A.C. Verkaik, B.W.A.M.M. Beulen, A.C.B. Bogaerds, M.C.M. Rutten, F.N.van de Vosse, Estimation of volume flow in curved tubes based on analytical and computational analysis of axial velocity profiles, Phys. Fluids 21 (2009) 023602-1-13.

[55] J.M. Tarbell, M.R. Samuels, Momentum and heat transfer in helical coils, Chem. Eng. J. 5 (1973) 117-127.

[56] S.V. Patankar, V.S. Pratap, D.B. Spalding, Prediction of laminar flow and heat transfer in helically coiled pipes, J. Fluid Mech. 62 (1974) 539-551.

[57] D.S. Austen, H.M. Soliman, Laminar flow and heat transfer in helically coiled tubes with substantial pitch, Exp. Therm. Fluid Sci. 1 (1988) 183-194.

[58] L.A.M. Janssen, C.J. Hoogendoorn, Laminar convective heat transfer in helical coiled tubes, Int. J. Heat Mass Transfer 21 (1978) 1197-1206.

[59] K.E. Kasza, M.M. Chen, Improvement of the performance of solar energy or waste heat utilization systems by using phase-change slurry as an enhanced heat-transfer storage fluid, J. Sol. Energy Eng. 107 (1985) 229-236.

[60] K. Narrein, H.A. Mohammed, Influence of nanofluids and rotation on helically coiled tube heat exchanger performance, Thermochim. Acta 564 (2013) 13-23.

[61] G. Hetsroni, Particles-turbulence interaction, Int. J. Multiphase Flow 15 (1989) 735-746.

[62] G.J. Yoo, H.K. Choi, W.R. Dong, Fluid flow and heat transfer characteristics of spiral coiled tube: effects of Reynolds number and curvature Ratio, J. Cent. South Univ. 19 (2012) 471-476.

[63] W. Yu, D.M. France, E.V. Timofeeva, D. Singh, J.L. Routbort, Thermophysical property-related comparison criteria for nanofluids heat transfer enhancement in turbulent flow, Appl. Phys. Lett. 96 (2010) 1-3.

[64] H.A. Mohammed, K. Narrein, Thermal and hydraulic characteristics of nanofluid flow in a helically coiled tube heat exchanger, Int. Commun. Heat Mass Transfer 39 (2012) 1375-1383.

[65] A.K. Tiwari, P. Ghosh, J. Sarkar, Performance comparison of the plate heat exchanger using different nanofluids, Exp. Therm. Fluid Sci. 49 (2013) 141-151.

[66] M.F. Pakdaman, M.A.A. Behabadi, P. Razi, An experimental investigation on thermo-physical properties and overall performance of MWCNT/heat transfer oil nanofluid flow inside vertical helically coiled tubes, Exp. Therm. Fluid Sci. 40 (2012) 103-111.

[67] K.Q. Xing, Y.X. Tao, Y.L. Hao, Performance evaluation of liquid flow with PCM particles in microchannels, J. Heat Transfer 127 (2005) 931-940.

APPENDIX A

CALIBRATION OF THERMOCOUPLES

This section presents the procedures and the results for the thermocouple calibrations. Twenty four surface temperature thermocouples and ten fluid temperature thermocouples were used and calibrated before heat transfer experiments. The thermocouple calibration was conducted with pure water under isothermal conditions. All the temperatures were measured using an Agilent data logger at steady state conditions. The calibration process is as follows:

Experimental measurements were taken for all the thermocouples under equilibrium isothermal conditions for a period of 10 days. To get the average temperature value for each thermocouple, an arithmetic mean was taken and defined as:

$$T_{avg,i} = \frac{\sum_{n=1}^{10} T_{measured,i}}{10} \tag{A.1}$$

where *i* is the number of each thermocouple, which is from 1 to 34.

A total average temperature was calculated using the average temperature values of the thermocouples, as follows:

$$T_{avg,total} = \frac{\sum_{i=1}^{34} T_{avg,i}}{34} \tag{A.2}$$

Finally, correction factor (CF_i) was found for each of the corresponding thermocouple based on the deviation from the total average temperature value, as follows:

$$CF_i = T_{avg,total} - T_{avg,i} \tag{A.3}$$

The correction factors for all the thermocouples used in the experiments are shown in Table A.1 and were incorporated directly in the data acquisition system software.

Table A.1. Correction factors for thermocouples

Thermocouples	Average Temperature, $T_{avg,i}$ (˚C)	Correction Factor, CF_i (˚C)	% Difference (%)
TC1	18.18	0.29	1.6
TC2	18.20	0.27	1.5
TC3	18.14	0.33	1.8
TC4	18.37	0.10	0.5
TC5	18.57	-0.10	-0.5
TC6	18.36	0.11	0.6
TC7	18.53	-0.06	-0.3
TC8	18.41	0.06	0.3
TC9	18.52	-0.04	-0.2
TC10	18.43	0.05	0.3
TC11	18.49	-0.02	-0.1
TC12	18.50	-0.03	-0.1
TC13	18.40	0.08	0.4
TC14	18.40	0.07	0.4
TC15	18.53	-0.06	-0.3

TC16	18.19	0.28	1.5
TC17	18.27	0.20	1.1
TC18	18.74	-0.26	-1.4
TC19	18.51	-0.04	-0.2
TC20	18.49	-0.02	-0.1
TC21	18.65	-0.18	-1.0
TC22	18.56	-0.09	-0.5
TC23	18.58	-0.10	-0.6
TC24	18.64	-0.17	-0.9
TC25	18.61	-0.14	-0.7
TC26	18.64	-0.17	-0.9
TC27	18.80	-0.33	-1.8
TC28	18.56	-0.09	-0.5
TC29	18.58	-0.10	-0.6
TC30	18.55	-0.08	-0.4
TC31	18.36	0.11	0.6
TC32	18.29	0.18	1.0
TC33	18.46	0.01	0.0
TC34	18.57	-0.10	-0.5
Total Average Temperature, $T_{avg,total}$ ($^{\circ}$C)	18.47		